2272-101

REPORT DOCUMENTATION PAGE	1. REPORT NO. MA-RD-940-80056	2.	3. Recipient's Accession No

Title and Subtitle

Non-Linear Ship Springing Experiments

5. Report Date: February 1983

6.

Author(s)

Scott Slocum and Armin Troesch

8. Performing Organization Rept. No. 266

Performing Organization Name and Address

Department of Naval Architecture and Marine Engineering
The University of Michigan
Ann Arbor, MI 48109

10. Project/Task/Work Unit No.

11. Contract(C) or Grant(G) No.
(C)
(G)

12. Sponsoring Organization Name and Address

The American Bureau of Shipping, 65 Broadway, New York, NY 10006
and
U.S. Department of Transportation, Maritime Administration
Office of Research and Development, Washington, DC 20590

13. Type of Report & Period Covered: Final

14.

15. Supplementary Notes

16. Abstract (Limit: 200 words)

The results of an experimental study investigating the main hull girder vibrations of Great Lakes bulk carriers are presented. The source of excitation is the non-linear excitation due to two wave trains of different frequencies. Large resonance responses are recorded when the sum of the two encounter frequencies match the natural frequency of the hull.

17. Document Analysis a. Descriptors

Wave induced bending moments
Springing
Non-linear ship dynamics
Experimental springing results

b. Identifiers/Open-Ended Terms

c. COSATI Field/Group

Availability Statement	19. Security Class (This Report)	21. No. of Pages
Approved for Release National Technical Information Service Springfield, Virginia 22151	Unclassified	125
	20. Security Class (This Page) Unclassified	22. Price

ANSI-Z39.18) See Instructions on Reverse

OPTIONAL FORM 272 (4-77)
(Formerly NTIS-35)
Department of Commerce

MARAD Report No.
MA-RD-940-80056
UM/NAME Report
No. 266
February 1983

NON-LINEAR SHIP SPRINGING EXPERIMENTS

Prepared by:

Scott Slocum
and
Armin W. Troesch

September 9, 1982

Co-sponsored by

The American Bureau of Shipping

U.S. Department of Transportation, Maritime Administration

Office of Research and Development

Department of Naval Architecture
and Marine Engineering
College of Engineering
The University of Michigan
Ann Arbor, Michigan 48109

TABLE OF CONTENTS

LIST OF FIGURES

page

page

NOMENCLATURE

A_{ij} = generalized hydrodynamic added mass coefficient

a_{ii} = generalized ship mass coefficient

B_{ij} = generalized hydrodynamic damping coefficient

B = ship beam at midship

b_{22} = internal ship springing damping coefficient

C_{ij} = generalized hydrostatic restoring coefficient

c_{22} = internal spring constant

$E_2^{(k)}$ = amplitude of the kth order springing excitation

$e_i(t)$ = ith generalized wave excitation periodic in time

$e_2^{(k)}(t)$ = kth order of the generalized springing excitation periodic in time

F_n = Froude number

f_1 = external force applied at x_{cg_A}

f_2 = external force applied at x_{cg_F}

g = gravitational constant

H = total springing excitation transfer function

$H^{(k)}$ = kth order springing excitation transfer function

$H_R^{(k)}$ = kth order springing response transfer function

h_1 = linear impluse response function

h_2 = quadratic impulse response function

I = mass moment of inertia of the model about midship

I_A = mass moment of inertia of the after part of the model about x_{cg_A}

I_F = mass moment of inertia of the forward part of the model about x_{cg_F}

K_s = model midship spring constant

k = wave number of the incident wave ($=2\pi/\lambda$)

L = ship length

ℓ_A = magnitude of distance from midship to the center of gravity of the after model section

ℓ_F = magnitude of distance from midship to the center of gravity of the forward model section

M = mass of the model

M_A = mass of the after model section

M_F = mass of the forward model section

$M_0^{(k)}$ = amplitude of the kth order midship bending moment

$m_0(t)$ = midship bending moment periodic in time

$m_0^{(k)}(t)$ = kth order midship bending moment periodic in time

$q_i(t)$ = the ith generalized coordinate
i = 0 : vertical rigid body motion
i = 1 : rigid body rotation about the y axis
i = 2 : two noded body motion

$S^+(\omega)$ = one sided incident wave spectrum

$S^+_E(\omega)$ = one sided springing excitation spectrum

$S^+_M(\omega)$ = one sided midship bending moment spectrum

U = ship speed

U_m = model speed

x = the longitudinal ship coordinate axis, positive towards the bow

x_{cg_A} = x coordinate of the center of gravity of the after model section ($= -\ell_A$)

x_{cg_F} = x coordinate of the center of gravity of the forward model section ($= \ell_F$)

y = transverse ship coordinate axis, positive to port

$z_i(x)$ = ith vertical mode shape

z = vertical ship coordinate axis, positive up

α_i = ith phase angle of the $q_i(t)$ mode of motion

$\zeta(t)$ = time dependent water surface elevation due to waves

ζ_0 = damping ratio in springing

η = incident wave amplitude

θ_0 = midship deflection angle due to springing motion

λ = incident wave length

ξ_3 = rigid body heave amplitude

ξ_5 = rigid body pitch amplitude

σ = incident wave frequency as seen from a stationary observer

ω, ω_1, ω_2 = wave frequencies of encounter

ω_- = difference frequency ($=\omega_1 - \omega_2$)

ω_+ = sum frequency ($=\omega_1 + \omega_2$)

ω_0 = natural frequency of main hull girder

Executive Summary

Under the joint sponsorship of the American Bureau of Shipping and the Maritime Administration, a Research program investigating Great Lakes springing was funded at the University of Michigan. The emphasis of the project was placed on determining whether non-linear long wave springing excitation is important. Based upon the model tests conducted in the Ship Hydrodynamic Laboratory's towing tank and based upon the analytical work done, it is clear that the methodology used to analyze ship springing must include both a linear and a non-linear part.

Consider a bulk carrier operating on the Great Lakes. If it encounters an incident wave of frequency ω, then there will be a springing excitation at ω. This is the so-called "linear" excitation and will produce a linear response in the form of a midship bending moment. The term linear implies that if the incident wave height is doubled, then the bending moment is also doubled. Preliminary springing excitation and response experiments conducted by Troesch (1980) have shown that there is also a significant transfer of energy from the fundamental frequency of encounter, ω, to higher harmonics such as 2ω and, sometimes 3ω. Should 2ω or 3ω equal ω_o, the natural frequency of the hull, then there will be a substantial increase in the springing response, and, consequently, the midship bending moment.

The sea is not composed of a single wave component, but rather a complete spectrum. The steepness of the water surface and the interaction of different wave components introduce non-linearities. Wave components at one frequency will interact with components at other frequencies. The result will be waves with frequencies $\omega_i-\omega_j$ and $\omega_i+\omega_j$, where ω_i and ω_j are the frequencies of the first order wave components. The implication of this for ship spring-

ing is that, in addition to the long wave excitation resulting from 2ω and 3ω, there will also be long wave excitation from $\omega_i+\omega_j$.

This report describes how the non-linear behavior of Great Lakes ship springing was investigated through model tests. Both the harmonic ($\omega_o = 2\omega_1$) and the sum frequency ($\omega_o = \omega_1 + \omega_2$) conditions were investigated. A description of the experimental equipment and data collection procedures is included. An empirical form of the equation describing the non-linear springing response is given and verification offered. The use of the model test results in statistically evaluating the importance of the non-linear springing is shown through an example.

Based upon the results of this report, it is possible to draw the following conclusions:

- The non-linear excitation and consequently the response to the non-linear excitation are dependent upon ship speed, wave frequency of encounter, and wave height.

- The non-linear effects tend to be quadratic in wave amplitude. (The distinction between linear and quadratic systems is the following: As stated earlier, a linear system with an incident wave of encounter frequency ω will produce a response at that same frequency, and if the wave height is doubled, the response will also double. In a quadratic system, an incident wave of encounter frequency ω will produce a response at twice that frequency, or 2ω. Of equal importance, however, is that if the wave height is doubled the response at 2ω will increase by a *factor of four*.)

- For Great Lakes bulk carriers, particularly the "thousand footers," heave and pitch motions are considered to be small. However, both the non-linear excitation and non-linear response are influenced by the magnitude of these relatively small motions.

In addition to the above conclusions, an example is given in the text where the non-linear effects are included in estimating the area under the springing spectrum. It is found that the non-linearities account for approximately 25% of the total area.

I. INTRODUCTION

Under the joint sponsorship of the American Bureau of Shipping and the Maritime Administration, a Research program investigating Great Lakes springing was funded at the University of Michigan. The emphasis of the project was placed on determining the answer to two questions: (1) Can a linear theory predict springing response? and (2) Is non-linear long wave excitation important? The unexpected answer to both is yes! Based upon the model tests conducted in the Ship Hydrodynamic Laboratory's towing tank and based upon the analytical work done, it is clear that the methodology used to analyze ship springing must include both a linear and a non-linear part.

Most current ship motions and wave loading programs use a linear theory. (An exception is the work described by Jensen and Pedersen (1981)). This implies that any of the quantities of interest, i.e., the heave amplitude or midship bending moment, are directly proportional to the incident wave height. Also implied is that the response has the same frequency as the encounter frequency of the incident wave. Specifically omitted from the model is the possibility that low frequency, long waves will excite high frequency ship springing. While the linear model has worked well in past applications, the work done here at the University demonstrates that it will only partially describe the springing excitation and response of the Great Lakes ore carriers.

An analytical linear theory has been developed by Bishop and Price (1977) and Maeda (1980). Parts of this linear model have been validated by towing tank experiments; see, for example Troesch (1980). One of the theory's deficiencies, however, is its inability to accurately predict a springing damping coefficient. While damping prediction is an important problem, this report will address another aspect of ship springing. If all the waves on the Great

Lakes were short, then a linear theory, with perhaps an empirical damping coefficient, would be sufficient. This has been demonstrated with the short wave experiments described by Troesch (1980). However, an ore carrier will encounter long waves in addition to short waves. Preliminary springing excitation and response experiments conducted by Troesch (1980) have shown that there could be a significant transfer of energy from the fundamental frequency of encounter to higher harmonics. If the incident wave elevation was given as $\zeta(t)$, where

$$\zeta(t) = \eta \cos(\omega t) ,$$

then there was a measurable springing excitation at 2ω and, sometimes 3ω . Here ω is the encounter frequency and η is the incident wave amplitude. Should 2ω or 3ω equal ω_o , the natural frequency of the hull, there will be a substantial increase in the springing response.

The sea is not composed of a single wave component, but rather a complete spectrum. The steepness of the water surface and the interaction of different wave components introduce non-linearities. If we wish to describe the non-linear behavior of water waves, there are a number of approaches available. For example, if a perturbation technique is used, wave components at one frequency will interact with components at other frequencies. The result will be waves with frequencies $\omega_i - \omega_j$ and $\omega_i + \omega_j$, where ω_i and ω_j are the frequencies of the first order wave components. A good description of this theory is given by Longuet-Higgins (1963). The implication of this for ship springing is that, in addition to the long wave excitation resulting from 2ω and 3ω , there will also be long wave excitation from $\omega_i + \omega_j$. This is shown schematically in Figure 1.

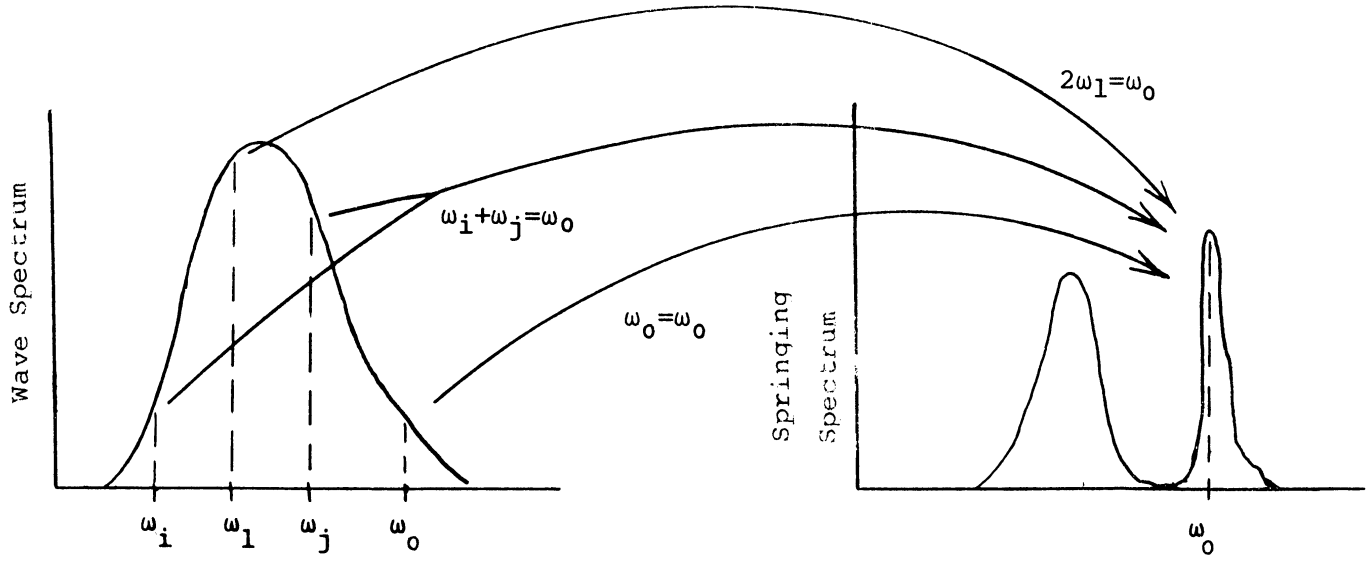

Figure 1: Linear and Non-Linear Transfer of Energy

In Figure 1, the spectra of the incident waves and the resulting springing response are indicated. The hull has a natural frequency of ω_0. The response at ω_0 is the result of the following sources of excitation:

i) Waves with an encounter frequency of ω_0. (This is the linear case. We are able to estimate this excitation using the theory developed by Bishop and Price (1977) or Maeda (1979)).

ii) Waves with an encounter frequency of ω_1, where $2\omega_1 = \omega_0$. (This is the non-linear excitation due to harmonics of long waves).

iii) Waves with encounter frequencies of ω_i and ω_j where $\omega_1 + \omega_j = \omega_0$. (This is also a non-linear excitation caused by the interaction of two different wave components).

A recent attempt to analyze the transfer of energy from low frequencies to high frequencies is described in articles by J. Jensen and P.T. Pedersen (1978) and (1981). In those articles the authors calculate the wave-induced

bending moments in ships by a quadratic theory. There are a number of difficulties associated with their theory, however, one being the improper handling of the free surface condition. This problem, though, only effects their ability to predict the magnitude of the non-linear bending moment. In principle, their procedure is correct. Specifically, they give the total bending moment response as follows:

$$m(x,t) = m^{(1)}(x,t) + m^{(2)}(x,t) + \ldots$$

where $m^{(1)}(x,t)$ is the linear moment due to wave excitation as previously described in case i) and $m^{(2)}(x,t)$ is the non-linear moment due to wave excitation described by ii) and iii). While it is extremely difficult to analytically estimate $m^{(2)}(x,t)$, it should be possible to determine its value experimentally.

Jensen and Pedersen (1981) also show how a spectral density function of the bending moment can be calculated if the spectrum of the incident wave is known and if the bending moment response amplitude operator (RAO) is given or can be determined. The RAO is the bending moment due to waves of unit height and may include the effects due to non-linearities. The bending moment spectrum would then include both linear and non-linear parts.

This report will describe how the non-linear behavior of Great Lakes ship springing was investigated through model tests. Both the harmonic ($\omega_o = 2\omega_1$) and the sum frequency ($\omega_o = \omega_1 + \omega_2$) conditions were investigated. A description of the experimental equipment and data collection procedures is included. An empirical form of the equation describing the non-linear springing response is given and verification offered. The use of the model test results in statistically evaluating the importance of the non-linear springing is shown in an example.

II. INSTRUMENTATION AND EQUIPMENT

The fiberglass model used in the experiments described by Troesch (1980) was used again for the non-linear experiments described in this report. A description of the model and test apparatus will be included here for completeness.

A 15 foot fiberglass model of the *S.J. Cort* was constructed for the earlier project. In a manner similar to that described by Hoffman and van Hooff (1976), the model was made in two halves connected by a spring at midships. See Table I for the model characteristics and Figure 2 for the body plan. See Figure 3 for a description of the quantities measured.

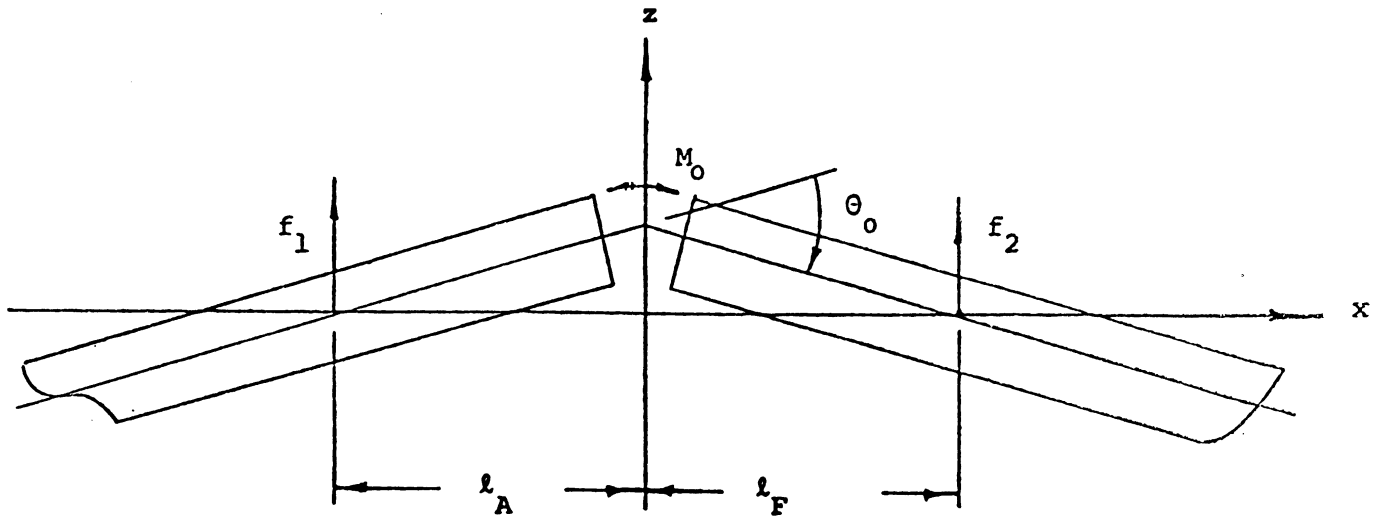

Figure 3: Schematic of Model for Springing Experiments

In Figure 3, f_1 and f_2 are external forces, M_o is the midship bending moment, $\ell_A = -x_{cg_A}$ where x_{cg_A} is the x coordinate of the center of gravity of the after part of the model and $\ell_F = x_{cg_F}$ where x_{cg_F} is the x coordinate of the center of gravity of the forward part of the model.

The model has three degrees of freedom. The normalized linear coupled equations of motion can be written in the following form.

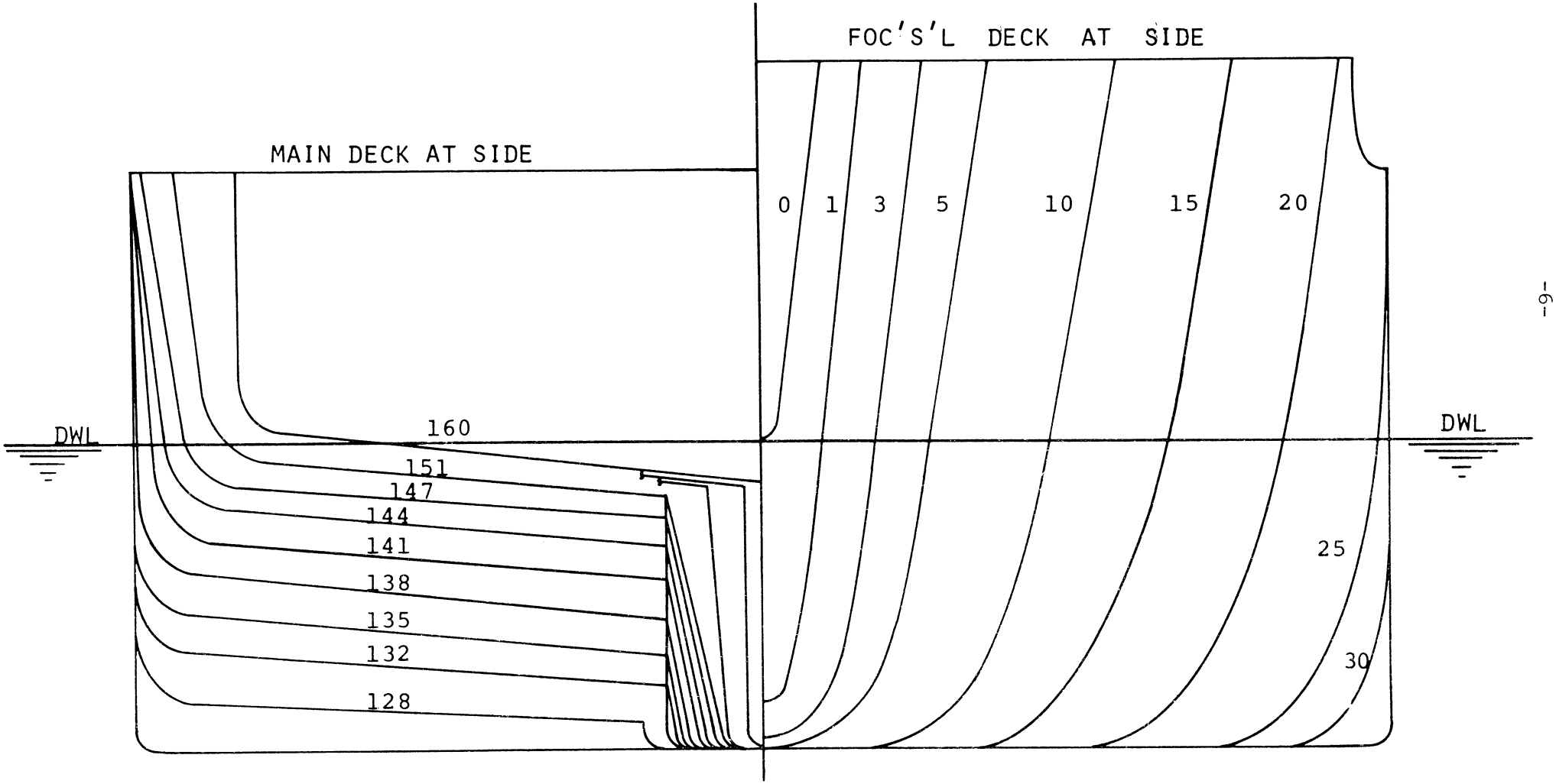

FIGURE 2: BODY PLAN OF THE S.J. CORT (WITH FRAME NUMBERS).

Table I: Model Characteristics

Characteristics - Total Model		
scale	66.67:1	
Length Overall, m(ft)	4.572	(15.00)
Length between Perpendiculars, m(ft)	4.569	(14.99)
Beam, m(ft)	0.4783	(1.569)
Draft (mean), m(ft)	0.1179	(0.387)
Displacement, N(lbs)	2,245.	(504.8)
Longitudinal Center of gravity (% L fwd midships)		0.1%
Moment of Inertia about Midships, kg-m^2 (slugs-ft^2)	331.6	(244.6)
Characteristics - Fore Body		
Length Overall, m(ft)	2.286	(7.50)
Displacement, N(lbs)	1,142.	(256.7)
Longitudinal Center of Gravity (% L fwd midships)		22.5%
Moment of Inertia about Forebody LCG, kg-m^2 (slugs-ft^2)	40.86	(30.14)
Characteristics - After Body		
Length Overall, m(ft)	2.286	(7.50)
Displacement, N(lbs)	1.103	(248.1)
Longitudinal Center for Gravity (% L aft midships)		23.1%
Moment of Inertia about Afterbody LCG, kg-,m^2 (slugs-ft^2)	41.86	(30.88)

$$\ddot{q}_0(t)a_{00} + \sum_{j=0}^{2} [A_{0j}\, q_j(t) + B_{0j}\, \dot{q}_j(t) + C_{0j}\, q_j(t)] = f_1 + f_2 + e_0 \qquad (1)$$

$$\ddot{q}_1(t)a_{11} + \sum_{j=0}^{2} [A_{1j}\, q_j(t) + B_{1j}\, \dot{q}_j(t) + C_{1j}\, q_j(t)] = x_{cq_A} f_1 + x_{cq_A} f_2 + e_1 \qquad (2)$$

$$\ddot{q}_2(t)a_{22} + \dot{q}_2(t)b_{22} + \sum_{j=0}^{2} [A_{2j}\, q_j(t) + B_{2j}\, \dot{q}_j(t) + C_{2j}\, q_j(t)] = + m_0 \left[1 - \frac{x_{cq_A}}{x_{cq_F}} \right] + e_2 \qquad (3)$$

The generalized coordinates are given as

$$q_0(t) = \xi_3\, e^{i\omega t + i\alpha_0}$$

$$q_1(t) = \xi_5\, e^{i\omega t + i\alpha_1}$$

$$q_2(t) = [\theta_0/(1+\ell_A/\ell_F)]\, e^{i\omega t + i\alpha_2}$$

where

ξ_3 is the heave amplitude,

ξ_5 is the pitch amplitude,

and θ_0 is the midship deflection angle.

The mode shapes, z_i, are defined as follows:

$$z_0 = 1$$

$$z_1 = x$$

$$z_2 = \begin{cases} \ell_A + x & \text{for } x \leq 0 \\ (\ell_A/\ell_F)(\ell_F - x) & \text{for } x \geq 0 \end{cases}$$

The midship bending moment, m_0, is given as

$$m_0(t) = -K_s(1 + \ell_A/\ell_F)q_2(t)$$

where K_s is a spring constant.

The coefficients have the following forms:

$a_{00} = M$, the mass of the model,

$a_{11} = I$, the mass moment of inertia of the model about midships,

$a_{22} = I_A + \frac{\ell_A}{\ell_F} I_F$ where I_A and I_F are the mass moments of inertias about the centers of gravity of the after part and forward part respectively.

$e_i = \int_L dx\ z_i(x)\ f_e(x,t)$ where f_e is the sectional hydrodynamic exciting force and periodic in time,

and $C_{ij} = \int_L dx\ z_i(x)\ z_j(x) \rho g\ B(x)$ where ρg is the weight density of the fluid and B is the beam of the ship.

Also A_{ij} represents the i-th generalized hydrodynamic force due to an acceleration in the j-th mode,

B_{ij} represents the i-th generalized hydrodynamic force due to a unit velocity in the j-th mode,

and b_{22} represents the springing internal mechanical damping.

Note that f_e is a result of the integration of the hydrodynamic pressures on a hull section and may include forward speed effects if the model is moving forward. For the complete theoretical expressions of these coefficients, see the corresponding formulas given by Maeda (1980).

As explained in the linear theory section of Troesch (1980), the vertical displacements are expanded in terms of the dry modes. For our particular case this is heave, pitch, and springing. These mode shapes must satisfy a condition of orthogonality that requires

$$M_A + M_F = M \ ,$$

$$M_A \ell_A = M_F \ell_F \ ,$$

and

$$I_A = (\ell_A/\ell_F) I_F \ .$$

here M_A and I_A and M_F and I_F are the mass and mass moment of inertia of the after part and forward part respectively.

The rationalization of using dry mode expansions instead of the more common wet mode expansions will be briefly explained. The hydrodynamic pressures are treated as external incremental forces allowing the hydrodynamic coefficients to be expanded in terms of the orthogonal dry mode shapes. This permits both the added mass and damping coefficients to be expressed in the same rigorous, consistent manner. When the frequency of oscillation become sufficiently high and the damping forces go to zero, either the wet or dry mode expansions are correct. However, the relatively low springing frequency (that is relative to typical ship vibration frequencies) causes hydrodynamic reactive forces that are in phase with both the acceleration and velocity of the displacement. The non-conservative nature of the external forces suggests the use of the dry mode shapes. The derivation of the general equations of motion for an elastic ship's hull is given in detail by Bishop and Price (1977) or Maeda (1979).

In the experiments, measurements were made of the midship bending moment and the incident wave. The motions were not measured since the incident waves were typically shorter than the model and thus did not noticeably excite heave or pitch.

If the springing excitation was to be measured, then the spring constant, K_S , must be large enough so that the contribution of the dynamic terms in the equation of motion, equation (3), be effectively zero. This was accomplished by using a stiff 4450N (1000 lb) load cell. The actual experimental configuration is detailed by Troesch (1980). When measuring the springing response, the load cell was replaced with a relatively soft spring that gave the model a full scale, two noded, natural frequency of approximately 0.30 cycles per second.

The wave elevation was measured using a Wesmar LM7000 sonic wave probe. The probe was attached to the carriage approximately 2m (7 ft) in front of the model's bow.

The output from the instruments were in analog form. These signals were converted to digital form on a Tektronix 4052 minicomputer equipped with a Trans Era A/D converter, Memory module, and special purpose FFT ROM pack. The record length was 4096 sample points per channel, and all record processing was done on the Tektronix. Each signal was Fourier transformed and the spectral peaks in the wave record were located. Given the incident wave transform and the convolution of that transform, the first and second order transfer function could be determined. The actual data reduction method is described in detail in the Appendix.

As described earlier, the non-linear experiments consisted of both harmonic and sum frequency tests. The harmonic tests followed a format similar to

Troesch (1980). In those tests, the wave maker produced waves of a single frequency with the non-linear excitation or response occurring at twice the encounter frequency. In order to conduct the sum frequency tests, two wave trains were generated. Since waves are dispersive (i.e., the speed at which they travel depends upon their frequency), the wave maker was driven by a predetermined signal that had the two wave groups meet at a particular location in the tank. By properly coordinating the start of the towing carriage and the start of the wave generator, the model and the wave groups arrived at the same place at the same time. This produced a springing excitation of five distinct frequencies. If the frequencies of the two wave groups are given as ω_1 and ω_2, then the linear responses were at ω_1 and ω_2. The three non-linear responses were at $\omega_1 + \omega_2$, $2\omega_1$, and $2\omega_2$. The location of non-linear responses could be accurately determined by simply viewing the convolution of the Fourier transform of the incident wave signal.

The graphics screen of the Tektronix 4052 was used to monitor the input signals from the load cells/strain gages and wave probe. It also was used to display various quantities of interest at selected steps in the data reduction procedure. Examples of the traces shown on the screen are reproduced in Figures 4 through 7. The time, frequency, and magnitude axes are indicated. Figure 4 shows the time histories of the incident wave and resulting bending moment for the harmonic response test. The fundamental and harmonic content of the response are clearly visible. The relative magnitudes can be seen in Figure 5 where the Fourier Transform of the bending moment is graphed. The transform of the incident wave and the convolution of that transform are also presented. The use of the convolution is described in the Appendix. Figure 6 shows the time histories of the wave and bending moment for the sum frequency

Harmonic Springing Response Test
($2\omega_1 = \omega_o$)
Encounter Frequency $\omega_1 \simeq 7.55$ rad/sec
Froude Number $F_n = 0.132$

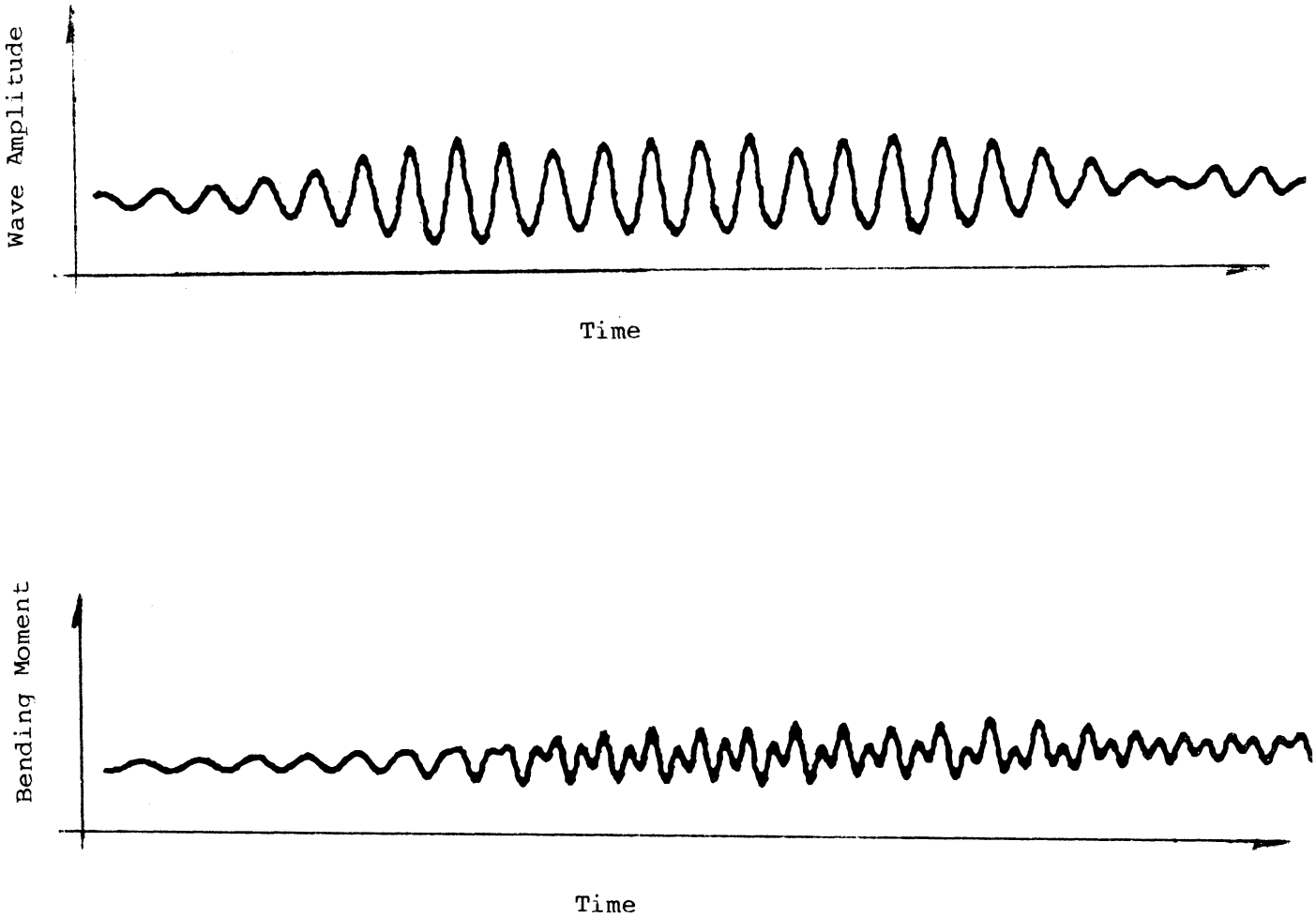

FIGURE 4: TIME HISTORY OF A SINGLE WAVE GROUP AND THE RESULTING MIDSHIP BENDING MOMENT.

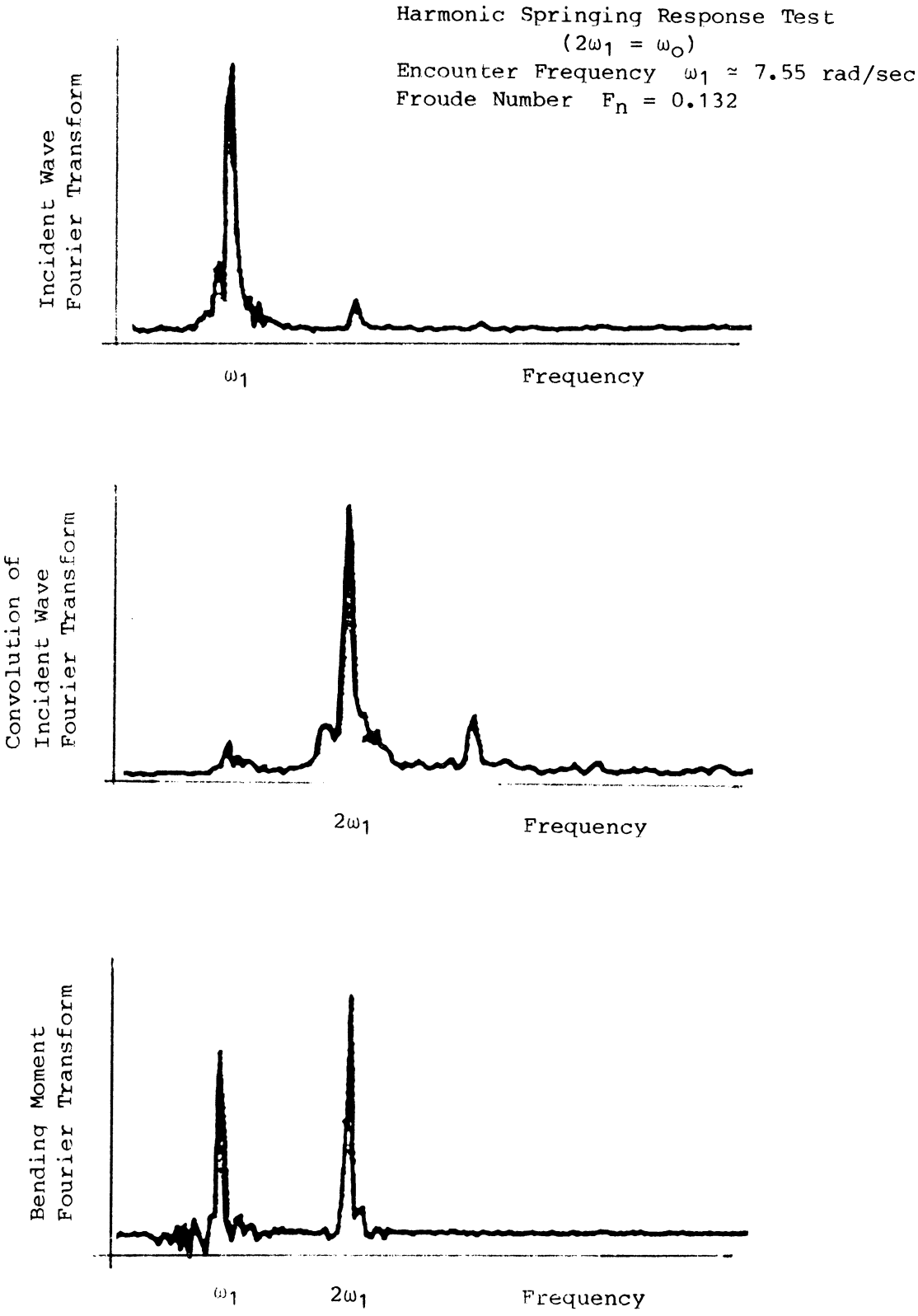

FIGURE 5: FREQUENCY DOMAIN REPRESENTATION OF A SINGLE WAVE GROUP AND THE RESULTING MIDSHIP BENDING MOMENT.

Sum Frequency Springing Response Test
($\omega_1 + \omega_2 = \omega_0$)
Encounter Frequencies $\omega_1 \simeq 8.80$ rad/sec
$\omega_2 \simeq 6.30$ rad/sec
Froude Number $F_n = 0.132$

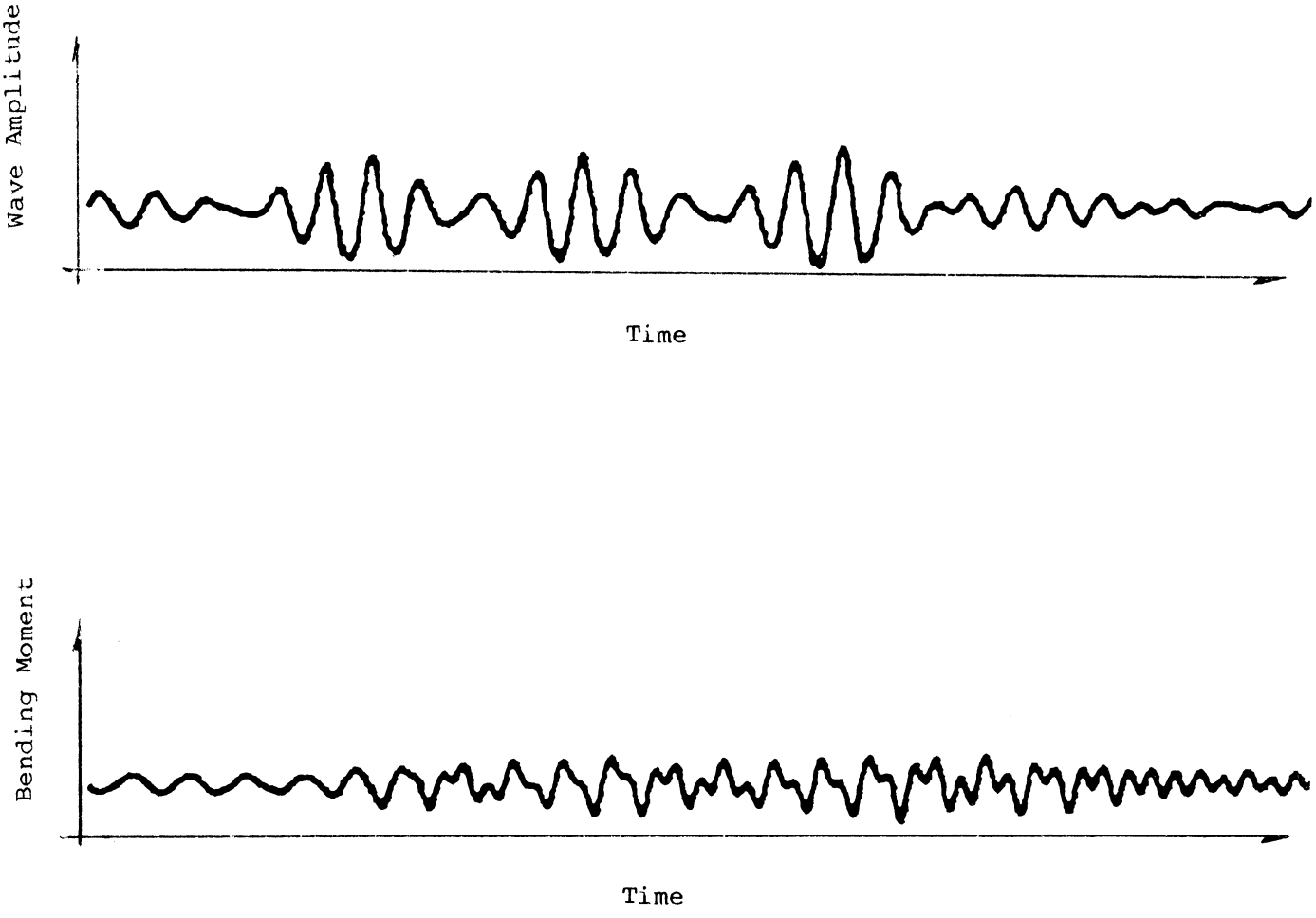

FIGURE 6: TIME HISTORY OF A TWO COMPONENT WAVE GROUP AND THE RESULTING MIDSHIP BENDING MOMENT.

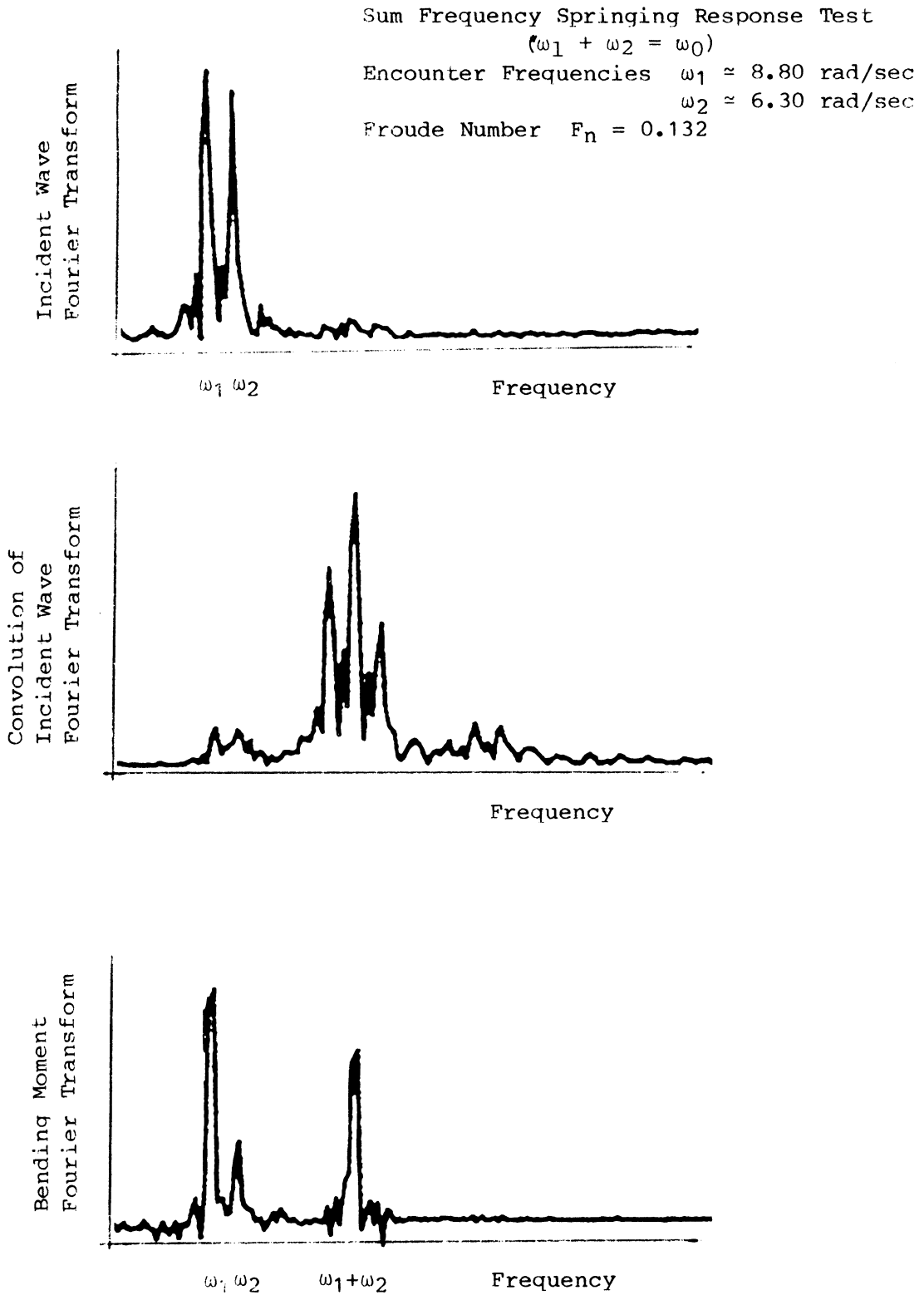

FIGURE 7: FREQUENCY DOMAIN REPRESENTATION OF A TWO COMPONENT WAVE GROUP AND THE RESULTING MIDSHIP BENDING MOMENT.

response test. The beat phenomenon that occurs when waves of two slightly different frequencies interact is present. Figure 7 contains the Fourier Transforms of the incident waves and bending moment and also the convolution of the wave transform. The doubly spiked graph of the wave transform demonstrates the two wave component nature of the incident wave. The bending moment transform shows the linear response at ω_1 and ω_2 and the non-linear sum frequency response at $\omega_1+\omega_2$. The difference in the magnitude of the response at ω_1 relative to that at ω_2 again demonstrates the hump-hollow behavior of the linear excitation curve as shown by Troesch (1980).

III. EXPERIMENTAL RESULTS

Introduction to the Experimental Results

Let the springing excitation transfer function, H, be the sum of the first order excitation, $H^{(1)}$, and the second order excitation, $H^{(2)}$. Since the transfer function $H^{(2)}(\omega_1,\omega_2)$ is a function of two frequency arguments, its magnitude might be presented in the form of a three-dimensional graph. For example, if we take the ω_1-axis to lie in the x-direction, and the ω_2-axis to extend in the y-direction, we can plot the transfer function magnitude in the z-direction as a function of ω_1 and ω_2.

Alternatively, we can represent the transfer function by a series of two-dimensional curves, each showing a sectional vertical cut of the three-dimensional surface $H^{(2)}(\omega_1,\omega_2)$. This was the method used here. The directions in which the sectional cuts were taken were chosen to provide the most useful quantitative and qualitative information in view of the computational formulas presented in section IV. Let us define the encounter frequency sum ω_+ by

$$\omega_+ = \omega_1 + \omega_2 , \tag{4}$$

and the encounter frequency difference ω_- by

$$\omega_- = \omega_1 - \omega_2 . \tag{5}$$

We can then write

$$H^{(2)}(\omega_1,\omega_2) = H^{(2)}\left[\frac{1}{2}(\omega_+ + \omega_-),\ \frac{1}{2}(\omega_+ - \omega_-)\right] . \tag{6}$$

As can be seen from the formulas in section IV, the calculation of the non-linear excitation spectral density at a given frequency ω_n requires a knowledge of the behavior of the transfer function as ω_- varies and ω_+ is

non-linear excitation spectral density at several different frequencies ω_n, we are also interested in the behavior of the transfer function for constant ω_- and varying ω_+.

In order to illustrate the relationship between the arguments ω_1 and ω_2 and the newly defined parameters ω_+ and ω_-, lines of constant ω_+ and lines of constant ω_- are plotted on the ω_1,ω_2 plane in Figure 8. We emphasize here that the arguments ω_+ and ω_- are used merely as an alternative (and more appropriate) set of coordinates with which to specify a location on the ω_1,ω_2 plane. We are in all cases interested in non-linear effects at the "sum frequency" ω_+, and use of the frequency difference parameter ω_- does not in any instance imply that we are investigating non-linear "difference frequency" phenomena.

The non-linear transfer function was determined experimentally by testing the model in wave systems composed of two wave components, one at encounter frequency ω_1 and the other at encounter frequency ω_2. (A description of the analysis procedure used to calculate the transfer function is given in the appendix). The behavior of $H^{(2)}\left[\frac{1}{2}(\omega_+ + \omega_-),\frac{1}{2}(\omega_+ - \omega_-)\right]$ for varying ω_+ was investigated by changing the wave frequencies ω_1 and ω_2 for each test run such that ω_- was held constant at some chosen value and ω_+ was systematically varied. The results of these tests are plotted versus ω_+, and the constant value of ω_- for a given set of runs is indicated in the caption to the corresponding data plot. Conversely, an investigation of ω_- dependency was conducted by allowing ω_- to vary while ω_+ was held constant. These results are plotted versus ω_-, and the constant value of ω_+ is given in the caption. Line segments shown in Figure 9 indicate the regions of the ω_1, ω_2 plane for which experimental data was obtained.

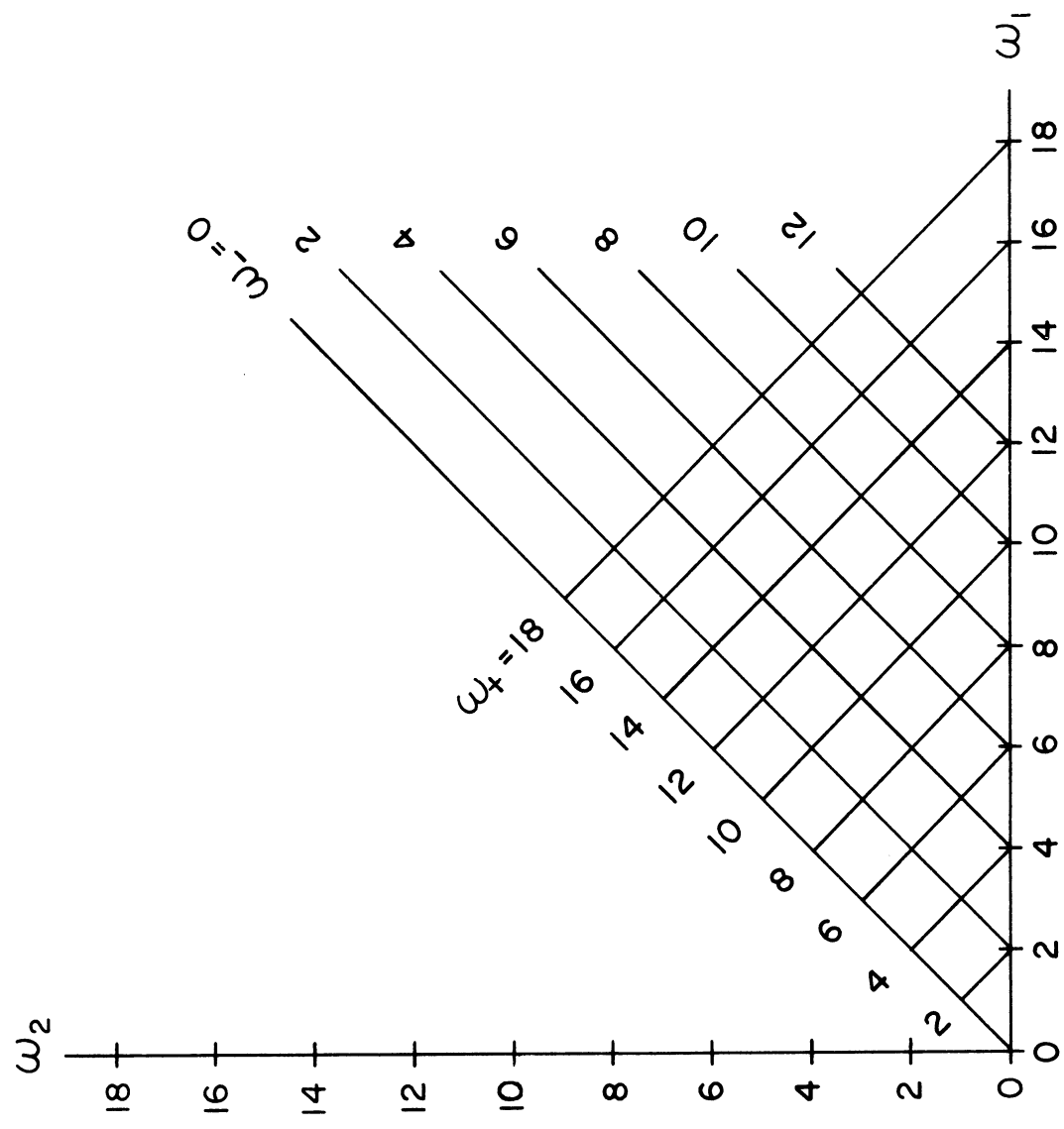

FIGURE 8: LINES OF CONSTANT ω_+ AND LINES OF CONSTANT ω_- PLOTTED IN THE ω_1, ω_2 PLANE.

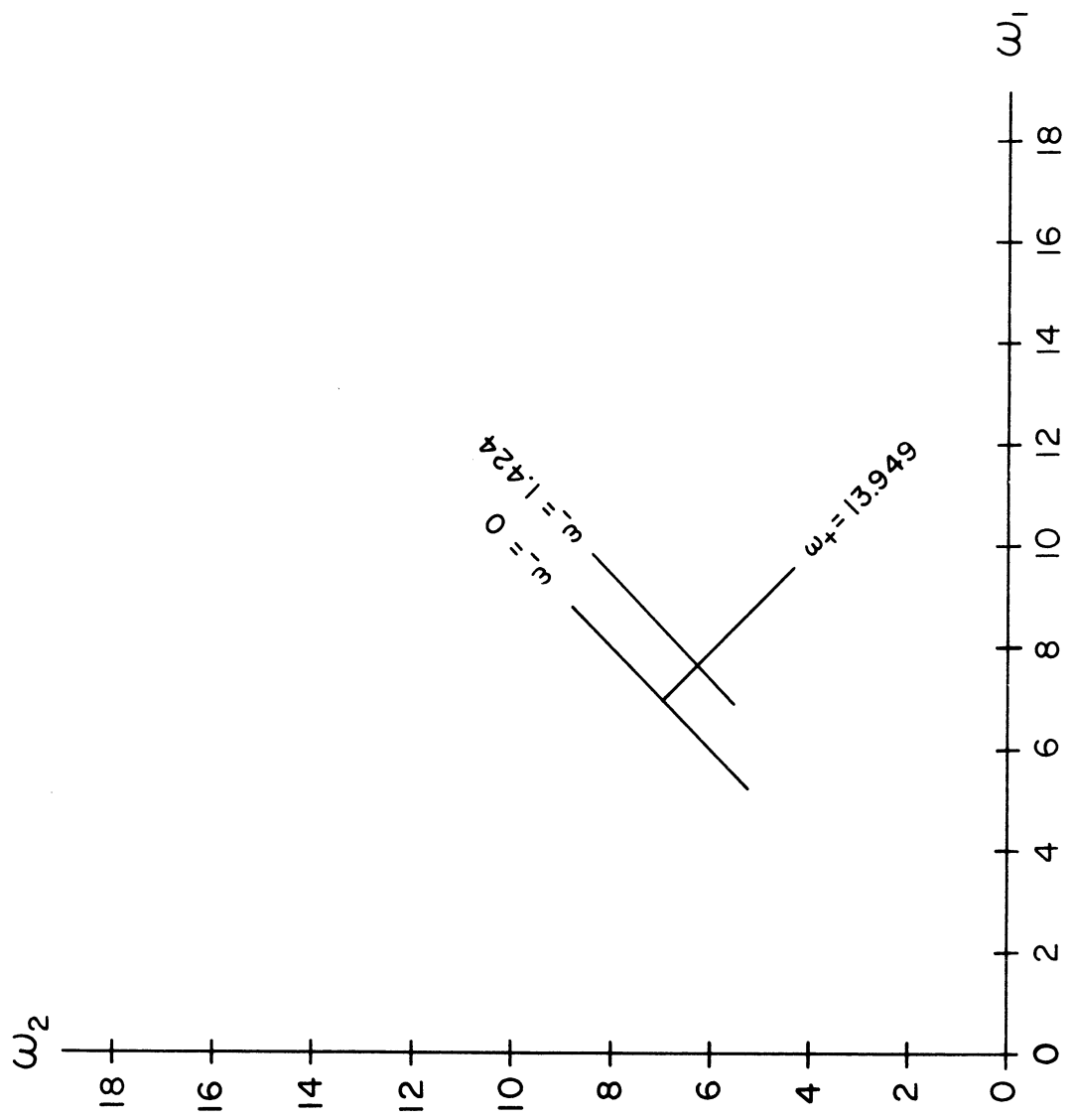

FIGURE 9: LINE SEGMENTS IN THE $\omega 1, \omega 2$ PLANE FOR WHICH EXPERIMENTAL DATA WAS OBTAINED.

Several tests were conducted for the important special case in which $\omega_- = \omega_1 - \omega_2 = 0$ and ω_+ varies. In this situation, the transfer function $H^{(2)}(\omega_1,\omega_1)$ was determined by testing the model in a monochromatic wave system. Since only one wave component was present in these tests, the results can be plotted against the ship length to wavelength ratio as well as the frequency sum (or, in this special case, the "harmonic" frequency) $\omega_+ = 2\omega_1$.

The linear transfer function $H^{(1)}(\omega)$ was determined from measurements taken in these "single wave" tests, and is in all cases plotted as a function of ship length to wavelength ratio.

Both the linear and non-linear excitation transfer functions are normalized by factors suggested by zero-speed Froude-Krylov calculations. The linear excitation data is given as

$$[H^{(1)}(\omega)]_{norm} = \frac{E_2^{(1)}(\omega)}{\rho g B L^2 \eta} \quad , \tag{7}$$

in which $E_2^{(1)}(\omega)$ is the amplitude of the linear generalized springing excitation measured at encounter frequency ω and η is the wave amplitude measured at the same frequency. The mass density of water is denoted by ρ , gravitational acceleration by g , B is the ship beam, and L denotes ship length. The non-linear excitation data is given as

$$[H^{(2)}(\omega_1,\omega_2)]_{norm} = \frac{E_2^{(2)}(\omega_1+\omega_2)}{\rho g B L^2 \sqrt{k_1 k_2}\, \eta_1(\omega_1)\eta_2(\omega_2)} \quad , \tag{8}$$

where $E_2^{(2)}(\omega_1+\omega_2)$ is the amplitude of the non-linear excitation at the frequency sum $\omega_+ = \omega_1 + \omega_2$, $\eta_1(\omega_1)$ and $\eta_2(\omega_2)$ are the measured wave amplitudes at encounter frequencies ω_1 and ω_2 , respectively, and k_1 and k_2 are wave numbers corresponding to ω_1 and ω_2 .

The relationship between the actual time history of the springing excitation, $e_2(t)$, and the amplitudes of the various components of the excitation, $E_2^{(1)}$, and $E_2^{(2)}$, is described in Section IV and the Appendix.

The non-linear response is plotted in the form

$$[H_R^{(2)}(\omega_1,\omega_2)]_{norm} = \frac{R_2^{(2)}(\omega_1+\omega_2)}{\rho g B L^2 \sqrt{k_1 k_2}\eta_1\eta_2} \qquad (9)$$

in which $R_2^{(2)}(\omega_1+\omega_2)$ is defined by the expression

$$R_2^{(2)}(\omega_1+\omega_2) = (1+\ell_A/\ell_F)M_0^{(2)}(\omega_1+\omega_2) \qquad (10)$$

with $M_0^{(2)}(\omega_1+\omega_2)$ denoting the amplitude of the non-linear bending moment at the frequency sum $\omega_+ = \omega_1 + \omega_2$.

Presentation of Experimental Data

(1) Figures 10 through 28: Experimental Data from Measurements of the Non-linear Springing Excitation

Figures 10 through 13 show the results of the primary thrust of the investigation. The normalized non-linear transfer function as defined by equation (8) is shown for each of the three line segments in the ω_1,ω_2 plane which are indicated in Figure 9. The data for all four plots was obtained from tests at Froude number $F_n = 0.132$ (model speed $U_m = 2.90$ ft/sec), with the model restrained in heave and pitch by rigid attachment at the node points.

Figure 10 shows the data taken in the "single wave" tests, in which ω_- was held constant at $\omega_- = 0$, and ω_+ was systematically varied. $[H^{(2)}(\omega_1,\omega_2)]_{norm}$ is plotted versus encounter frequency sum ω_+ (model scale).

Figure 11 shows the same data, plotted as a function of ship to wavelength ratio. This data agrees well with the non-linear excitation data given by Troesch (1980).

The data in Figure 12 was obtained in tests in which ω_- was held constant at $\omega_- = 1.424$ radians/sec (model scale) and ω_+ was varied. $[H^{(2)}(\omega_1,\omega_2)]_{norm}$ is plotted versus ω_+ (model scale). Note that there is little difference between the curves in Figures 10 and 12.

The purpose of taking the data in Figure 13 was to show the variation in the transfer function magnitude at constant ω_+ for different values of ω_-. $[H^{(2)}(\omega_1,\omega_2)]_{norm}$ is plotted versus ω_-, for $\omega_+ = 13.949$ radians/sec. Unfortunately the quality of this data is very poor, for reasons which have not yet been determined.

To investigate the effects of forward speed, the "single wave" tests ($\omega_- = 0$) were repeated for different Froude numbers, again with the model restrained. Figures 14 through 17 show the results of these tests plotted against ω_+. Figure 14 corresponds to tests at Froude number $F_n = 0.086$ (model speed $U_m = 1.90$ ft/sec). In Figure 15, $F_n = 0.109$ ($U_m = 2.40$ ft/sec). Figure 16 is a reproduction of the data in Figure 10, with $F_n = 0.132$ ($U_m = 2.90$ ft/sec). In Figure 17, $F_n = 0.155$ ($U_m = 3.40$ ft/sec). A curve has been faired through the data in each of these plots, and all four faired lines are shown together in Figure 18.

Figures 19 through 23 show the same data as Figures 14 through 18, but this time $[H^{(2)}(\omega_1,\omega_2)]_{norm}$ is plotted on a ship length/wavelength scale. We note that plotting the data on this scale seems to collapse the curves (compare Figures 18 and 23), indicating that the magnitude of the transfer

function is predominantly dependent upon the ship length/wavelength parameter. There is clearly a speed dependence, but it is not severe over small changes in Froude number.

In order to show that the transfer function itself is not dependent upon the wave amplitude, tests were conducted with reduced and increased wave amplitudes. Figure 24 shows the results of amplitude variation tests for $\omega_- = 0$ and varying ω_+. Figure 25 shows the data from amplitude variation tests for $\omega_- = 1.424$ radians/sec and varying ω_+. In both plots "medium amplitude" data was measured in waves with amplitudes of approximately 0.8-1.0 inches. This is the amplitude level maintained in all other tests. The "medium amplitude" data in Figures 24 and 25 is in fact the same as that shown in Figures 10 and 12, respectively. It is reproduced here for purposes of comparison. "High amplitude" data was measured in waves of approximately 2.0-2.3 inches in amplitude, a 130% increase. Data from "low amplitude" tests was measured in waves with amplitudes of approximately 0.5-0.7 inches, a 35% reduction. Figures 24 and 25 do not seem to support the statement that the transfer function is amplitude independent. We remark, however, that the results shown in these two plots are suspect. Since the non-linear excitation is small, there were inevitably some noise related problems in all of the excitation measurements. Waves of "medium" amplitude produced excitation signals which could be measured with reasonable accuracy. "Low" amplitude waves, however, produced signals which could not be analyzed with the same degree of confidence. In "high" amplitude waves, on the other hand, the model experienced a definite longitudinal impact as the bow entered each successive wave crest. This most likely caused a shudder in the support structure which would appear in the load cell signal as contaminant noise. In any event, the amplitude tests were repeated in the response experiments (in which the signal to noise problem was much

less severe) with a high degree of success (see Figure 43).

In order to investigate possible coupling effects between vertical rigid-body motions and the non-linear springing excitation, tests were conducted in for tests with $\omega_- = 0$, and ω_+ varying. Data from the restrained model test (Figure 10) is also plotted for purposes of comparison. Unlike the linear transfer function, which was shown by Troesch (1980) to be independent of heave and pitch, the non-linear transfer function appears to depend strongly upon vertical rigid-body motions.

In Figure 27 the data in Figure 26 is plotted against the ship length to wavelength ratio.

Figure 28 shows the results of tests with the model free to heave and pitch for $\omega_- = 1.424$ radians/sec and ω_+ varying. The normalized transfer function is plotted versus ω_+ . The quality of the data is poor for unknown reasons.

(2) Figures 29 through 44: Experimental Data from Measurements of the Non-linear Springing Response

Figures 29 through 32 show plots of the normalized non-linear response transfer function as defined by equation (9). These correspond to the excitation data in Figures 10 through 13. The data was obtained in tests at Froude number $F_n = 0.132$ ($U_m = 2.90$ ft/sec), with the model restrained in heave and pitch.

The data shown in Figure 29 was obtained in "single wave" tests, in which $\omega_- = 0$ and ω_+ varied. $[H_R^{(2)}(\omega_1,\omega_2)]_{norm}$ is plotted versus ω_+ (model scale).

Figure 30 shows the same data, plotted versus ship length/wavelength.

The data in Figure 31 was obtained in tests in which ω_- was held constant at $\omega_- = 1.424$ radians/sec and ω_+ varied. $[H_R^{(2)}(\omega_1,\omega_2)]_{norm}$ is plotted against ω_+ (model scale). Note that there is no significant difference between the curves in Figures 29 and 31.

Figure 32 shows the results of tests conducted with $\omega_+ = 13.949$ radians/sec and varying ω_-. $[H_R^{(2)}(\omega_1,\omega_2)]_{norm}$ is plotted versus ω_-. As was the case in the corresponding excitation tests (Figure 13), the data quality is poor for unknown reasons.

Speed variation tests equivalent to those conducted in the excitation measurements (Figures 14 through 23) were run to determine the effects of forward speed on the non-linear response. Figures 33, 34, 35, and 36 show the results for Froude numbers $F_n = 0.086$, 0.109, 0.132, and 0.155 respectively, with $\omega_- = 0$ in all cases. $[H_R^{(2)}(\omega_1,\omega_2)]_{norm}$ is plotted against ω_+, and faired lines are shown in each plot. The four faired curves are replotted for comparison in Figure 37.

The data from Figures 33 through 36 is plotted versus ship length/wavelength in Figures 38 through 41.

Faired lines are shown on a ship length/wavelength scale in Figure 42. Since the dynamic non-linear response is dependent primarily upon the proximity of the frequency sum ω_+ to the springing natural frequency (15.08 radians/sec for the model), plotting the response data on a ship length/wavelength scale does not collapse the data as was the case with the excitation data.

Amplitude variation tests were conducted to show that the normalized response transfer function is independent of the wave amplitude. Figure 43 shows the data obtained in tests with $\omega_- = 0$ and varying ω_+. "Low," "medium," and "high" amplitudes are defined in the same manner as in the excitation measurements. Since signal quality was not a problem in the response tests, the quality of the data for "high" and "low" amplitude waves is much better than that for the corresponding excitation tests. Figure 43 supports the statement that the normalized response transfer function tends to be independent of wave amplitude.

Equation (9) implies that the non-linear response at the sum frequency $\omega_1 + \omega_2 = \omega_+$ is proportional to the product. $\eta_1\eta_2[HR^{(2)}(\omega_1,\omega_2)]_{norm}$. If $[HR^{(2)}(\omega_1,\omega_2)]_{norm}$ is itself independent of the wave amplitudes η_1 and η_2, the non-linear response is wave amplitude dependent only through the quantity $\eta_1\eta_2$ and therefore is the result of non-linear effects are "quadratic" in wave amplitude. In the special "single wave" case, in which $\omega_1 = \omega_2$, this quantity becomes η^2, and the response obeys an "amplitude squared" law.

To investigate possible coupling effects between vertical rigid-body motions and non-linear springing response, tests were conducted in which the model was allowed to heave and pitch. Figure 44 shows the results for $\omega_- = 0$, with ω_+ varying. Data from the restrained model test (Figure 29) is also shown for comparison. The non-linear response appears to be strongly dependent upon vertical rigid-body motions.

(3) Figures 45 through 48: Experimental Data from Measurements of the Linear Springing Excitation

The linear excitation data, obtained from "single wave" tests ($\omega_- = 0$) is

shown in Figures 45 through 48 as $[H^{(1)}(\omega)]_{norm}$ versus ship length/wavelength. This data compares well with that given by Troesch (1980).

Figure 45 shows the data obtained in tests at Froude number $F_n = 0.132$ ($U_m = 2.90$ ft/sec) with the model restrained in heave and pitch.

Figure 46 is a plot of linear excitation data from the amplitude variation tests. "Low," "medium," and "high" amplitudes are defined as before. Clearly, the linear transfer function seems to be independent of wave amplitude.

Figure 47 shows the data obtained in speed variation tests, in which the linear transfer function was determined for Froude numbers $F_n = 0.086, 0.109, 0.132, 0.155$. This figure shows that small to moderate changes in forward speed have minor effects on the linear excitation, at least in the range of ship length/wavelength shown.

Figure 48 is a comparison which shows the effects of heave and pitch on the linear springing excitation. Data from Figure 45 (model restrained) is shown along with data obtained in tests in which the model was allowed to heave and pitch. The effects of vertical rigid-body motion are noticeable but tend to be small.

Comparison of Non-Linear Excitation and Response

Given the definitions (8), (9), and (10), we can show that the normalized excitation and response transfer functions are related by

$$[H_R^{(2)}(\omega_1,\omega_2)]_{norm} = \frac{[H^{(2)}(\omega_1,\omega_2)]_{norm}}{\left[\left(1 - \left(\frac{\omega_+}{\omega_o}\right)^2\right)^2 + \left(2\zeta\frac{\omega_+}{\omega_o}\right)^2\right]^{1/2}}\left[1 - \frac{C_{22}}{\omega_o^2(a_{22} + A_{22})}\right]. \tag{11}$$

(See equation (16) in Section IV.) This expression holds under the assumption that the second order excitation is the only source of non-linear effects.

In order to investigate the validity of this hypothesis, the normalized response transfer function $[H_R^{(2)}(\omega_1,\omega_2)]_{norm}$ was calculated from equation (11) using experimentally measured values of the normalized excitation transfer function $[H^{(2)}(\omega_1,\omega_2)]_{norm}$ as shown in equation (8). The calculated values were then compared to the measured values from the non-linear response tests.

Figure 49 shows this comparison for $\omega_- = 0$ and $F_n = 0.132$ with the model restrained in heave and pitch.

Figure 50 illustrates the analogous comparison for the case in which the model is free to heave and pitch.

Note that in the region near the resonance the measured response is in both cases lower than that predicted by equation (8). This indicates that there exists significant non-linear effects which are associated with the response, possibly influencing the motion through non-linear damping.

Conclusions

The following conclusions can be drawn from Figures 10 through 50:

1. The non-linear excitation is dependent upon both ship speed and wavelength. See Figure 23.

2. The non-linear excitation is only weakly dependent upon ship speed. For small changes in Froude number the speed dependence can be neglected. See Figure 23.

3. Both the non-linear excitation and non-linear response show only a slight dependence upon the encounter frequency difference parameter ω_- , at least for $\omega_- < 1.424$ radians/sec model scale. In some region near $\omega_- = 0$ both can be treated as a function only of the frequency sum parameter ω_+ . Compare excitation plots in Figures 10 and 12, and compare response plots in Figures 29 and 31.

4. The non-linear effects are "quadratic" in wave amplitude. See Figure 43 and the corresponding discussion.

5. Both the non-linear excitation and non-linear response are influenced by heave and pitch motions. See Figures 26 and 44.

6. Although second order excitation is the dominant source of non-linear effects, it appears that response dependent non-linearities are also significant. See Figures 49 and 50.

7. The linear excitation data agrees well with that obtained by Troesch (1980).

8. The linear excitation is independent of speed in the range of wave-lengths tested. See Figure 46.

9. The linear transfer function is independent of wave amplitude. See Figure 47.

10. The linear excitation is not greatly influenced by heave and pitch motions. See Figure 48.

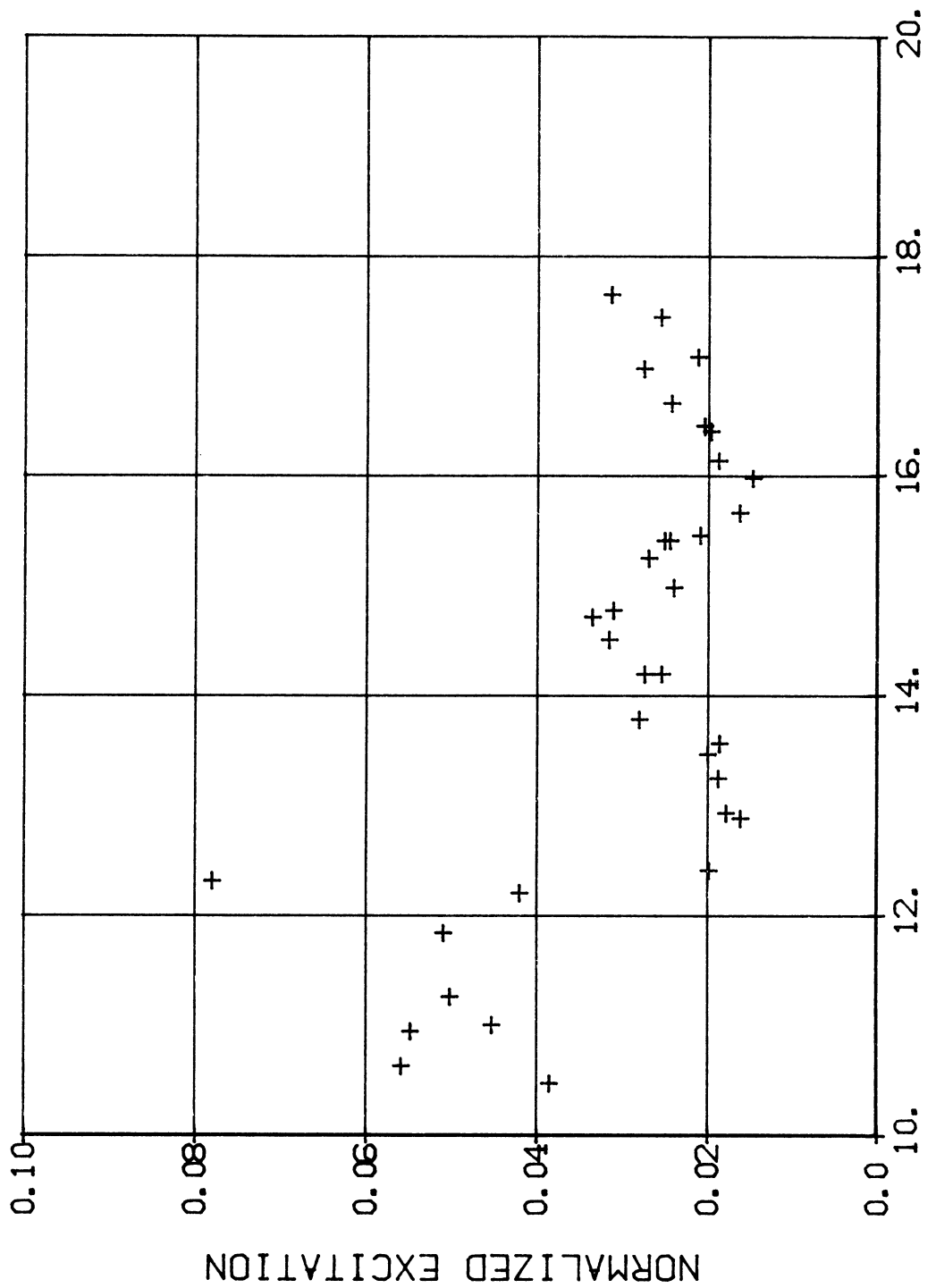

FIGURE 10: NORMALIZED NON-LINEAR EXCITATION VS. ENCOUNTER FREQUENCY SUM, ω_+ (MODEL SCALE).

$\omega_- = 0$. $F_N = 0.132$. MODEL RESTRAINED.

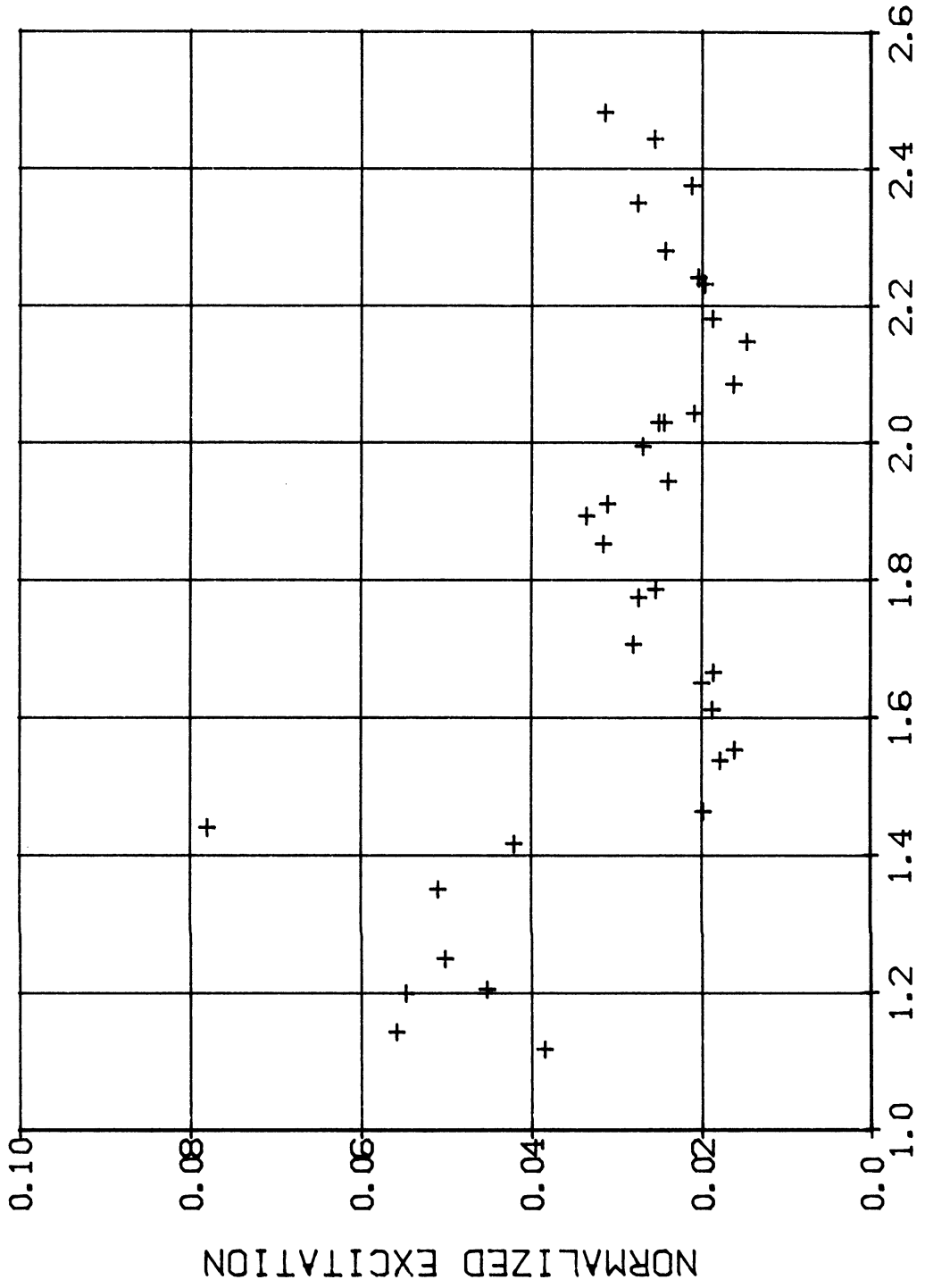

FIGURE 11: NORMALIZED NON-LINEAR EXCITATION VS. SHIP LENGTH/WAVELENGTH. $\omega_- = 0$. $F_N = 0.132$. MODEL RESTRAINED.

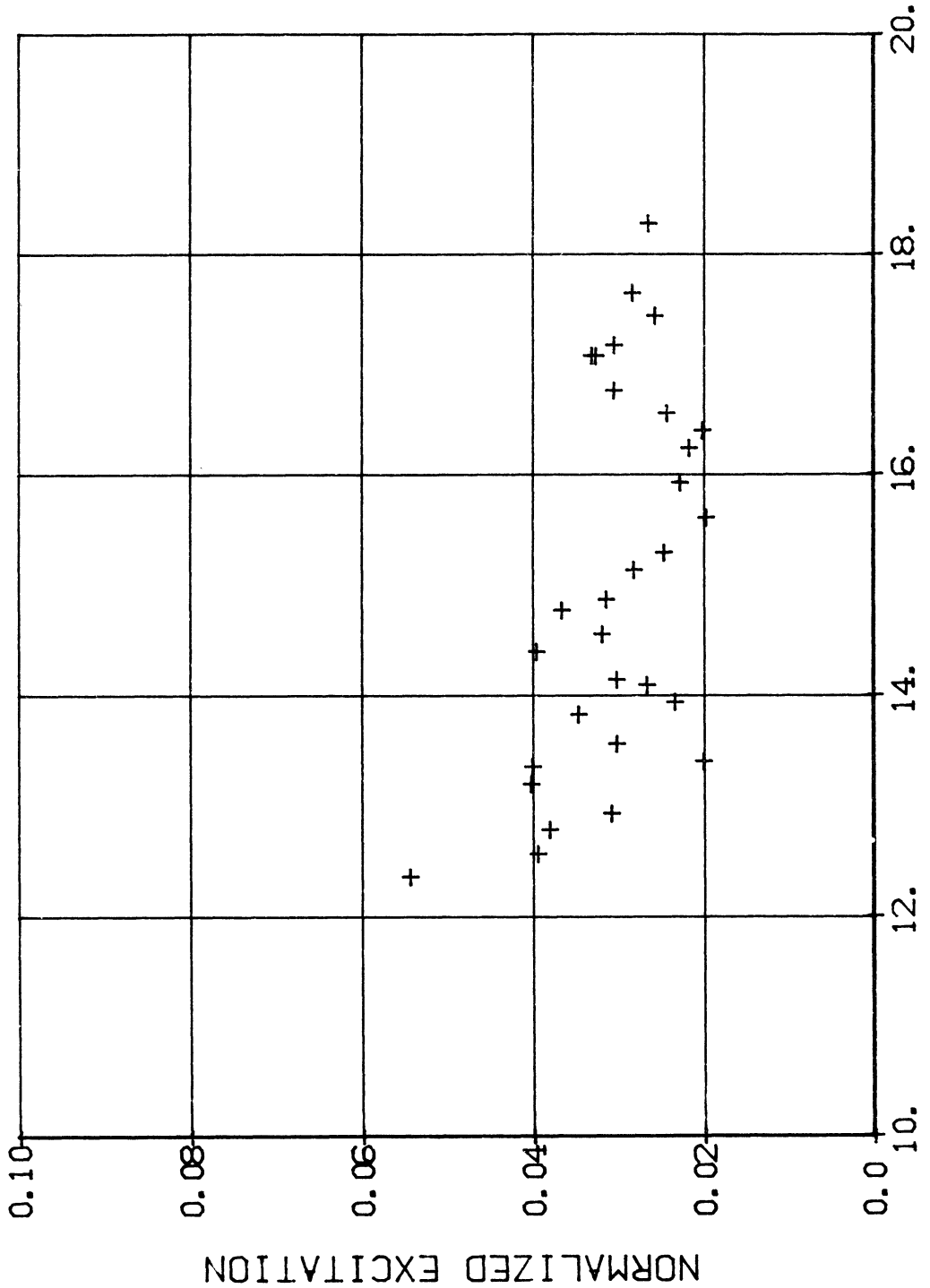

FIGURE 12: NORMALIZED NON-LINEAR EXCITATION VS. ENCOUNTER FREQUENCY SUM, ω_+ (MODEL SCALE).

$\omega_- = 1.424$ RAD/SEC. $F_N = 0.132$. MODEL RESTRAINED.

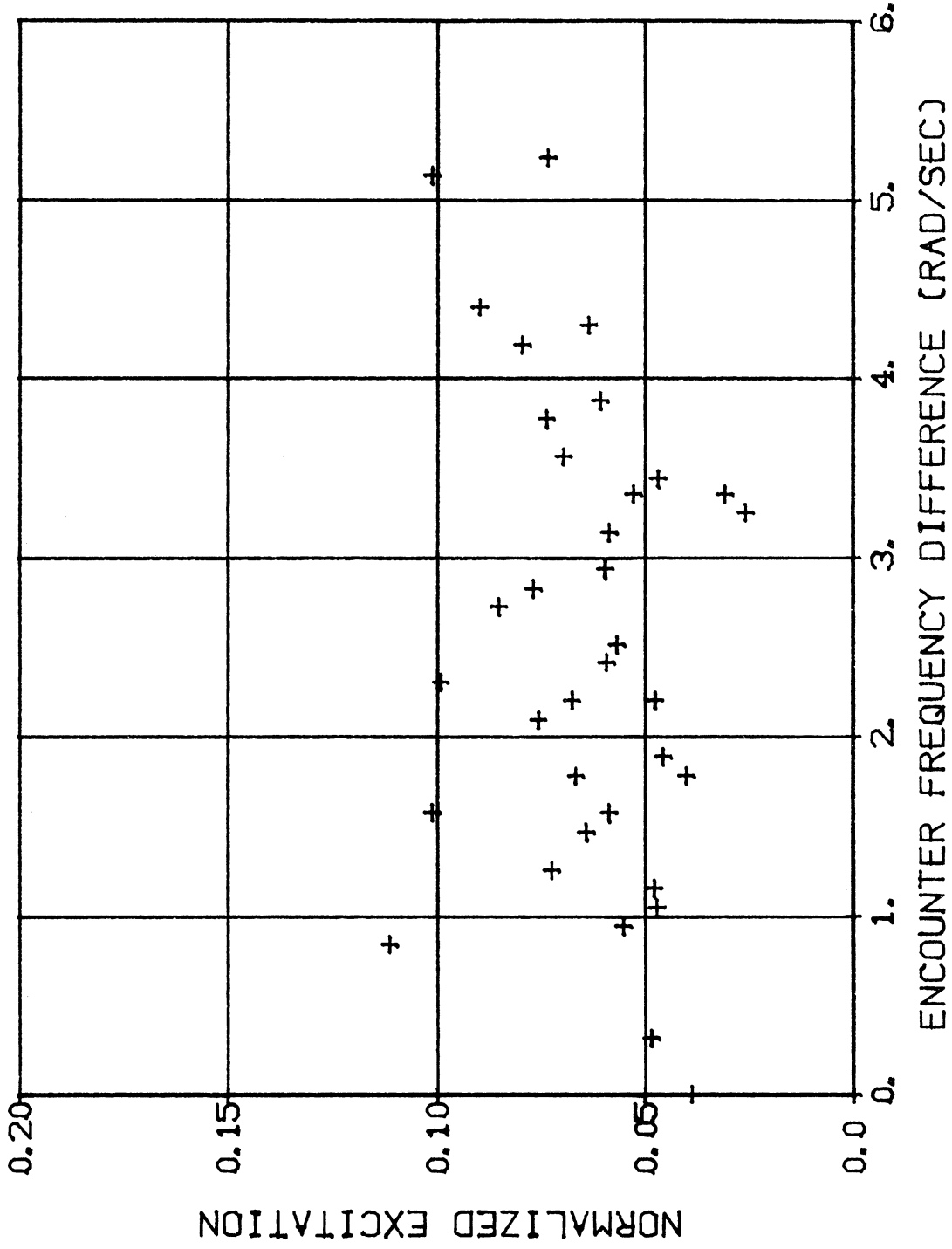

FIGURE 13: NORMALIZED NON-LINEAR EXCITATION VS. ENCOUNTER FREQUENCY DIFFERENCE, ω_- (MODEL SCALE). $\omega_+ = 13.949$ RAD/SEC. $F_N = 0.132$. MODEL RESTRAINED.

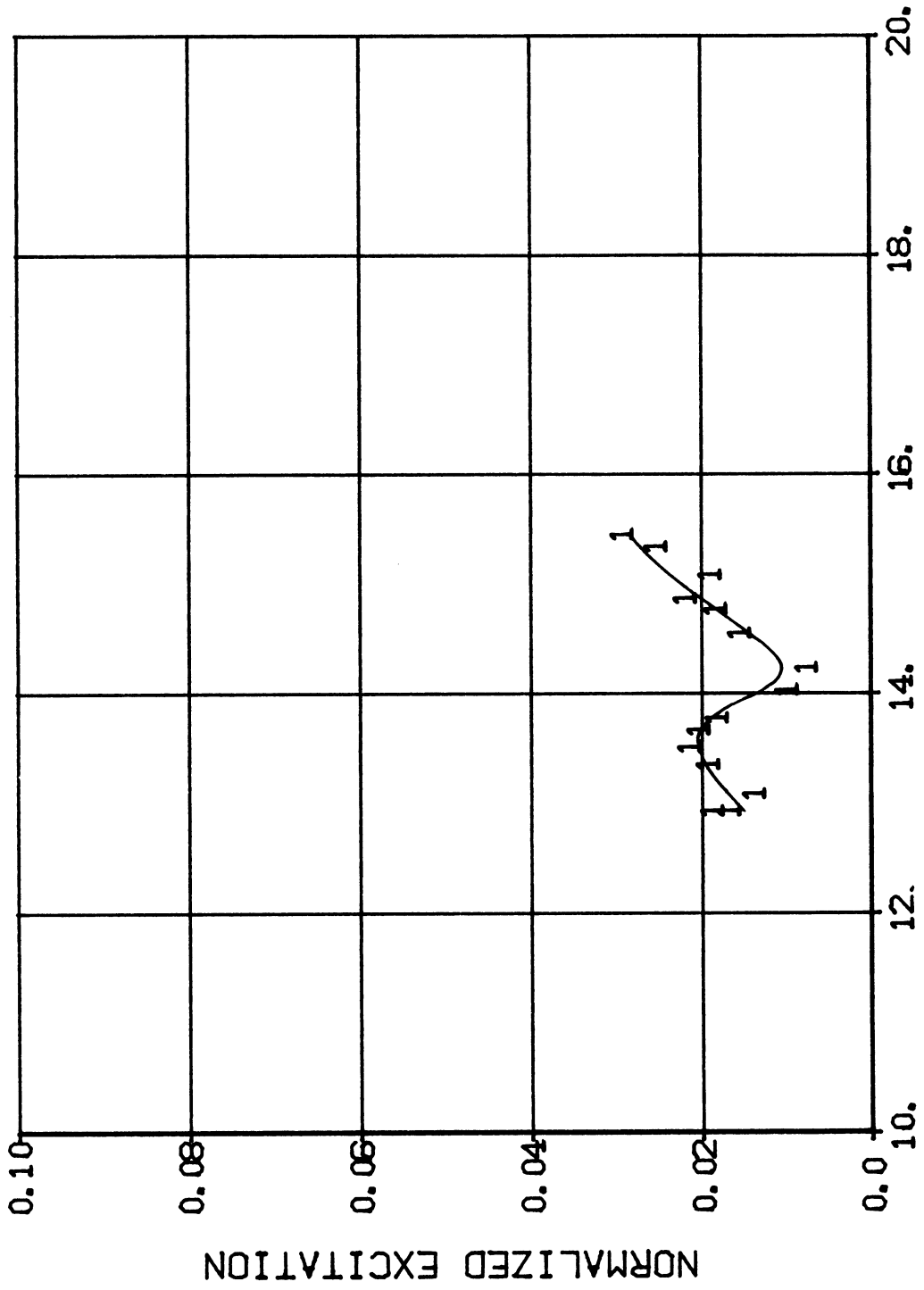

FIGURE 14: SPEED DEPENDENCE TEST, NORMALIZED NON-LINEAR EXCITATION VS. ENCOUNTER FREQUENCY SUM, $\omega+$ (MODEL SCALE).

$\omega-$ = 0. F_N = 0.086. MODEL RESTRAINED.

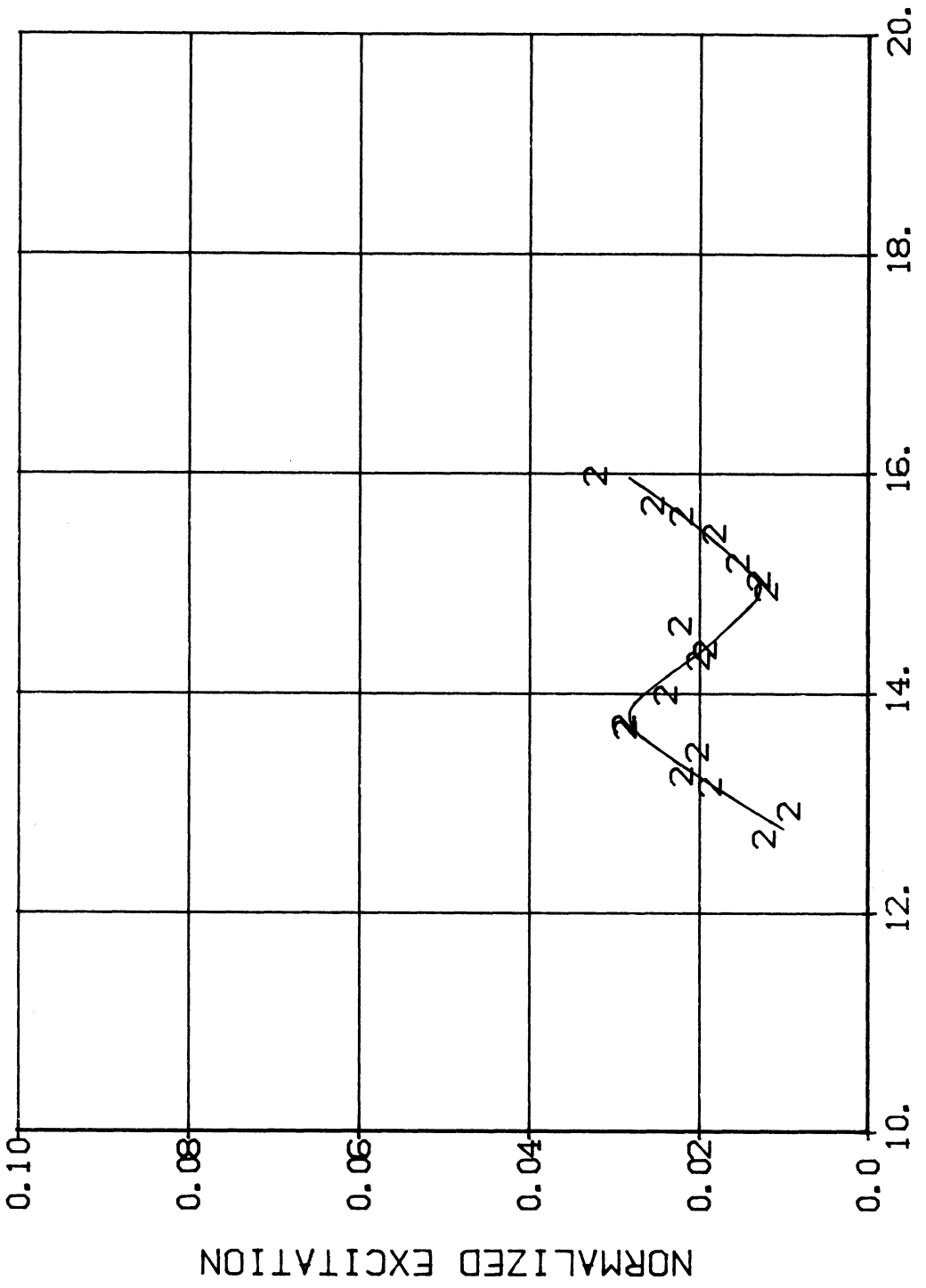

FIGURE 15: SPEED DEPENDENCE TEST, NORMALIZED NON-LINEAR EXCITATION VS. ENCOUNTER FREQUENCY SUM, ω_+ (MODEL SCALE).

$\omega_- = 0.$ $F_N = 0.109.$ MODEL RESTRAINED.

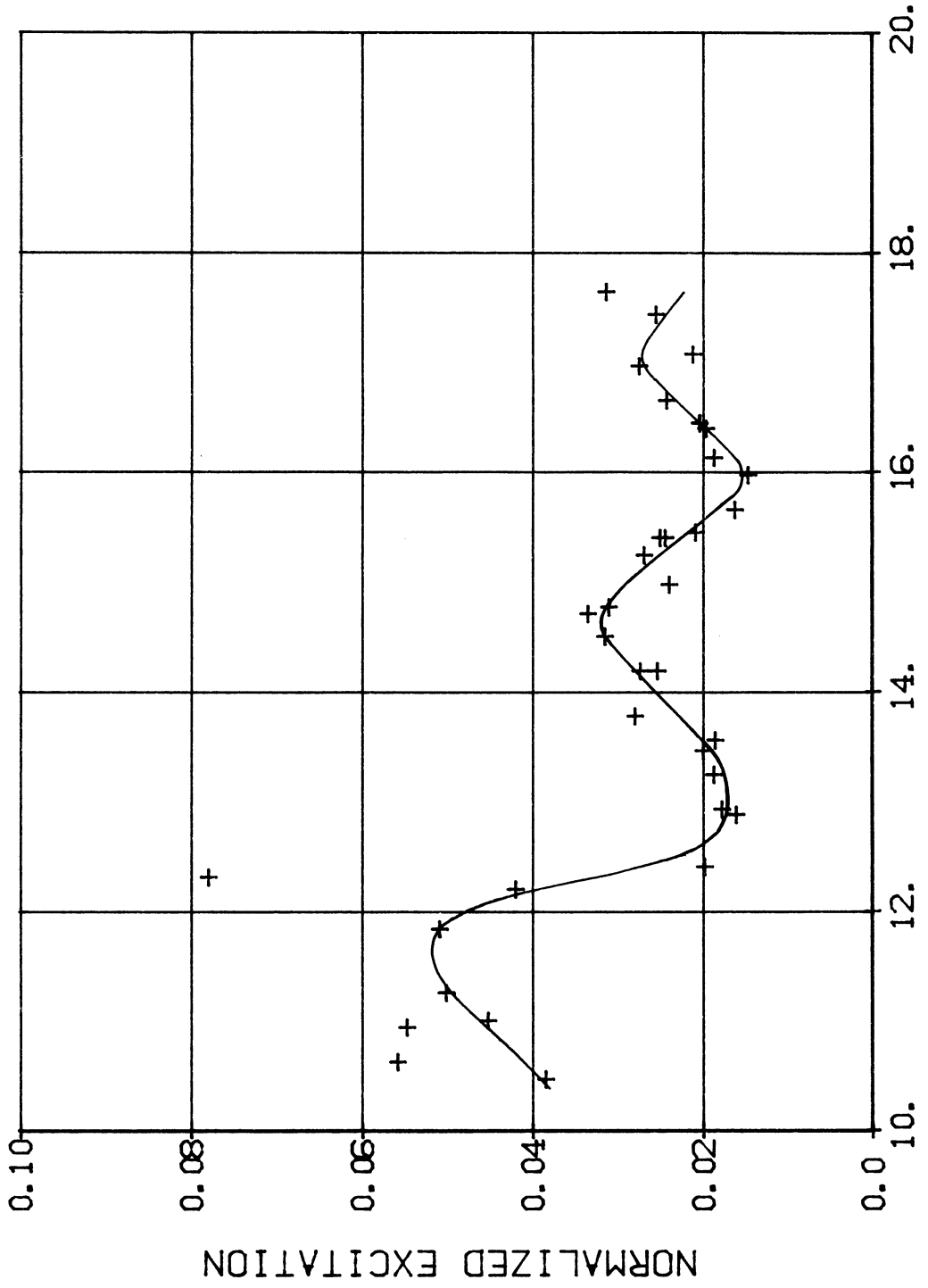

FIGURE 16: SPEED DEPENDENCE TEST, NORMALIZED NON-LINEAR EXCITATION VS. ENCOUNTER FREQUENCY SUM, ω_+ (MODEL SCALE).
$\omega_- = 0.$ $F_N = 0.132.$ MODEL RESTRAINED.

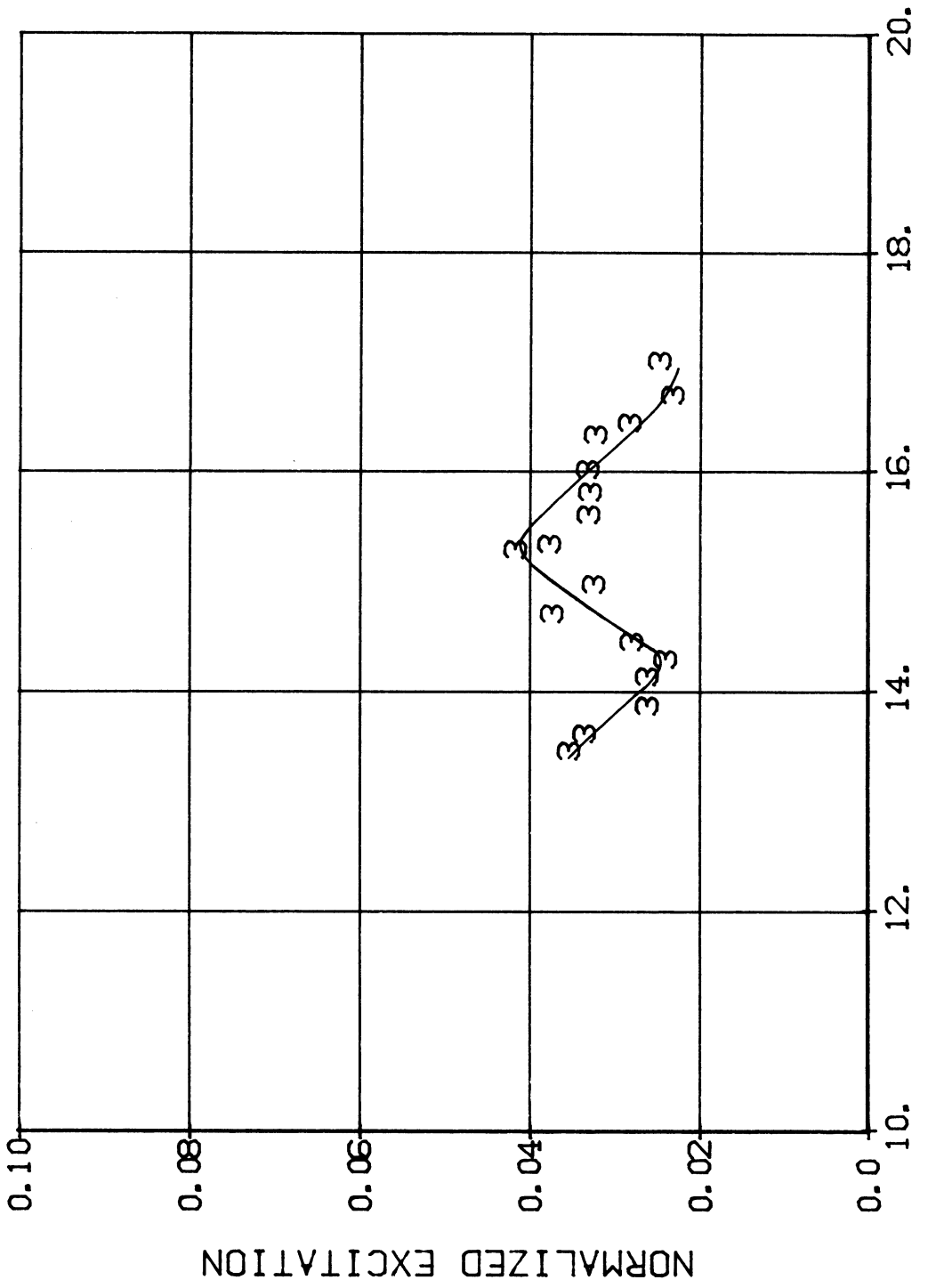

FIGURE 17: SPEED DEPENDENCE TEST, NORMALIZED NON-LINEAR EXCITATION VS. ENCOUNTER FREQUENCY SUM, ω_+ (MODEL SCALE). $\omega_- = 0.$ $F_N = 0.155.$ MODEL RESTRAINED.

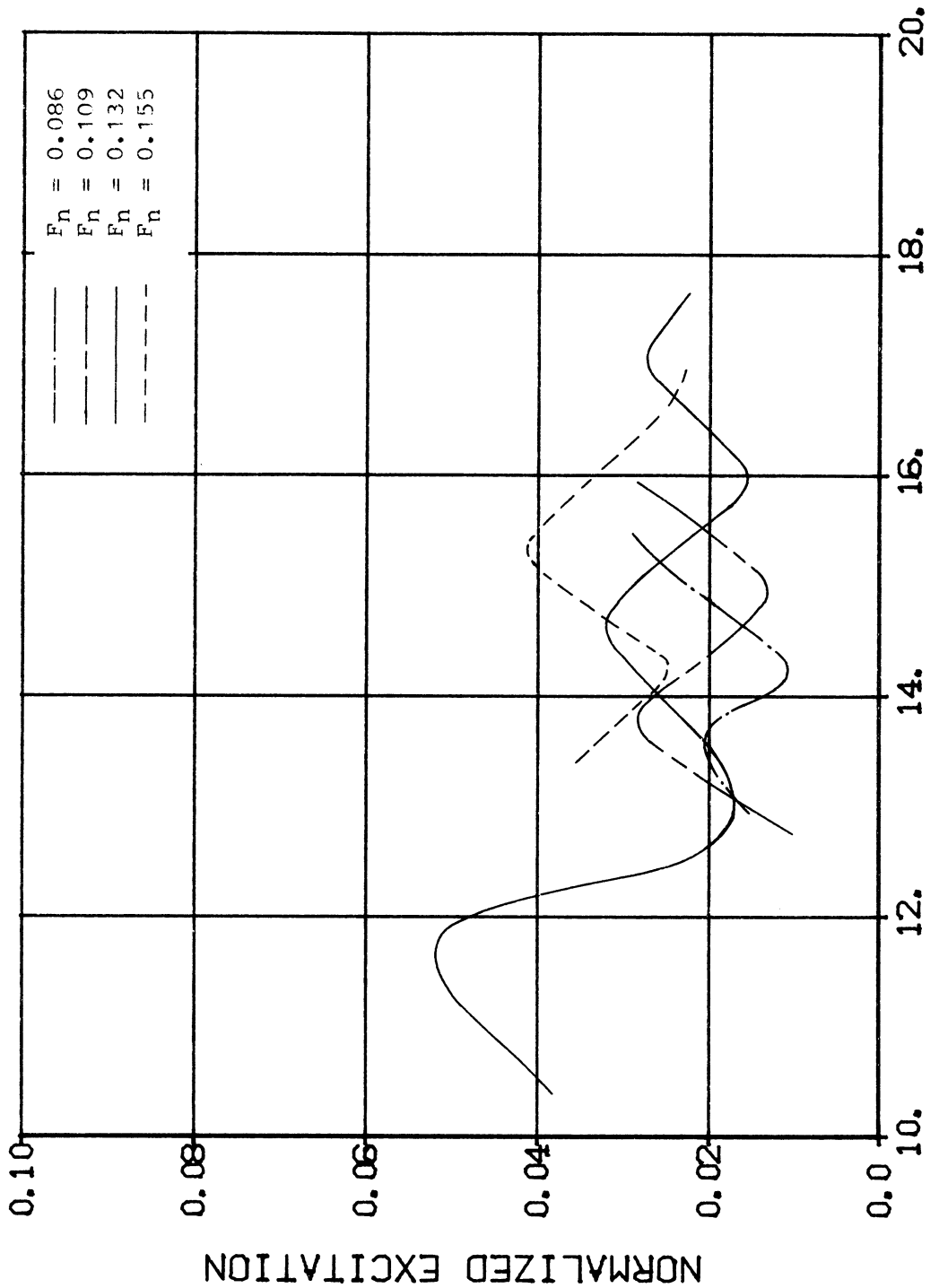

FIGURE 18: SPEED DEPENDENCE TEST, NORMALIZED NON-LINEAR EXCITATION VS. ENCOUNTER FREQUENCY SUM, $\omega+$ (MODEL SCALE). $\omega-$ = 0. F_N = 0.086, 0.109, 0.132, 0.155. MODEL RESTRAINED.

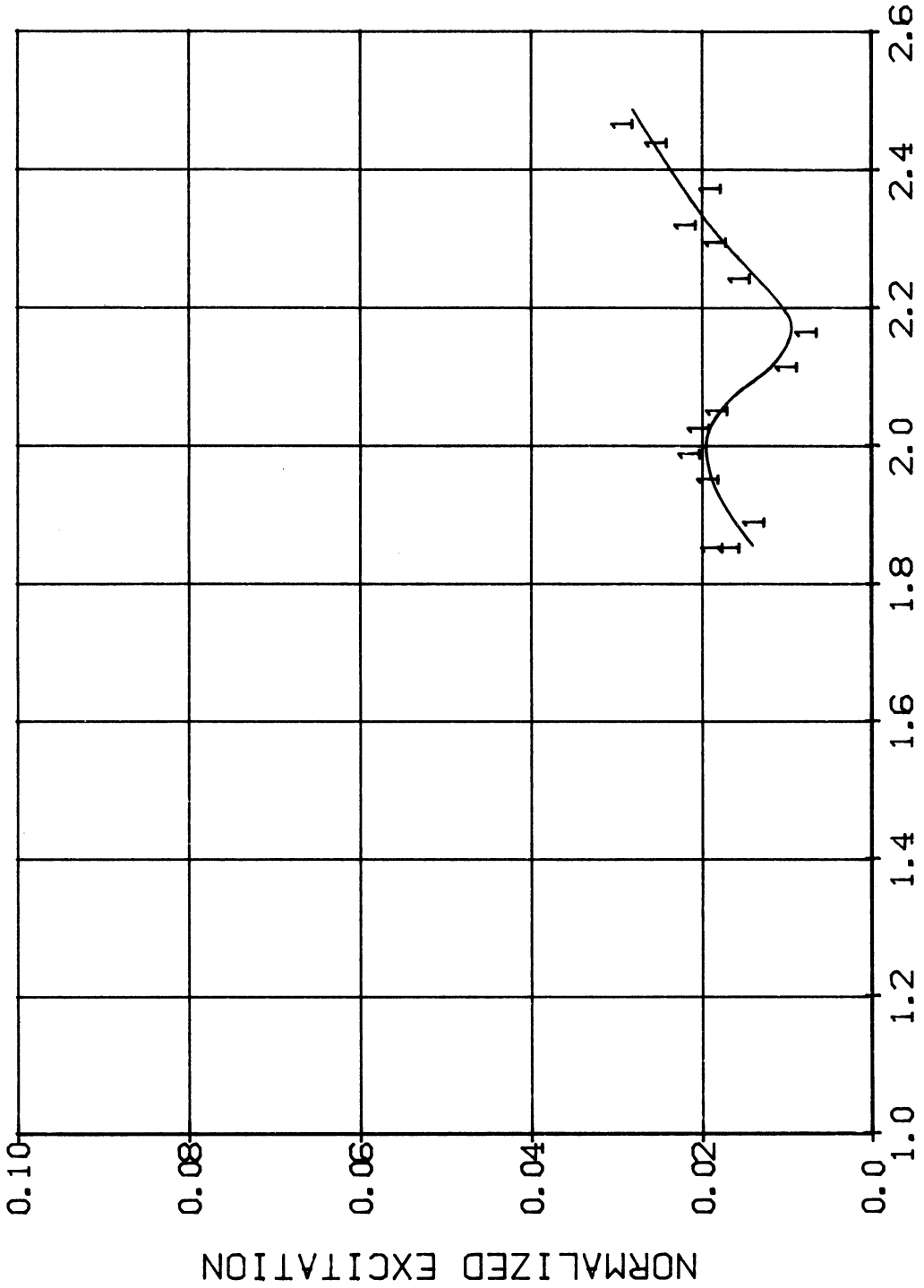

FIGURE 19: SPEED DEPENDENCE TEST, NORMALIZED NON-LINEAR EXCITATION VS. SHIP LENGTH/WAVELENGTH. $\omega_- = 0.$ $F_N = 0.086.$ MODEL RESTRAINED.

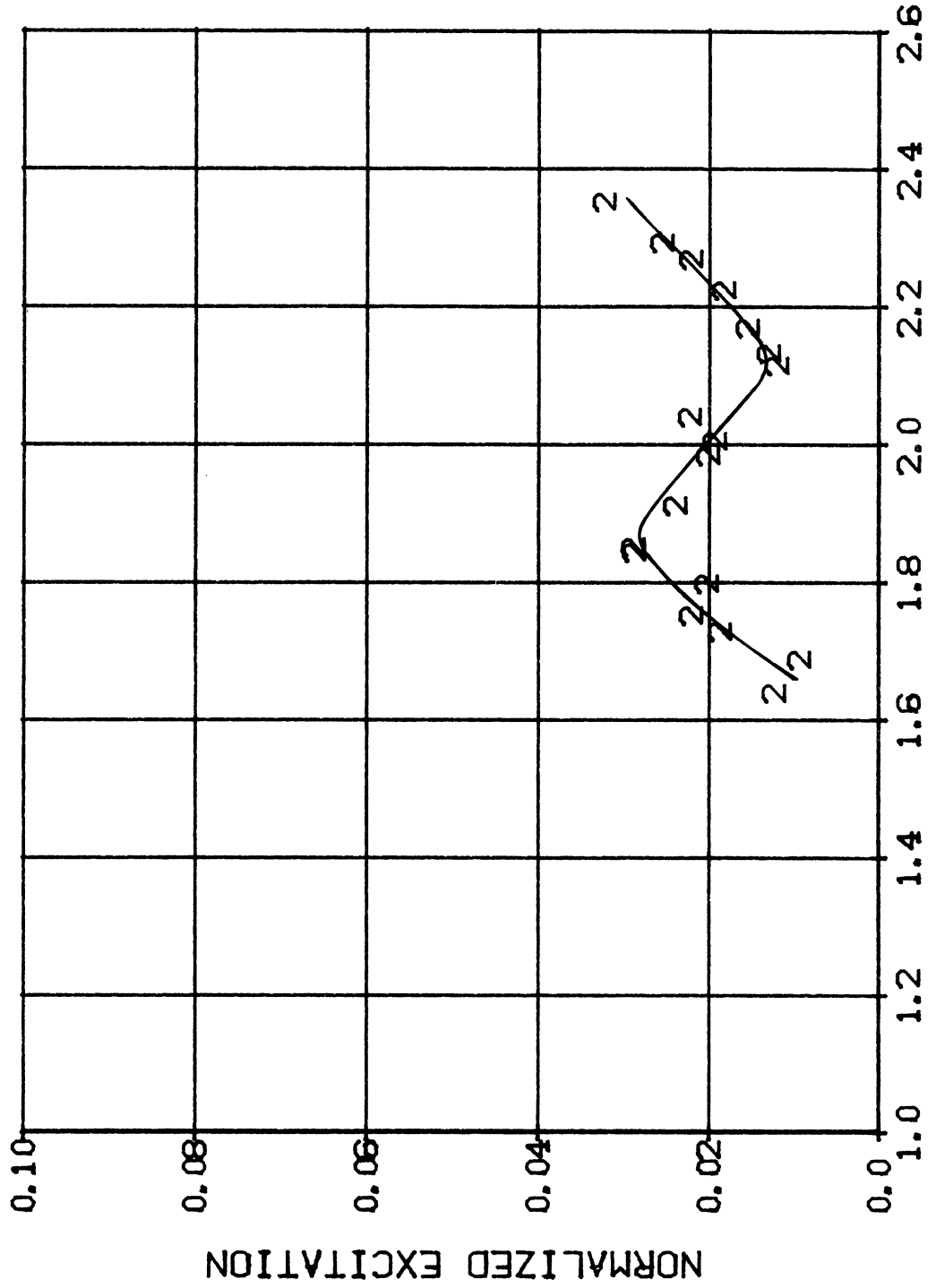

FIGURE 20: SPEED DEPENDENCE TEST, NORMALIZED NON-LINEAR EXCITATION VS. SHIP LENGTH/WAVELENGTH. $\omega_- = 0.$ $F_N = 0.109.$ MODEL RESTRAINED.

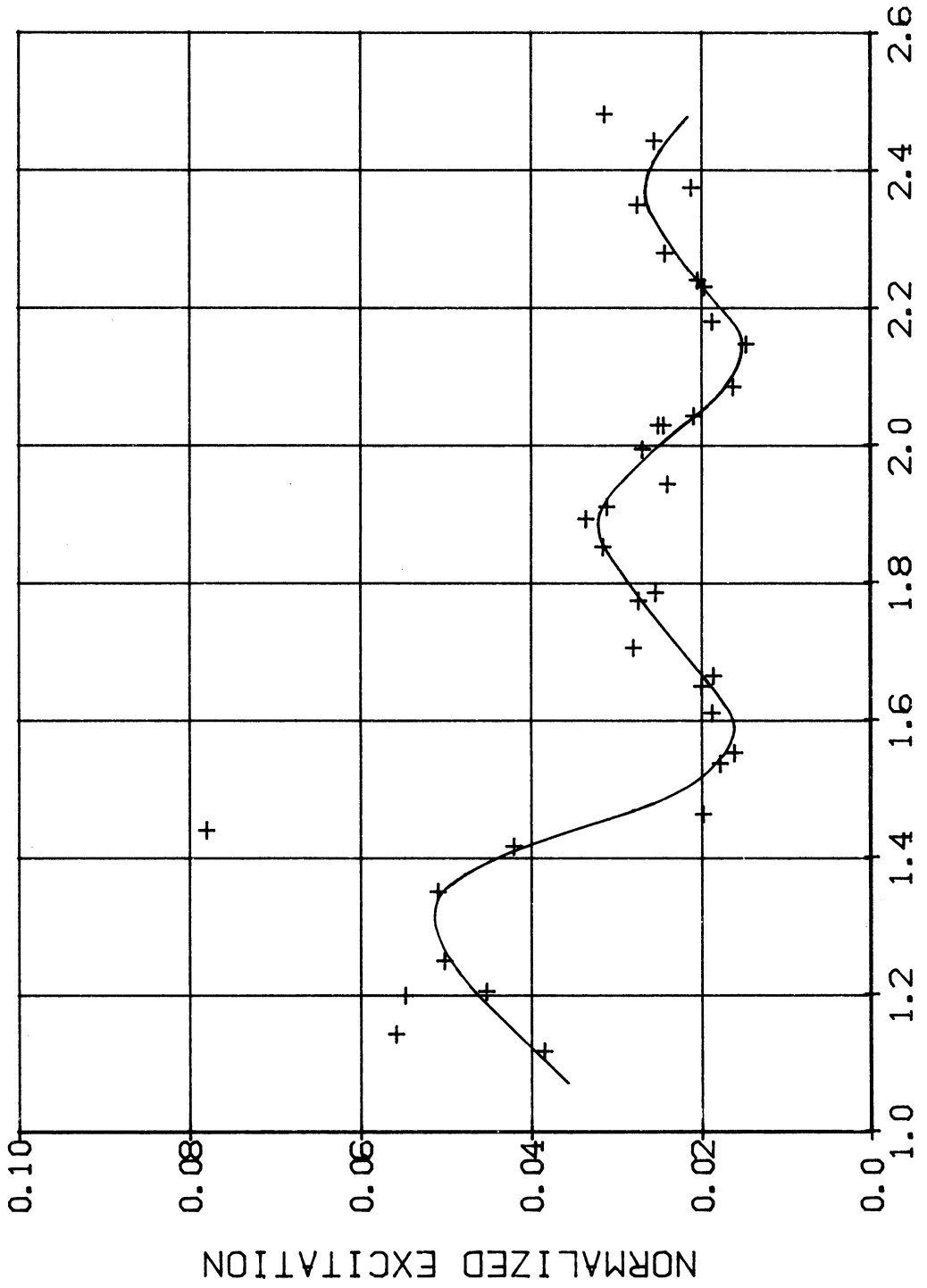

FIGURE 21: SPEED DEPENDENCE TEST, NORMALIZED NON-LINEAR EXCITATION VS. SHIP LENGTH/WAVELENGTH. $\omega_- = 0.$ $F_N = 0.132.$ MODEL RESTRAINED.

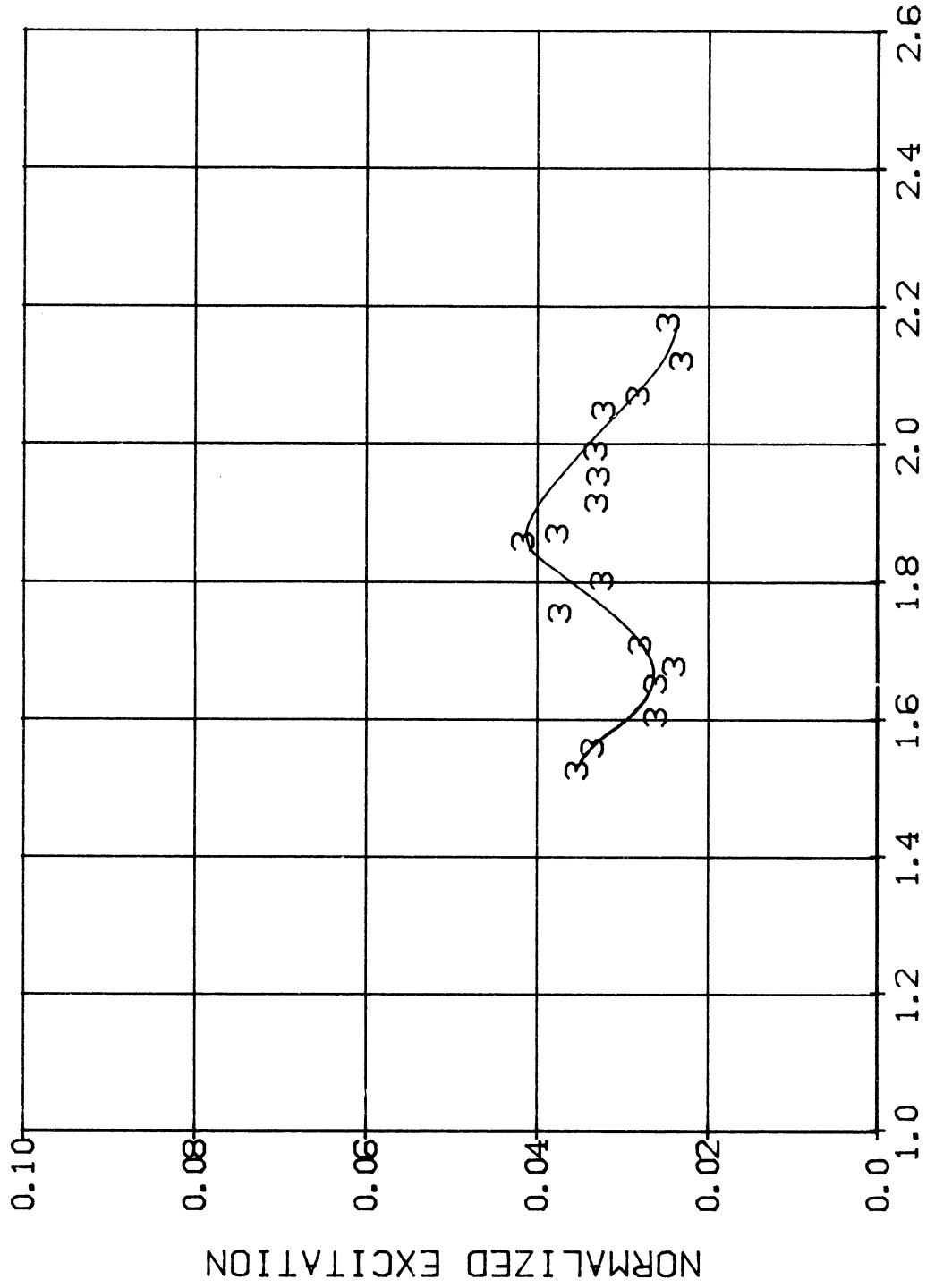

FIGURE 22: SPEED DEPENDENCE TEST, NORMALIZED NON-LINEAR EXCITATION VS. SHIP LENGTH/WAVELENGTH. $\omega_- = 0.$ $F_N = 0.155.$ MODEL RESTRAINED.

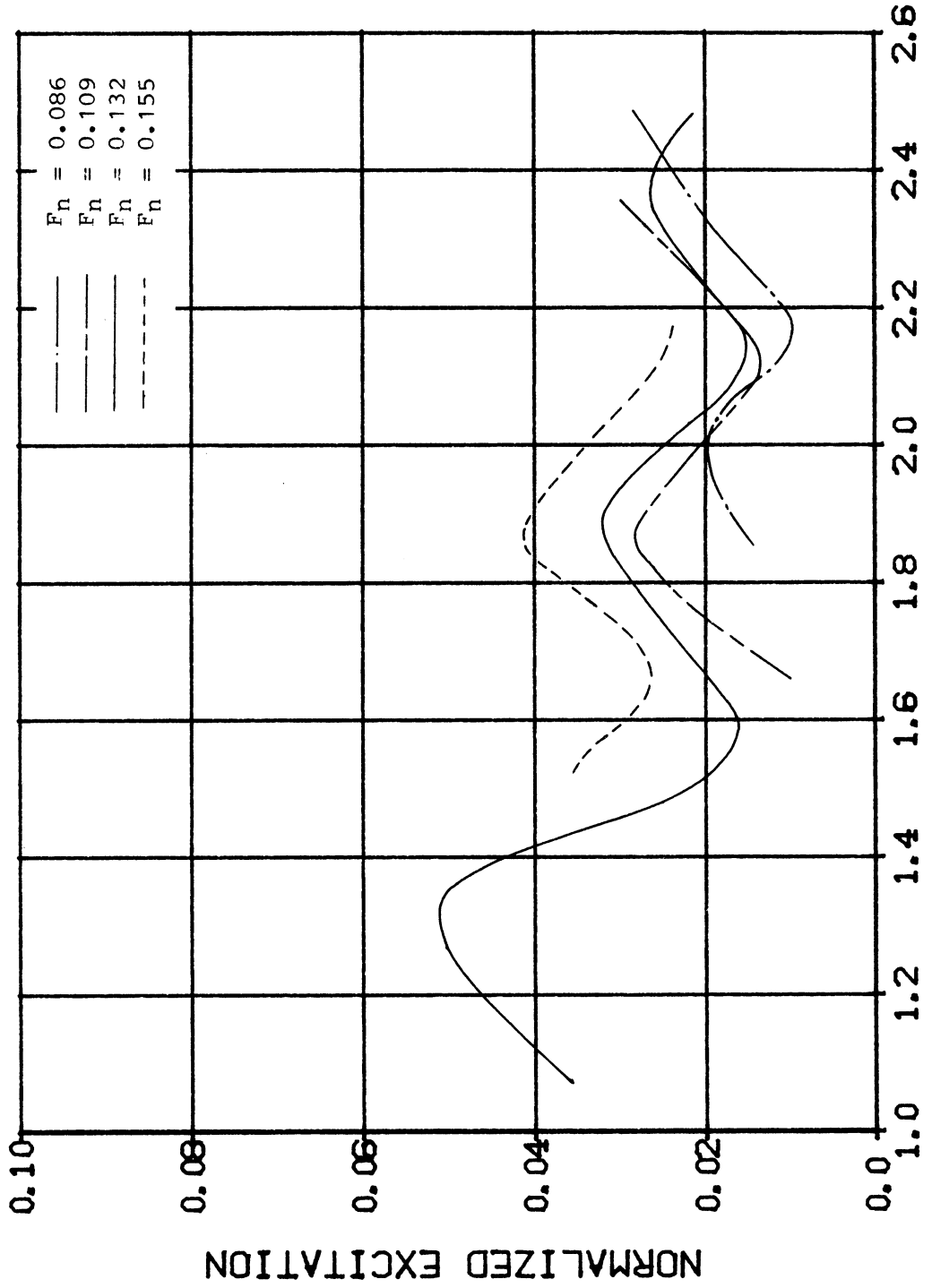

FIGURE 23: SPEED DEPENDENCE TEST, NORMALIZED NON-LINEAR EXCITATION VS. SHIP LENGTH/WAVELENGTH. $\omega_- = 0$. $F_N = 0.086$, 0.109, 0.132, 0.155. MODEL RESTRAINED.

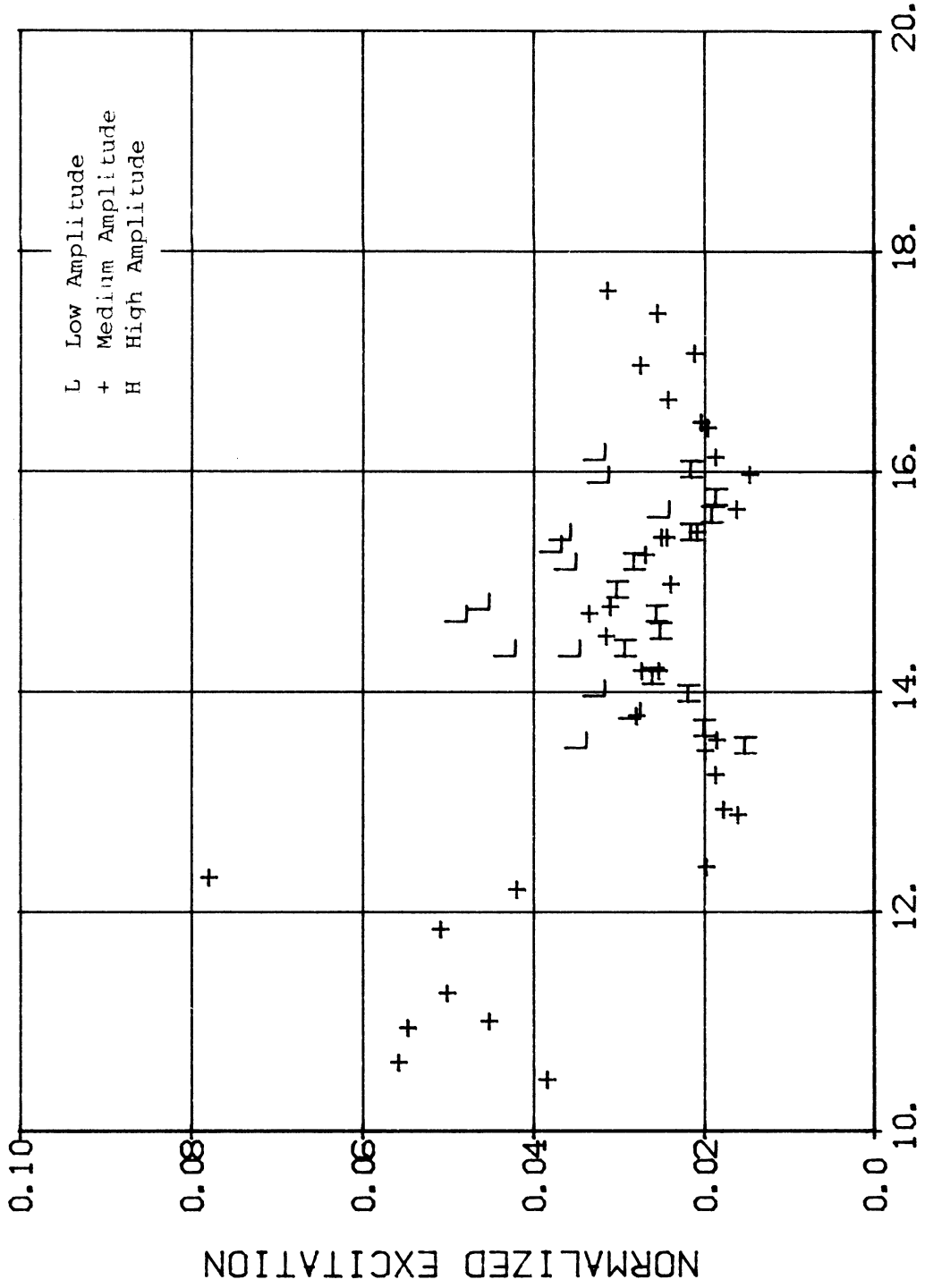

FIGURE 24: AMPLITUDE DEPENDENCE TESTS, NORMALIZED NON-LINEAR EXCITATION VS. ENCOUNTER FREQUENCY SUM, ω_+ (MODEL SCALE).

$\omega_- = 0.$ $F_N = 0.132.$ LOW, MEDIUM, AND HIGH AMPLITUDES.

MODEL RESTRAINED.

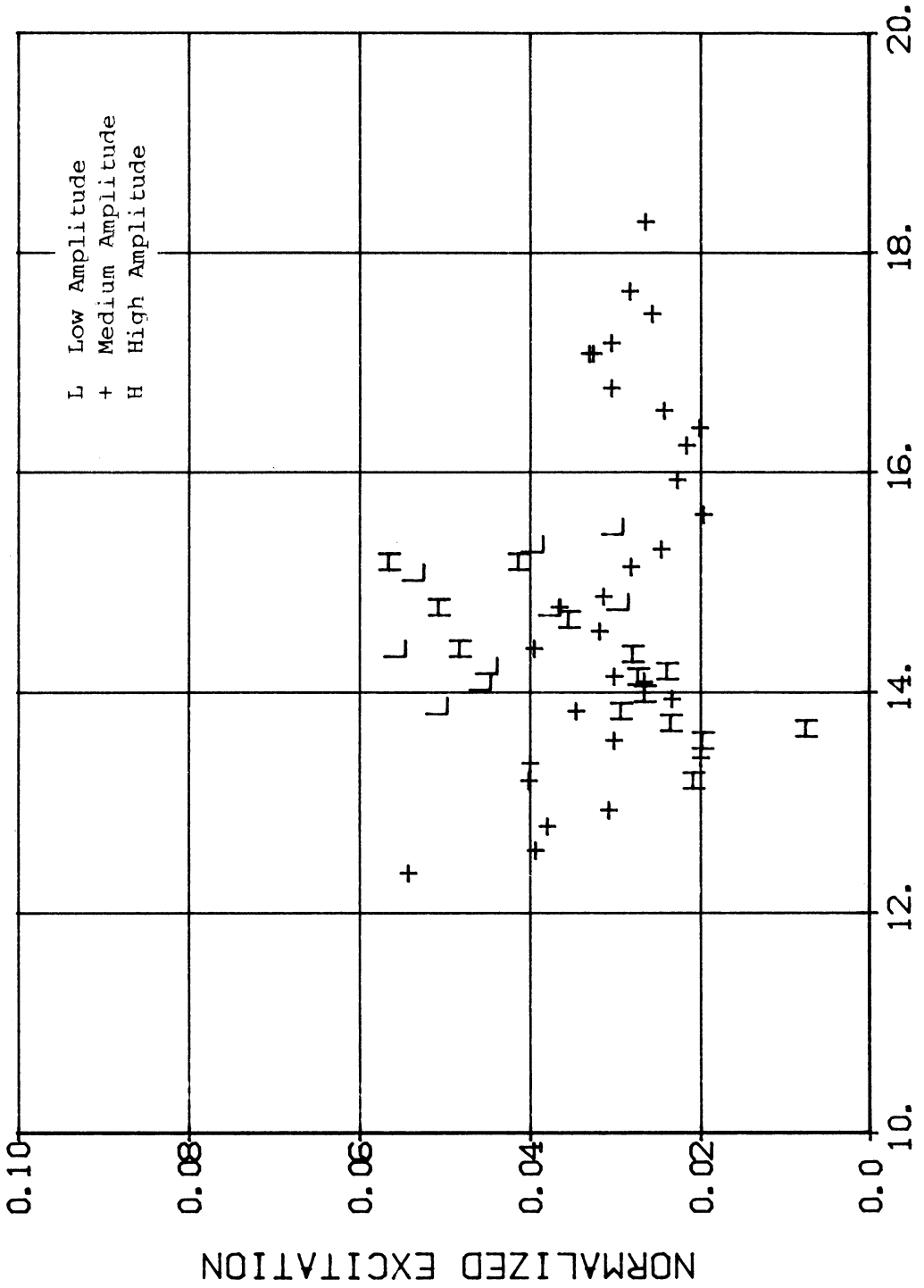

FIGURE 25: AMPLITUDE DEPENDENCE TESTS, NORMALIZED NON-LINEAR EXCITATION VS. ENCOUNTER FREQUENCY SUM, ω_+ (MODEL SCALE). $\omega_- = 1.424$. $F_N = 0.132$. LOW, MEDIUM, AND HIGH AMPLITUDES. MODEL RESTRAINED.

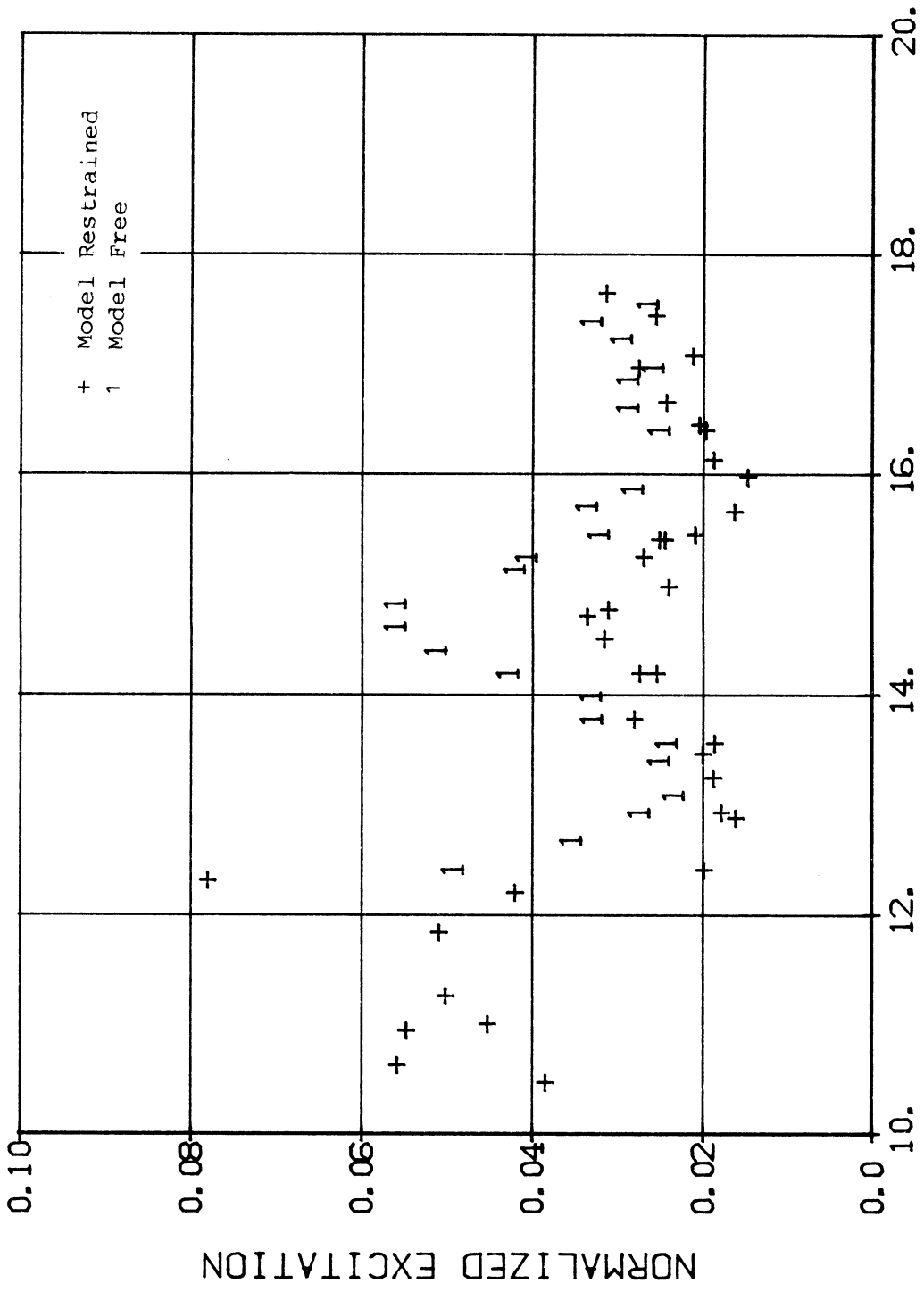

FIGURE 26: NORMALIZED NON-LINEAR EXCITATION VS. ENCOUNTER FREQUENCY SUM, ω_+ (MODEL SCALE). $\omega_- = 0.$ $F_N = 0.132.$ MODEL RESTRAINED AND MODEL FREE TO HEAVE AND PITCH.

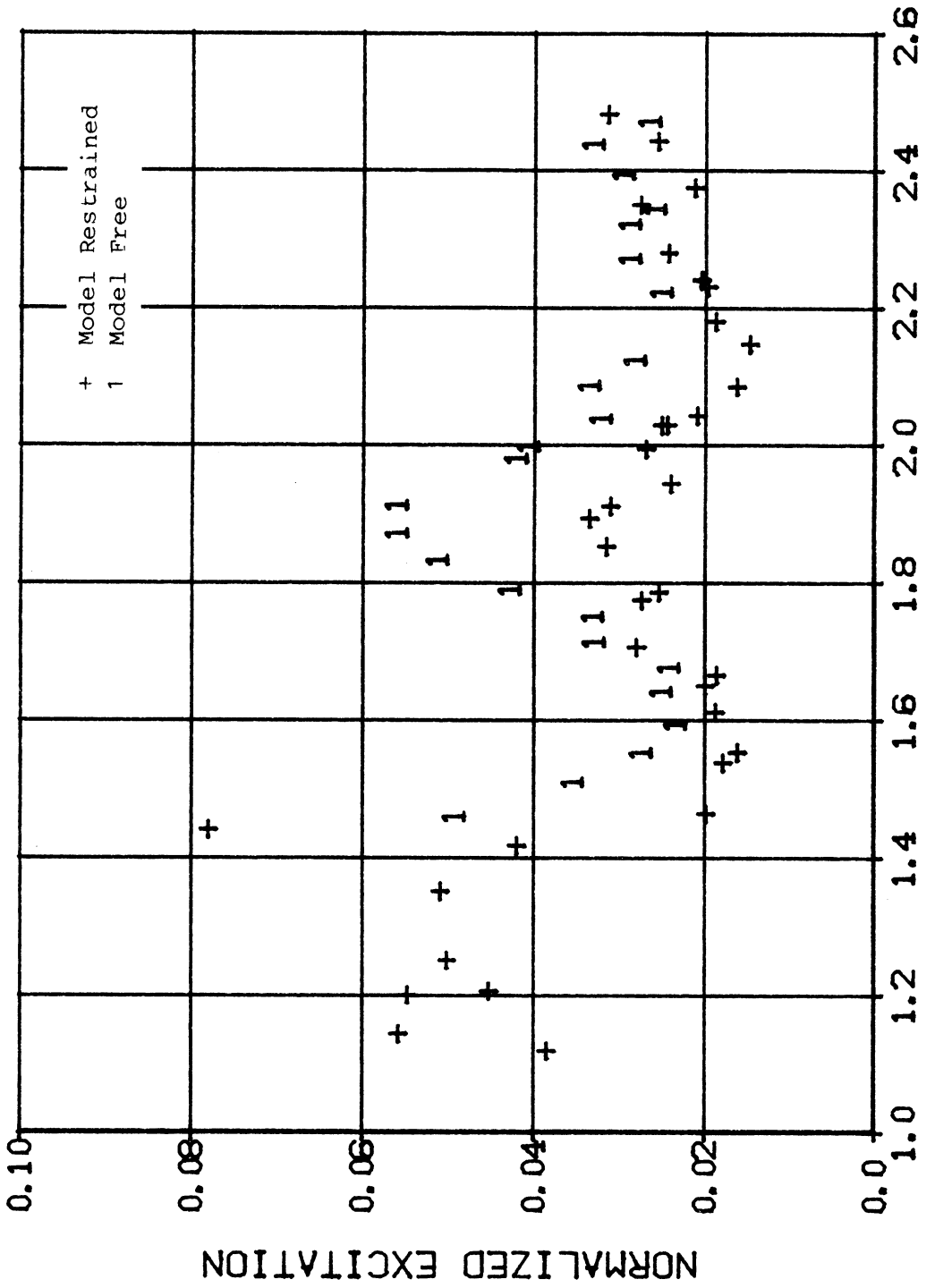

FIGURE 27: NORMALIZED NON-LINEAR EXCITATION VS. SHIP LENGTH/ WAVELENGTH. $\omega_- = 0.$ $F_N = 0.132.$

MODEL RESTRAINED AND MODEL FREE TO HEAVE AND PITCH.

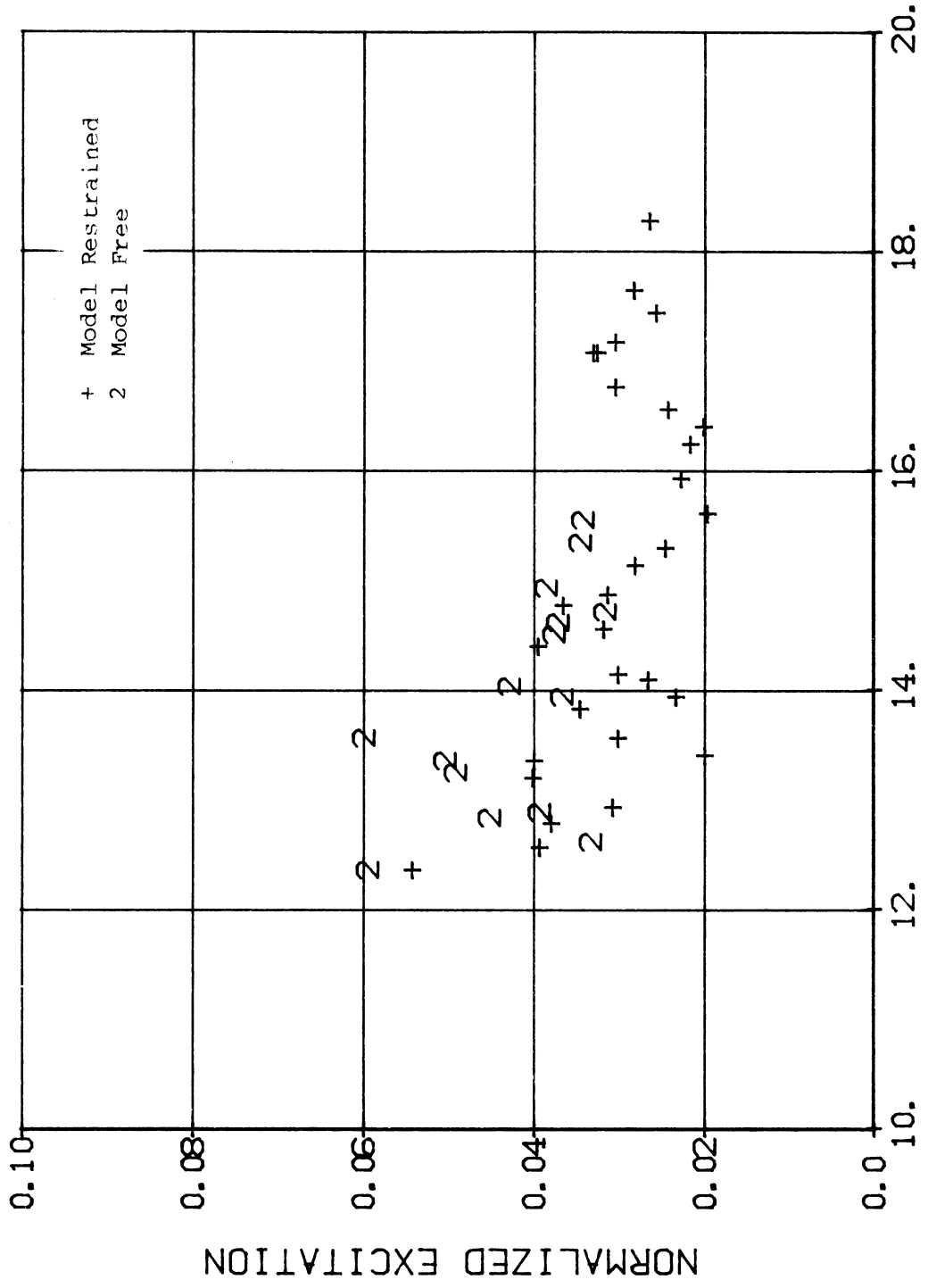

FIGURE 28: NORMALIZED NON-LINEAR EXCITATION VS. ENCOUNTER FREQUENCY SUM, ω_+ (MODEL SCALE). $\omega_- = 1.424$. $F_N = 0.132$. MODEL RESTRAINED AND MODEL FREE TO HEAVE AND PITCH.

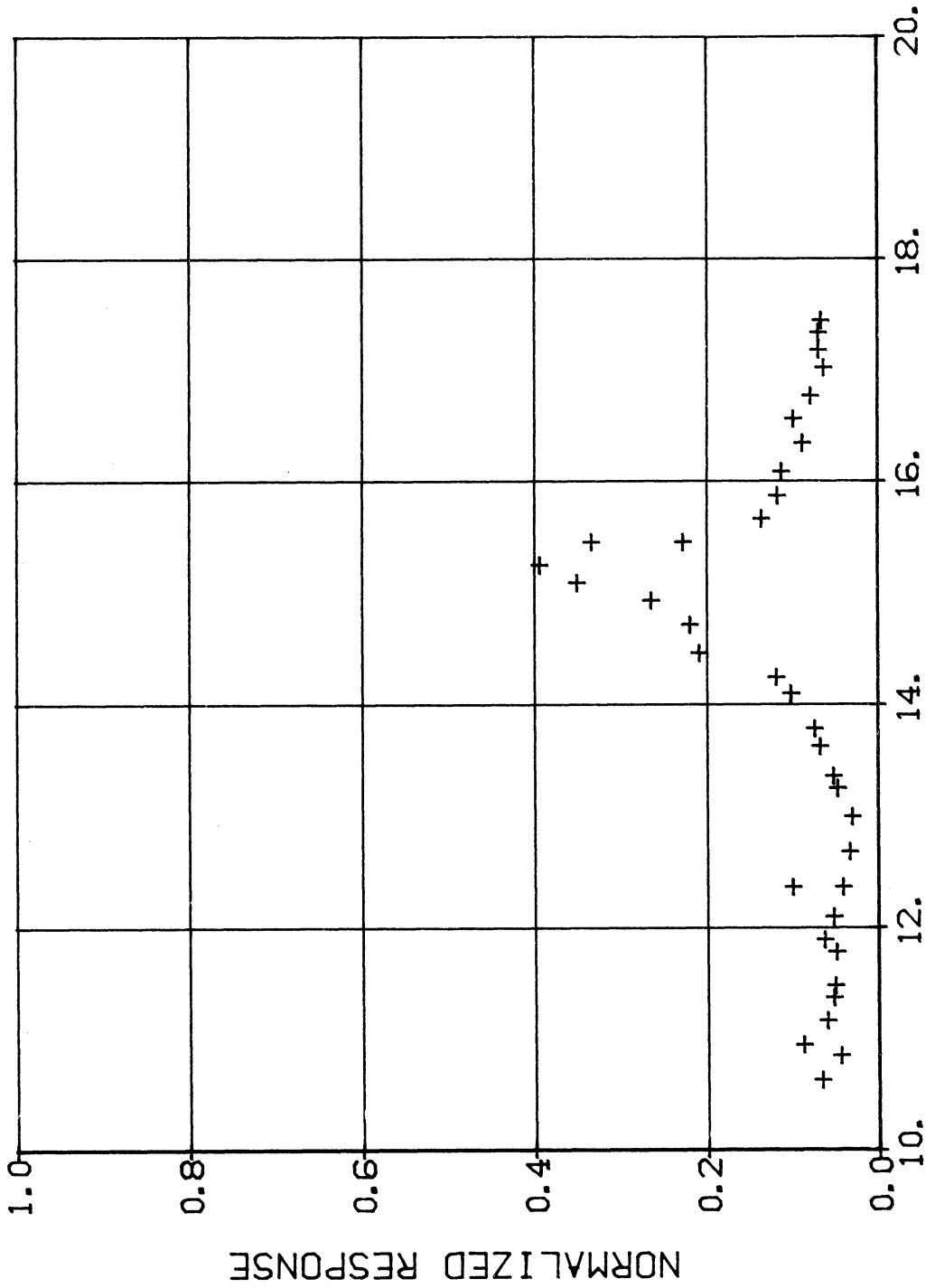

FIGURE 29: NORMALIZED NON-LINEAR RESPONSE VS. ENCOUNTER FREQUENCY SUM, ω_+ (MODEL SCALE). $\omega_- = 0.$ $F_N = 0.132.$ MODEL RESTRAINED.

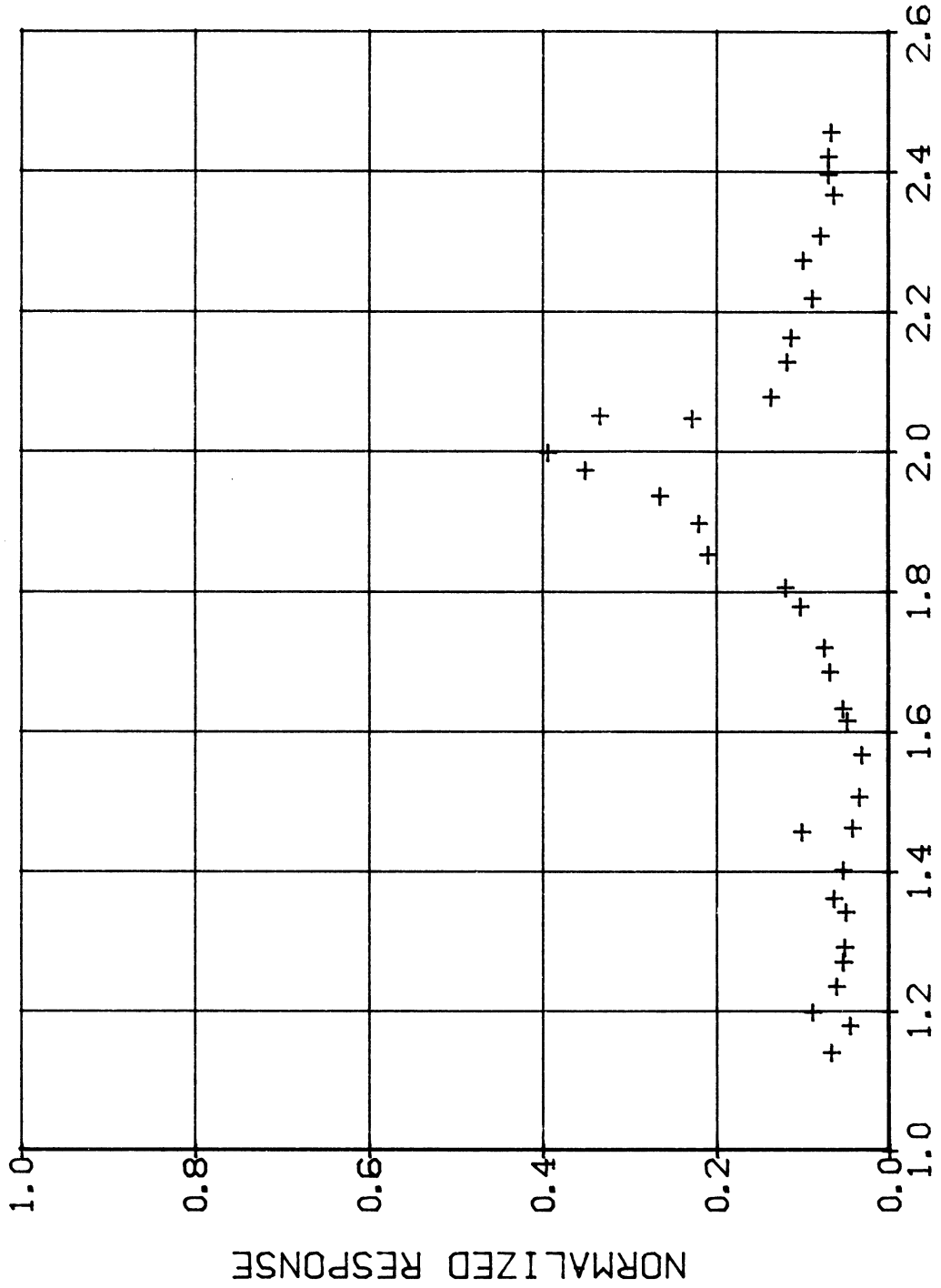

FIGURE 30: NORMALIZED NON-LINEAR RESPONSE VS. SHIP LENGTH/ WAVELENGTH. $\omega_- = 0.$ $F_N = 0.132.$ MODEL RESTRAINED.

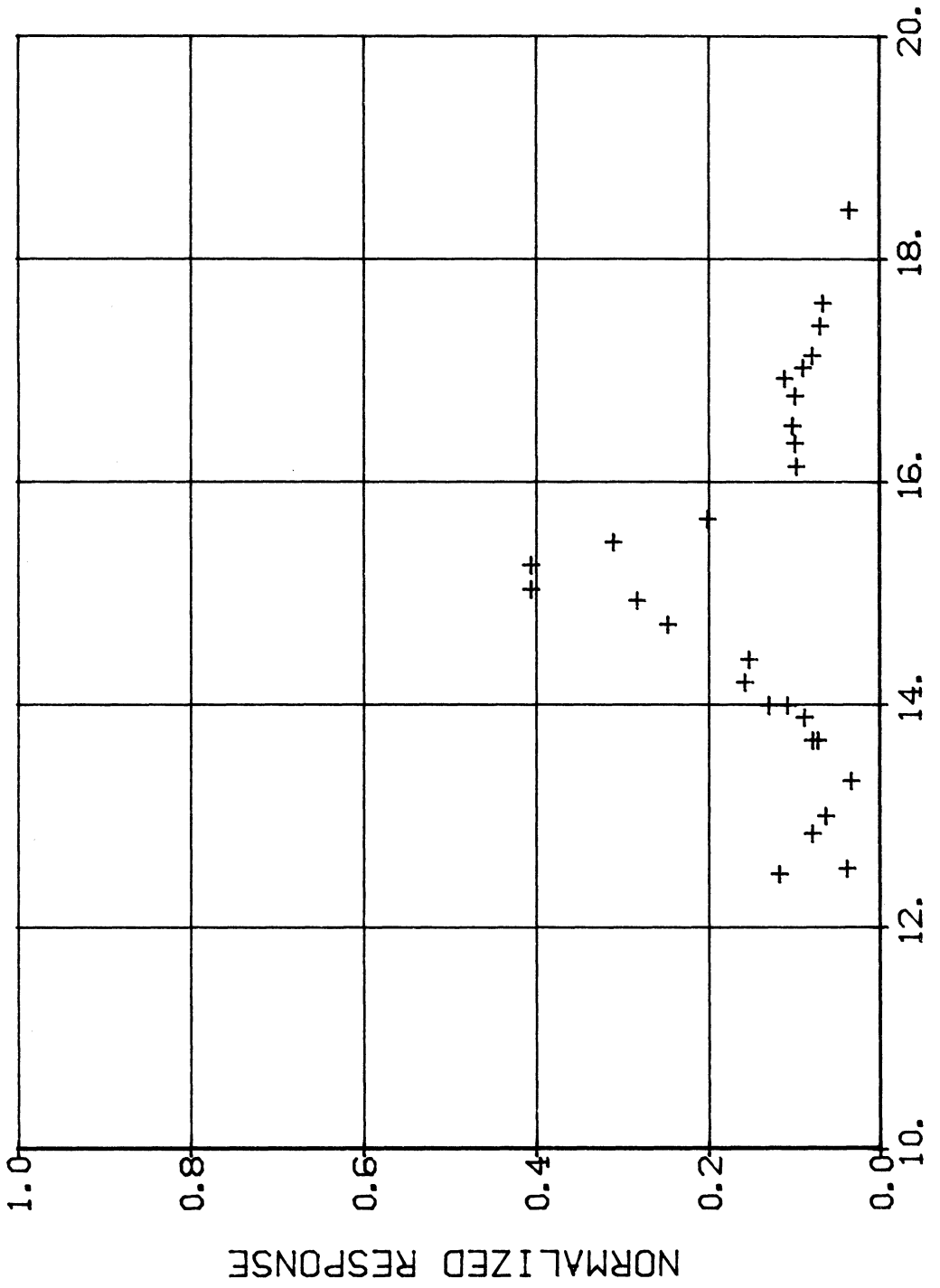

FIGURE 31: NORMALIZED NON-LINEAR RESPONSE VS. ENCOUNTER FREQUENCY SUM, ω_+ (MODEL SCALE). $\omega_- = 1.424$. $F_N = 0.132$.

MODEL RESTRAINED.

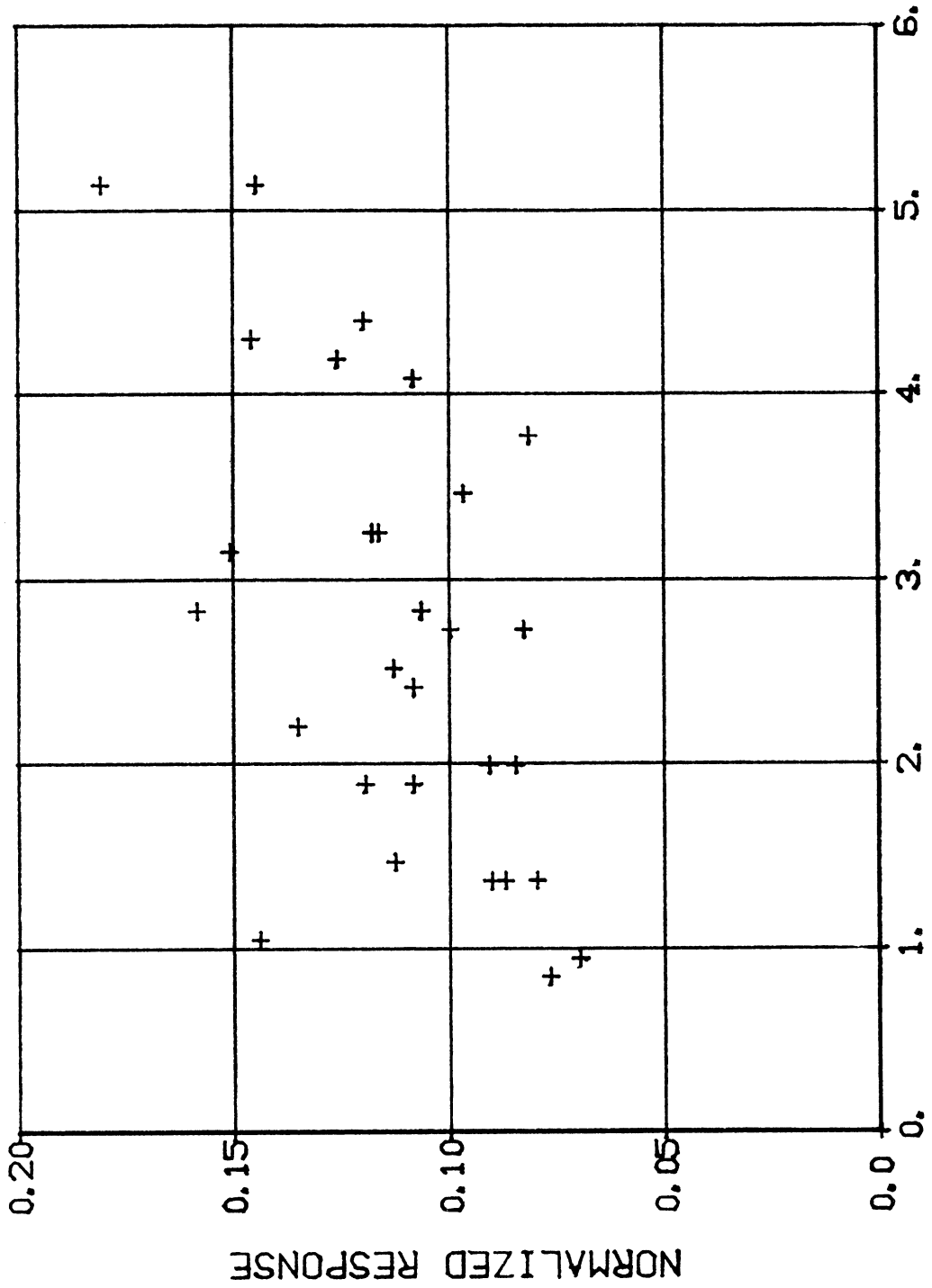

FIGURE 32: NORMALIZED NON-LINEAR RESPONSE VS. ENCOUNTER FREQUENCY DIFFERENCE, ω_- (MODEL SCALE). ω_+ = 13.949 RAD/SEC. F_N = 0.132. MODEL RESTRAINED.

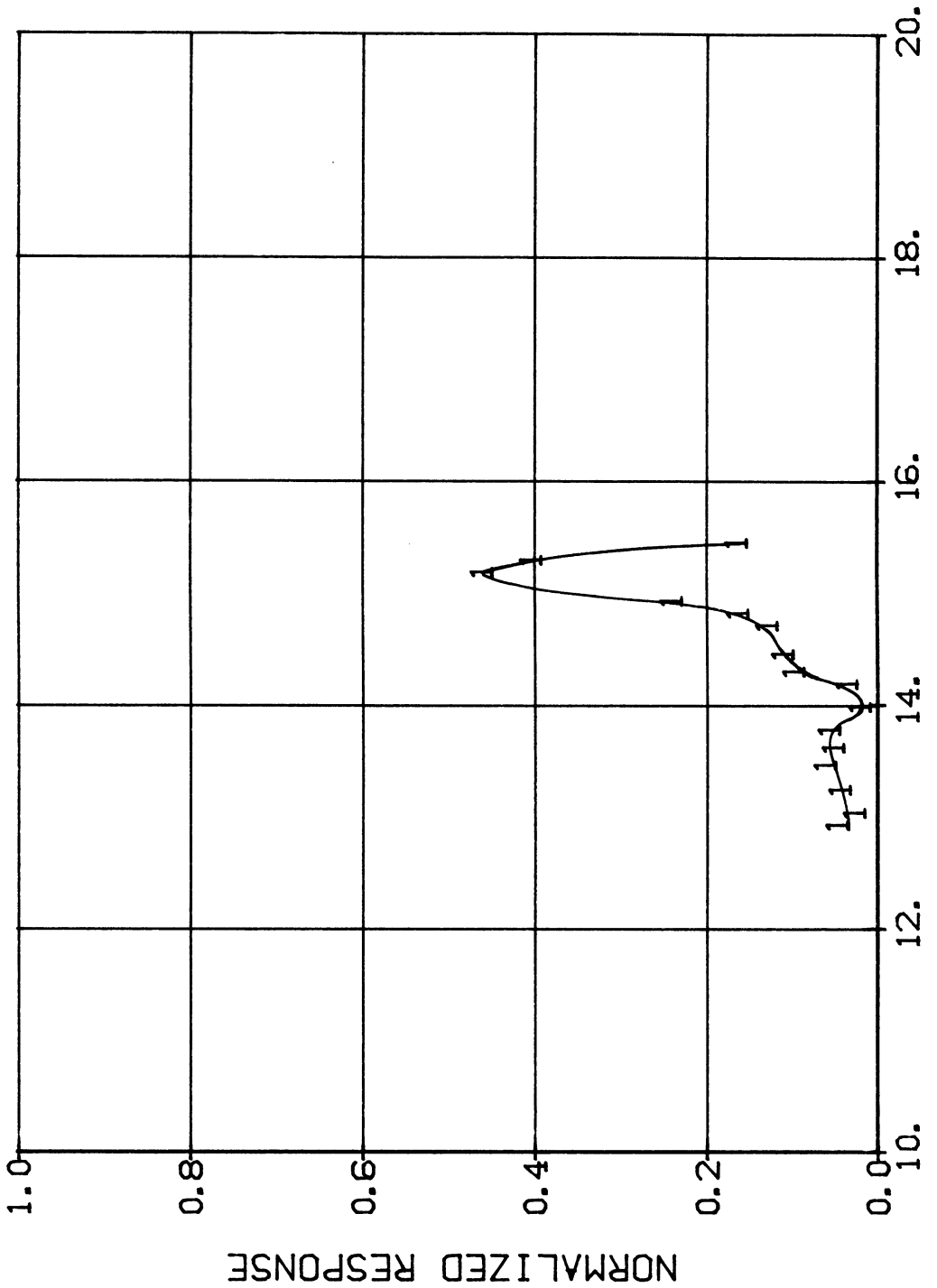

FIGURE 33: SPEED DEPENDENCE TEST, NORMALIZED NON-LINEAR RESPONSE VS. ENCOUNTER FREQUENCY SUM, ω_+ (MODEL SCALE).

$\omega_- = 0.$ $F_N = 0.086.$ MODEL RESTRAINED.

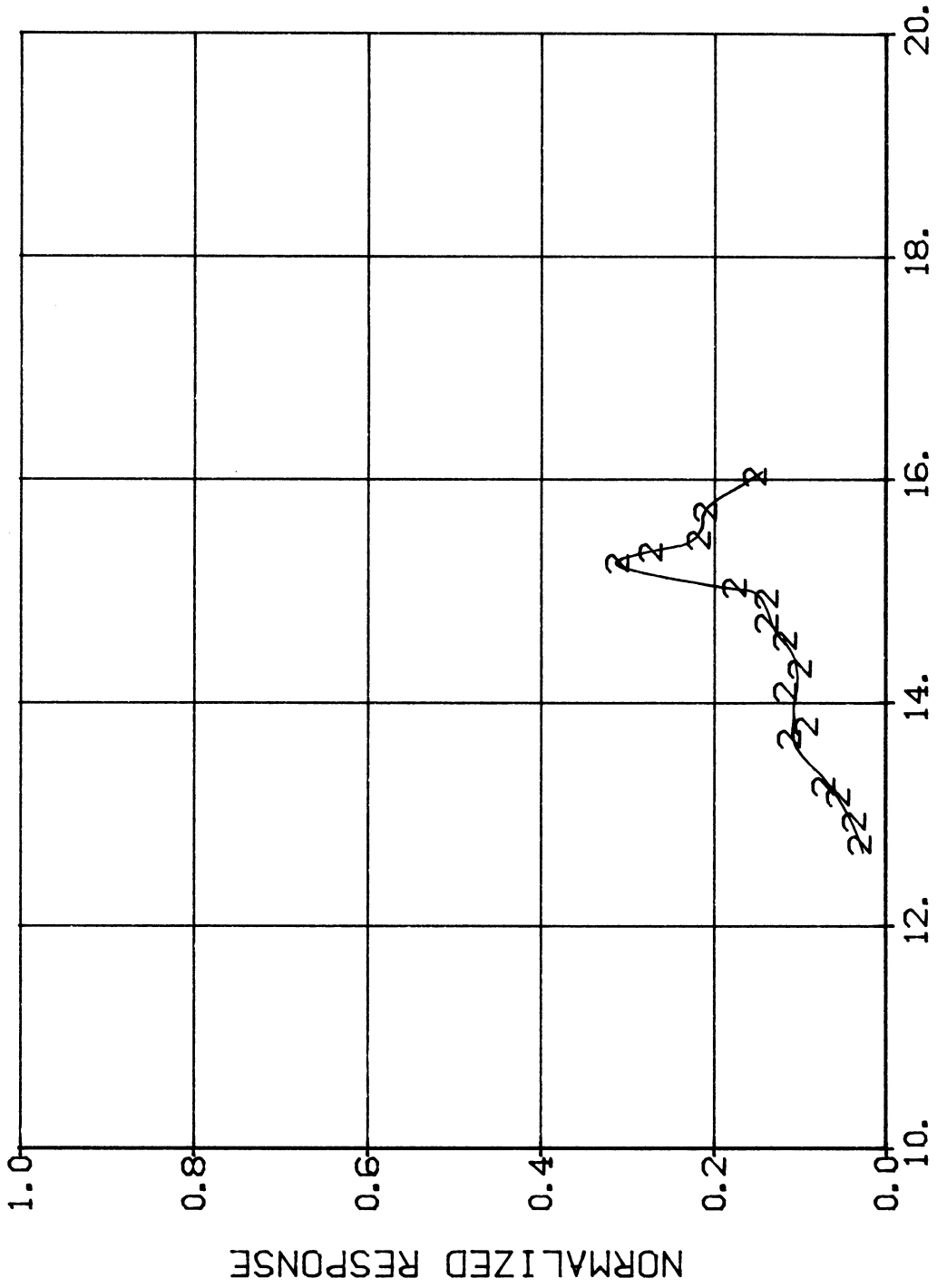

FIGURE 34: SPEED DEPENDENCE TEST, NORMALIZED NON-LINEAR RESPONSE VS. ENCOUNTER FREQUENCY SUM, ω_+ (MODEL SCALE).

$\omega_- = 0.$ $F_N = 0.109.$ MODEL RESTRAINED.

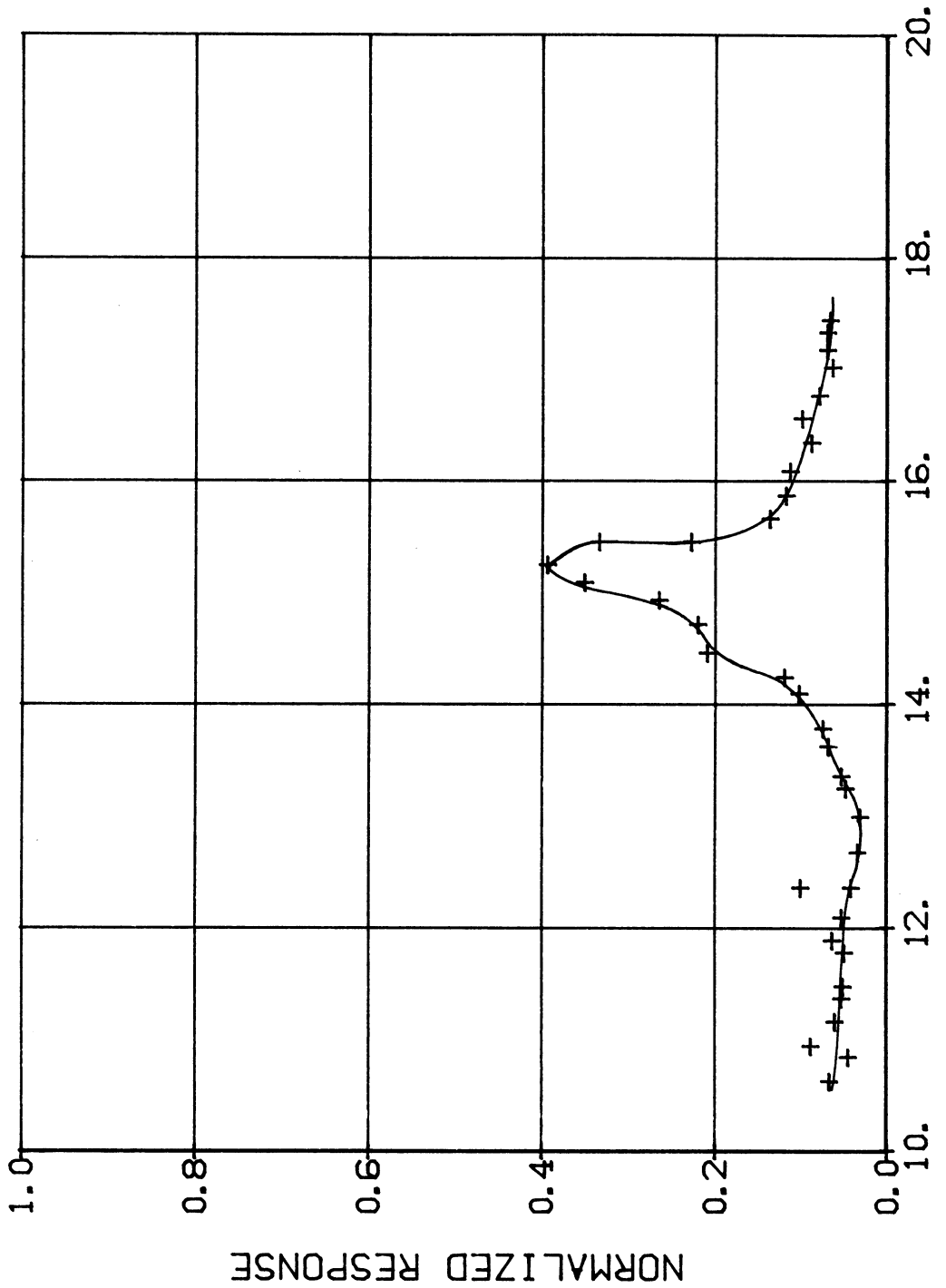

FIGURE 35: SPEED DEPENDENCE TEST, NORMALIZED NON-LINEAR RESPONSE VS. ENCOUNTER FREQUENCY SUM, ω_+ (MODEL SCALE).

$\omega_- = 0.$ $F_N = 0.132.$ MODEL RESTRAINED.

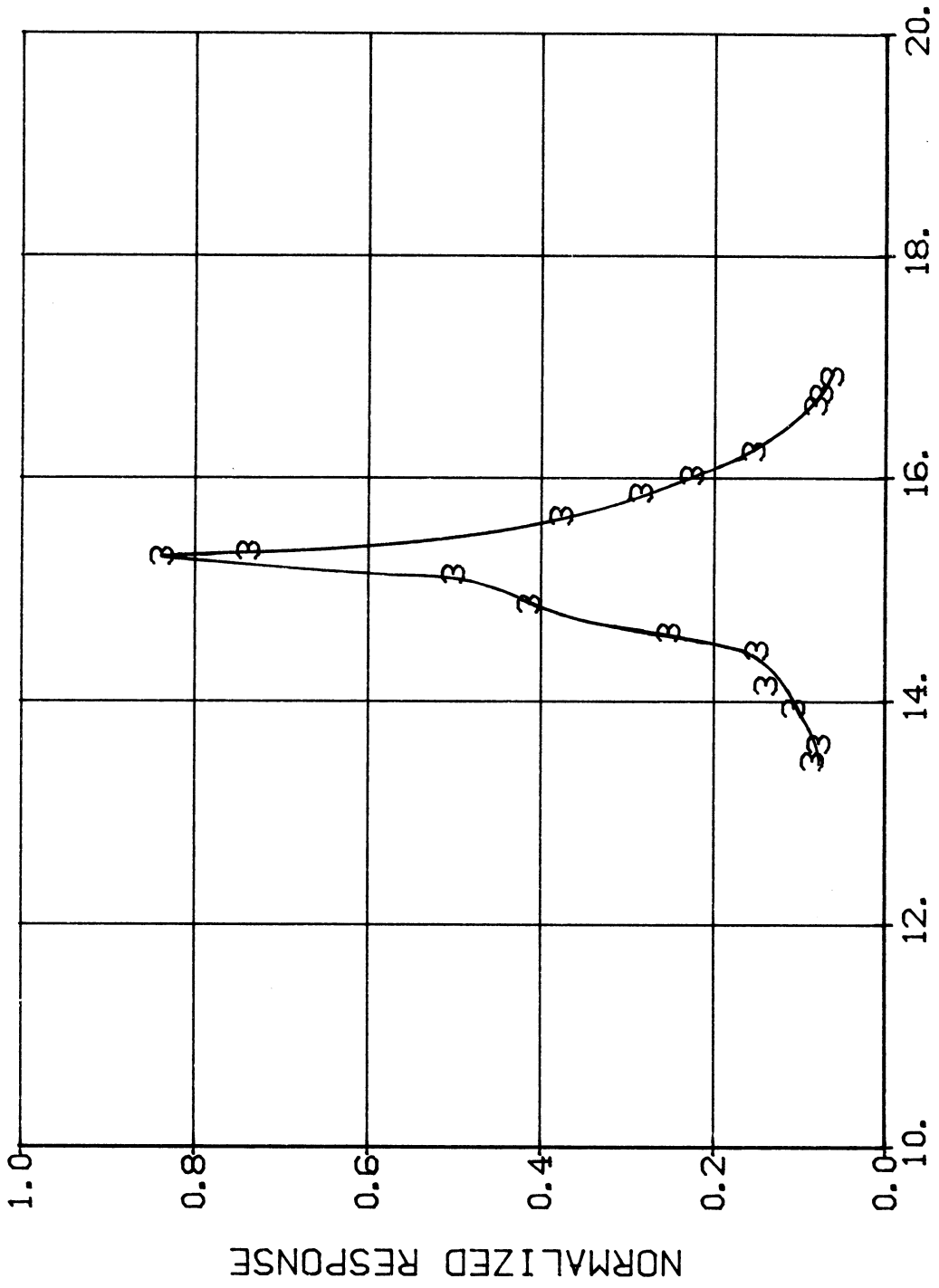

FIGURE 36: SPEED DEPENDENCE TEST, NORMALIZED NON-LINEAR RESPONSE VS. ENCOUNTER FREQUENCY SUM, ω_+ (MODEL SCALE). $\omega_- = 0.$ $F_N = 0.155.$ MODEL RESTRAINED.

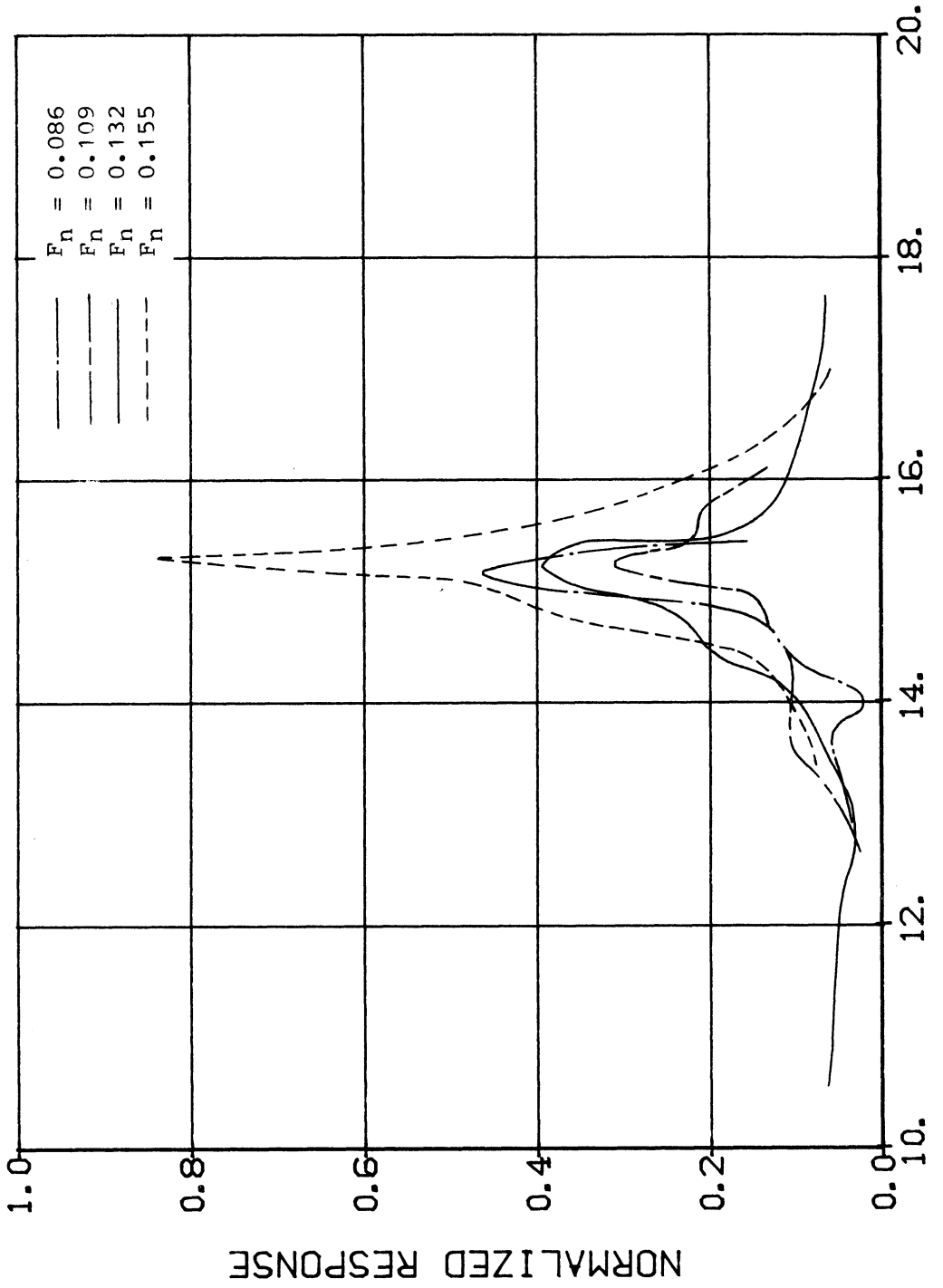

FIGURE 37: SPEED DEPENDENCE TEST, NORMALIZED NON-LINEAR RESPONSE VS. ENCOUNTER FREQUENCY SUM, $\omega+$ (MODEL SCALE).

$\omega- = 0.$ $F_N = 0.086, 0.109, 0.132, 0.155.$

MODEL RESTRAINED.

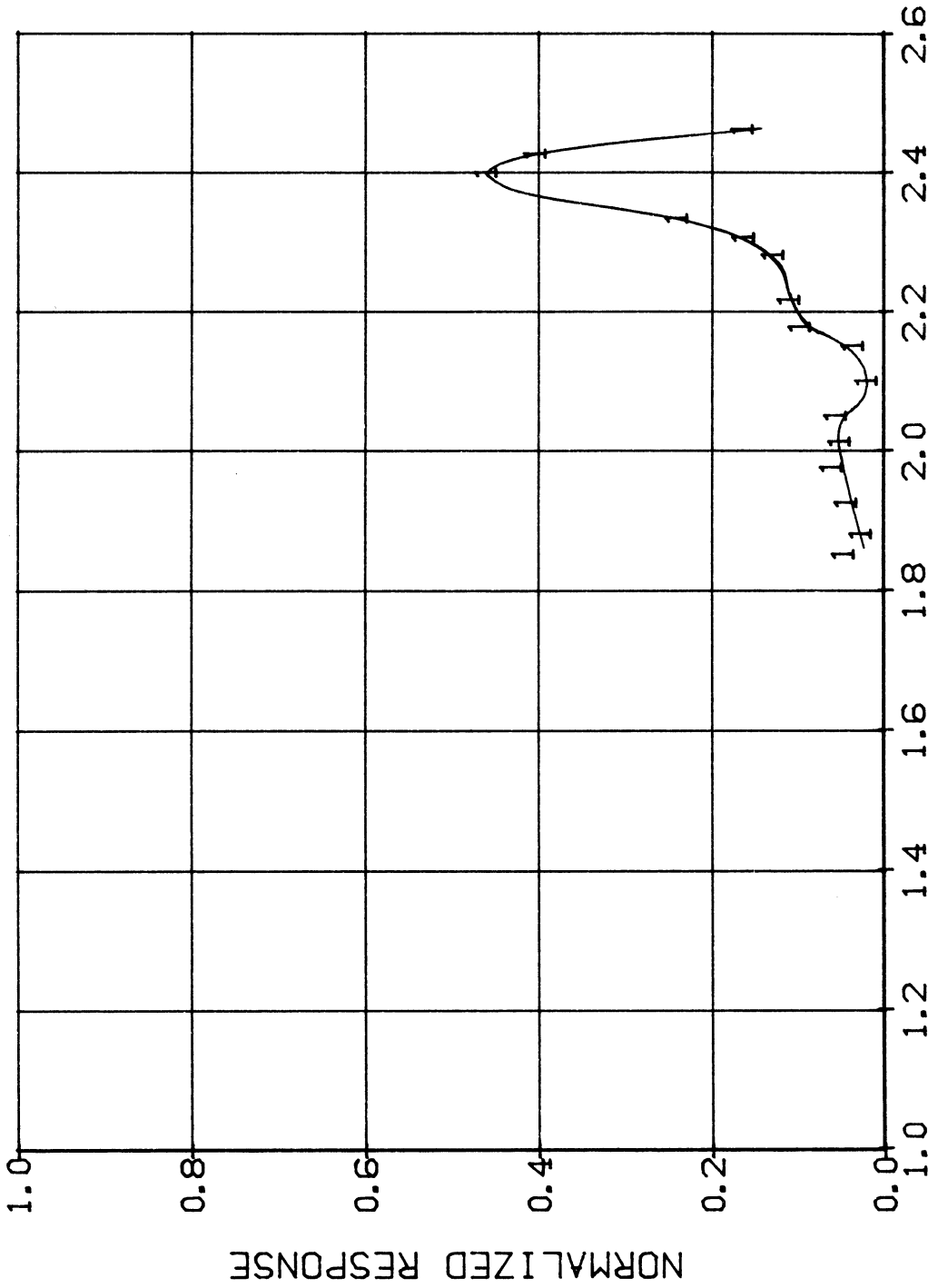

FIGURE 38: SPEED DEPENDENCE TEST, NORMALIZED NON-LINEAR RESPONSE VS. SHIP LENGTH/WAVELENGTH. $\omega_- = 0.$ $F_N = 0.086.$ MODEL RESTRAINED.

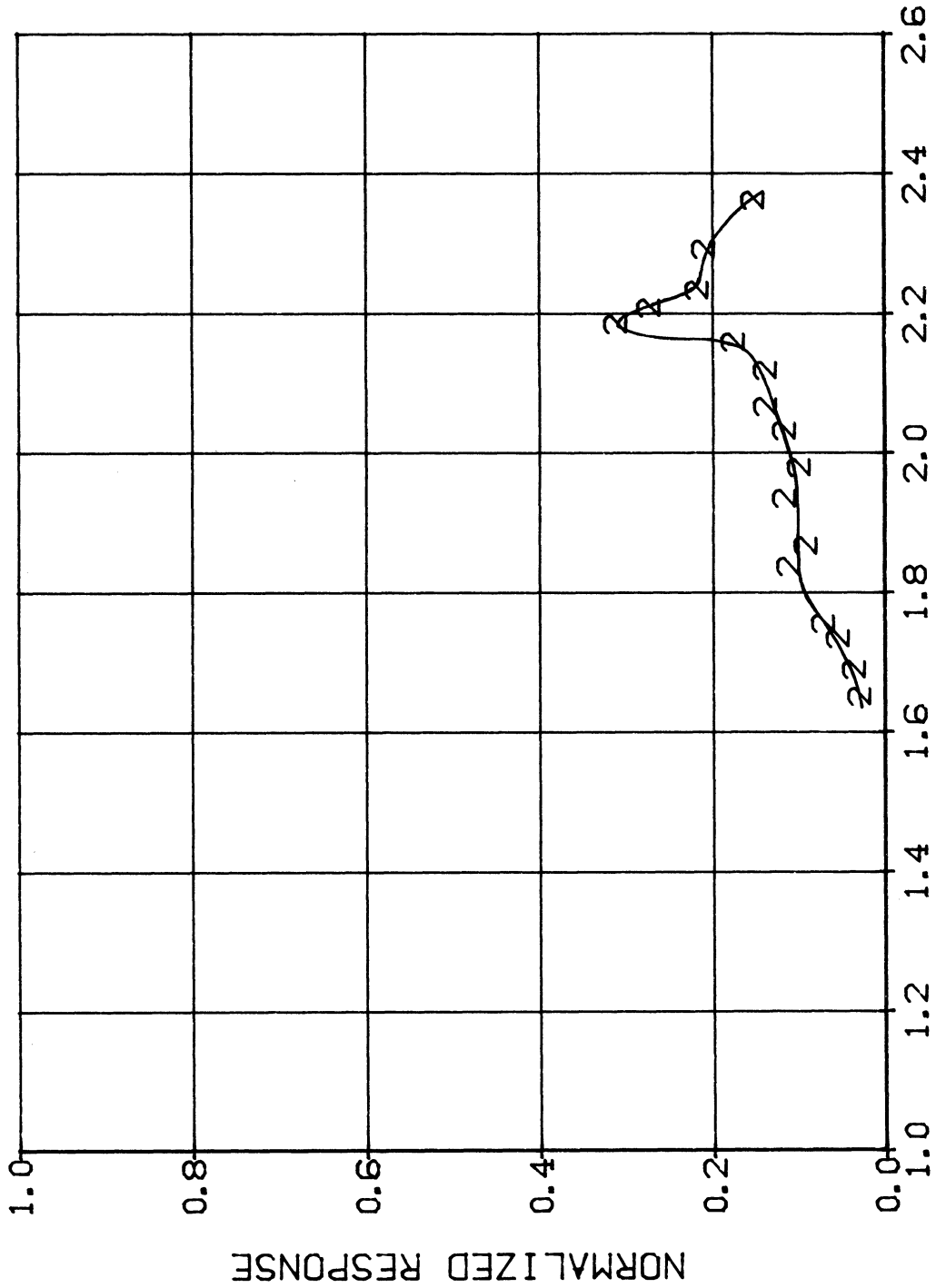

FIGURE 39: SPEED DEPENDENCE TEST, NORMALIZED NON-LINEAR RESPONSE VS. SHIP LENGTH/WAVELENGTH. $\omega_- = 0.$ $F_N = 0.109.$ MODEL RESTRAINED.

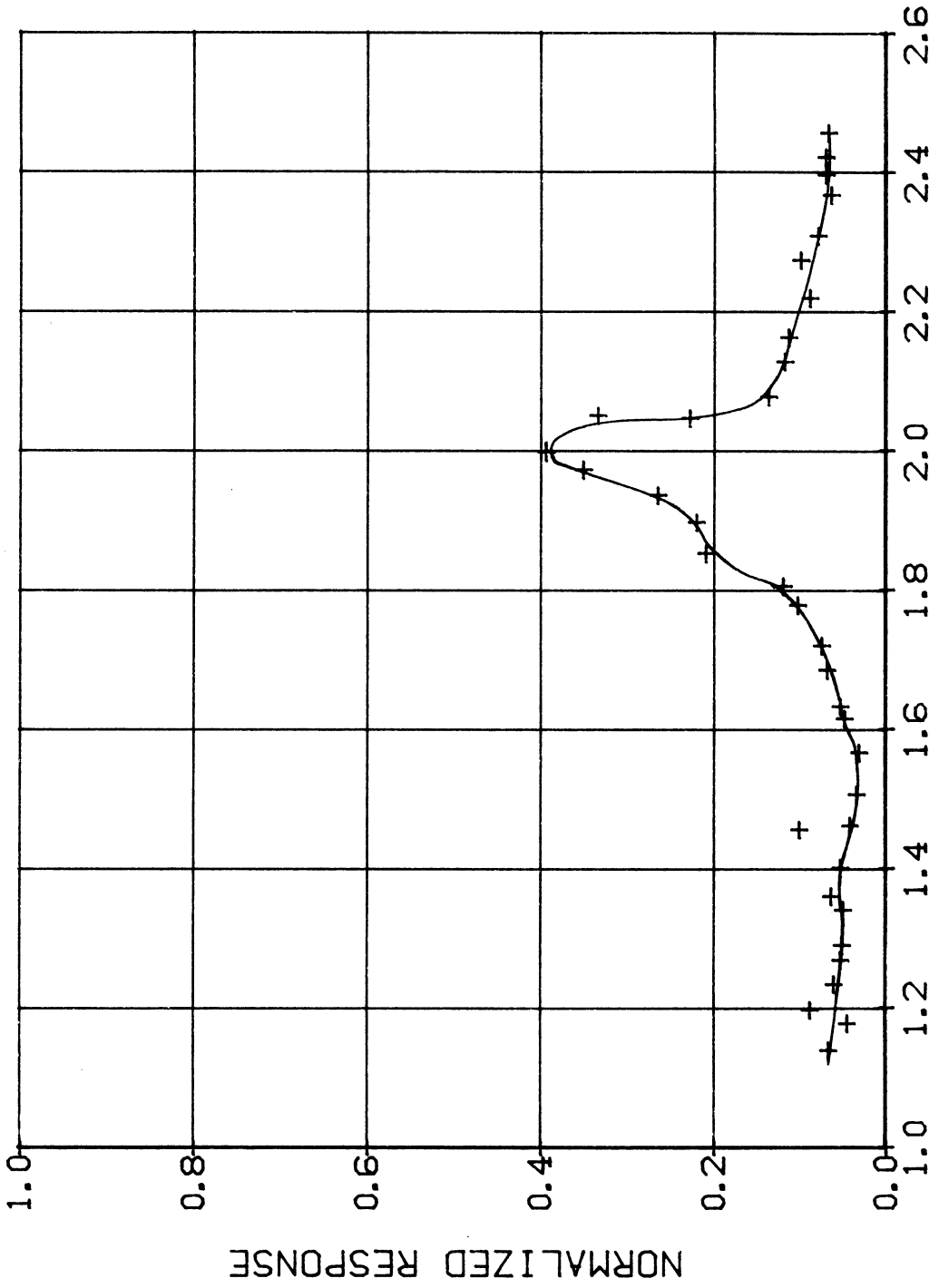

FIGURE 40: SPEED DEPENDENCE TEST, NORMALIZED NON-LINEAR RESPONSE VS. SHIP LENGTH/WAVELENGTH. $\omega_- = 0.$ $F_N = 0.132.$ MODEL RESTRAINED.

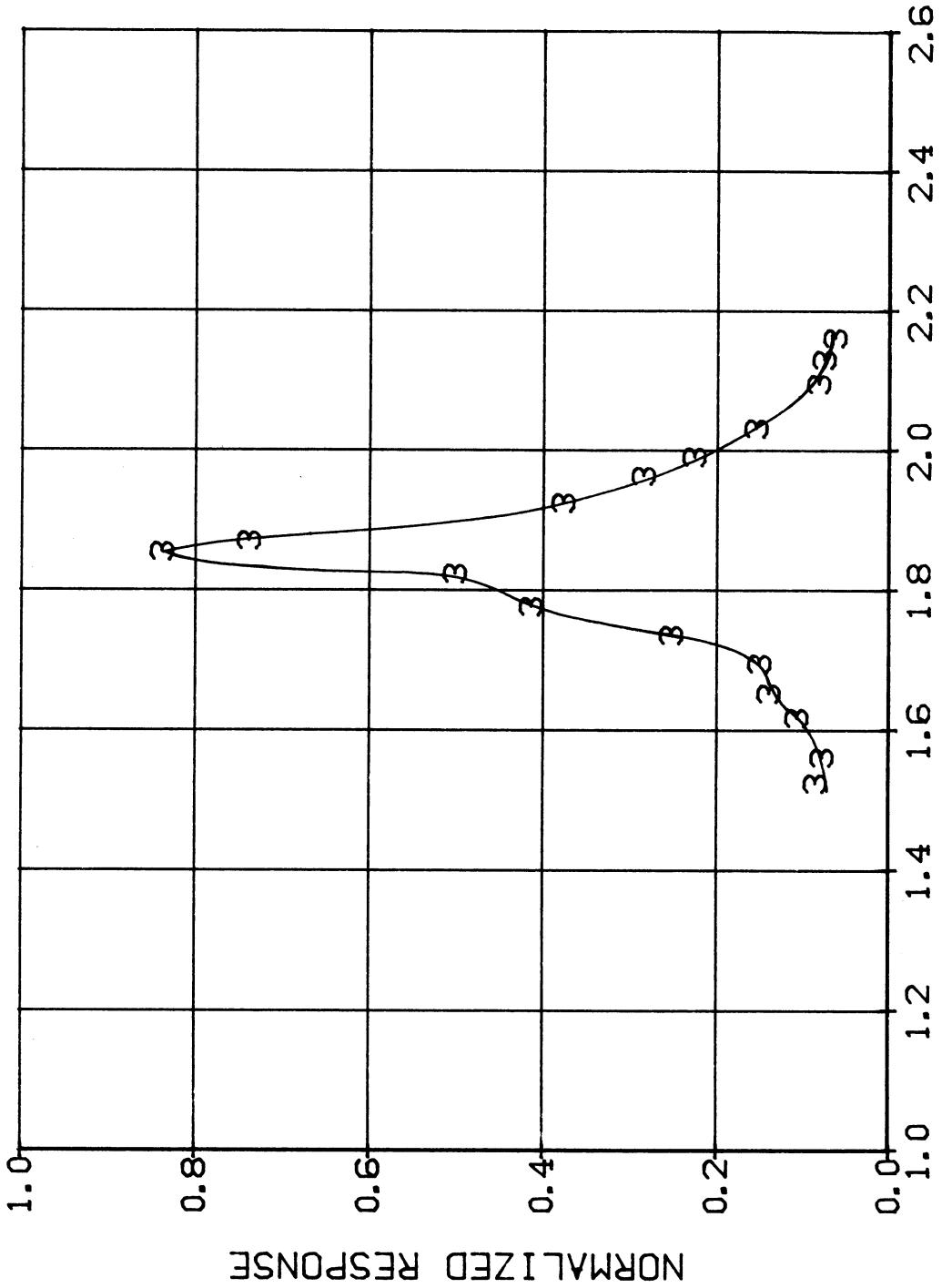

FIGURE 41: SPEED DEPENDENCE TEST, NORMALIZED NON-LINEAR RESPONSE VS. SHIP LENGTH/WAVELENGTH. $\omega_- = 0.$ $F_N = 0.155.$ MODEL RESTRAINED.

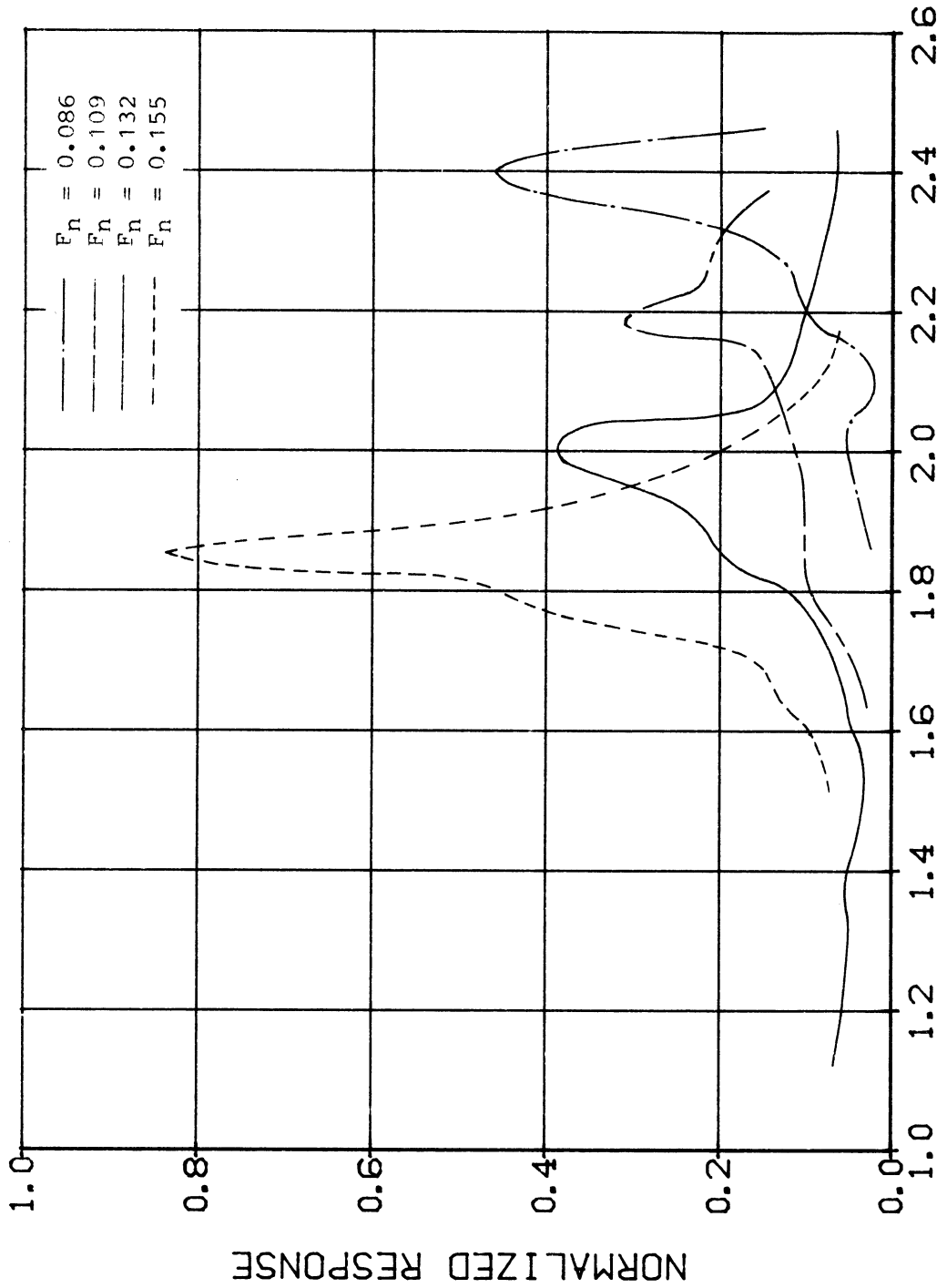

FIGURE 42: SPEED DEPENDENCE TEST, NORMALIZED NON-LINEAR RESPONSE VS. SHIP LENGTH/WAVELENGTH. $\omega_- = 0.$ $F_N = 0.086$, 0.109, 0.132, 0.155. MODEL RESTRAINED.

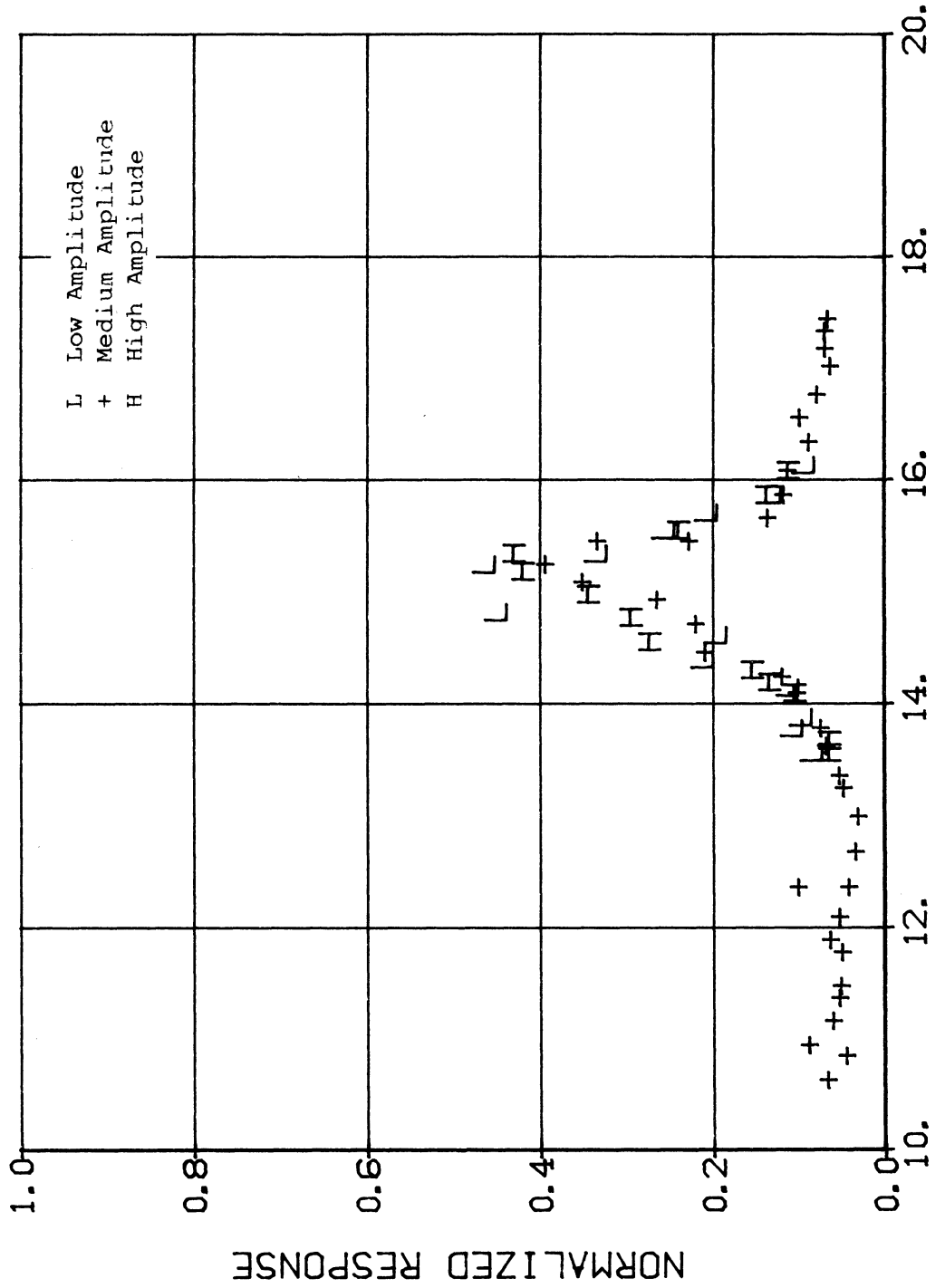

FIGURE 43: AMPLITUDE DEPENDENCE TESTS, NORMALIZED NON-LINEAR RESPONSE VS. ENCOUNTER FREQUENCY SUM, ω_+ (MODEL SCALE).
$\omega_- = 0.$ $F_N = 0.132.$ LOW, MEDIUM, AND HIGH AMPLITUDES.
MODEL RESTRAINED.

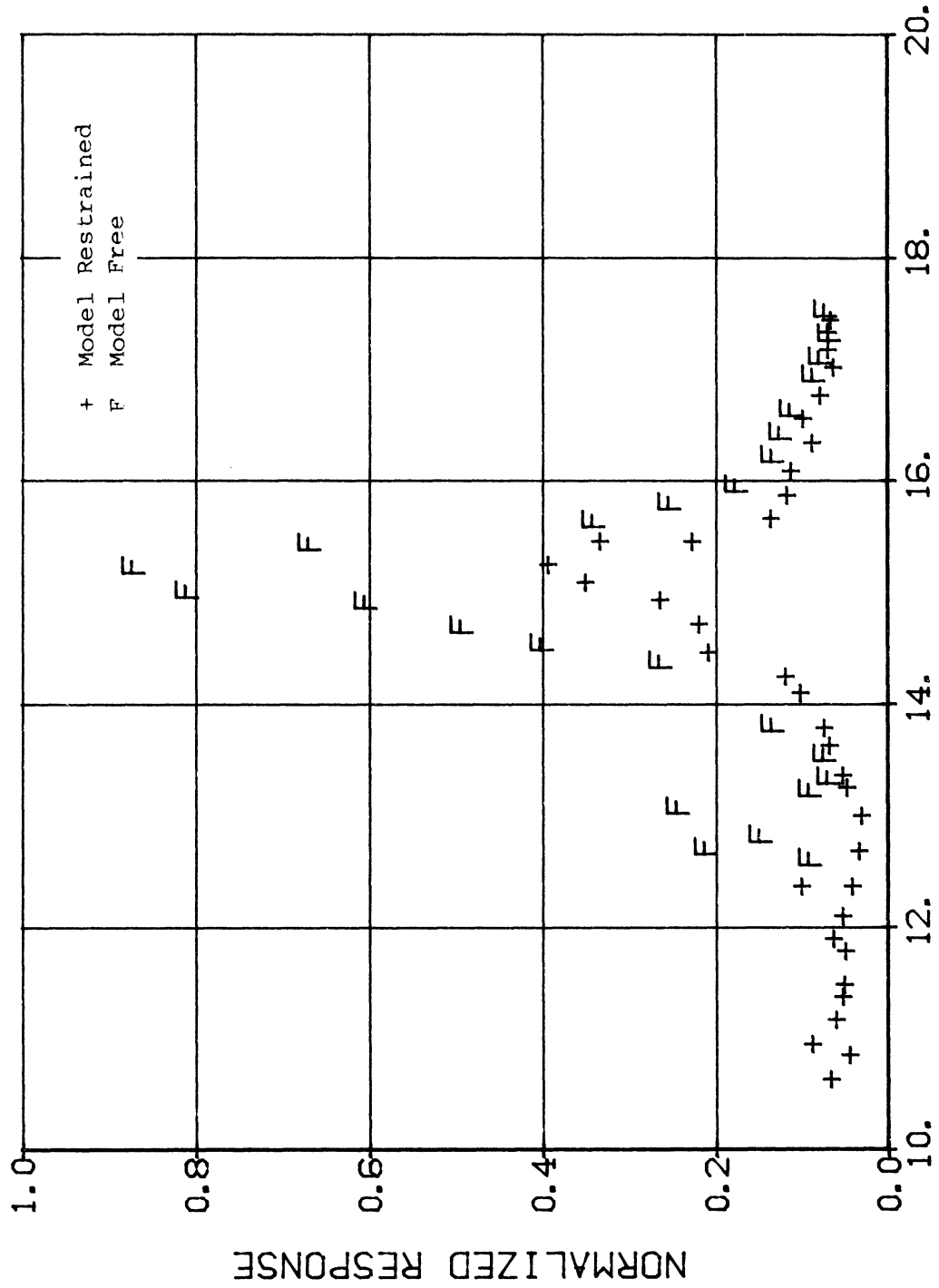

FIGURE 44: NORMALIZED NON-LINEAR RESPONSE VS. ENCOUNTER FREQUENCY SUM, ω_+ (MODEL SCALE). $\omega_- = 0$. $F_N = 0.132$. MODEL RESTRAINED AND MODEL FREE TO HEAVE AND PITCH.

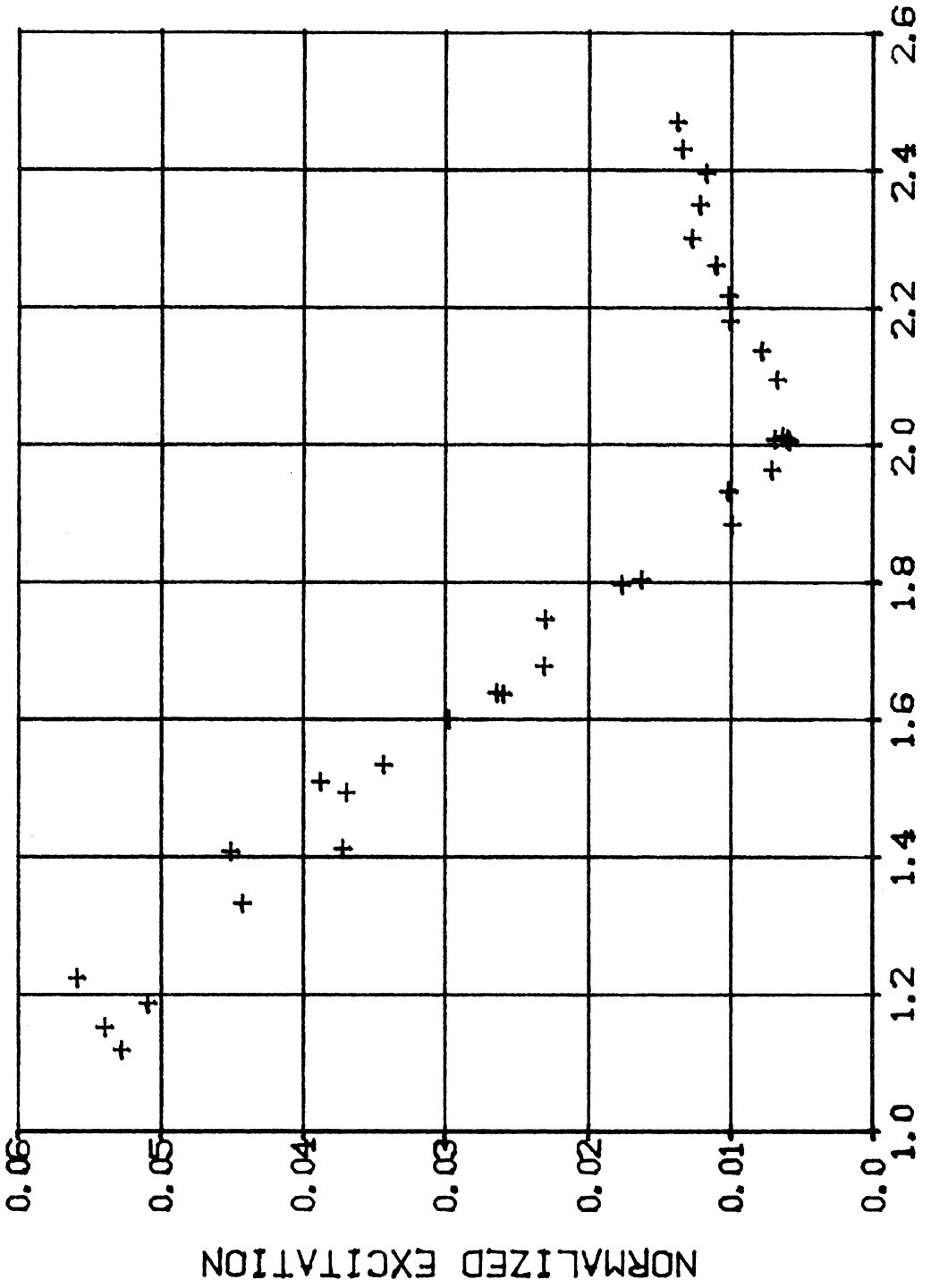

FIGURE 45: NORMALIZED LINEAR EXCITATION VS. SHIP LENGTH/ WAVELENGTH. $F_N = 0.132$. MODEL RESTRAINED.

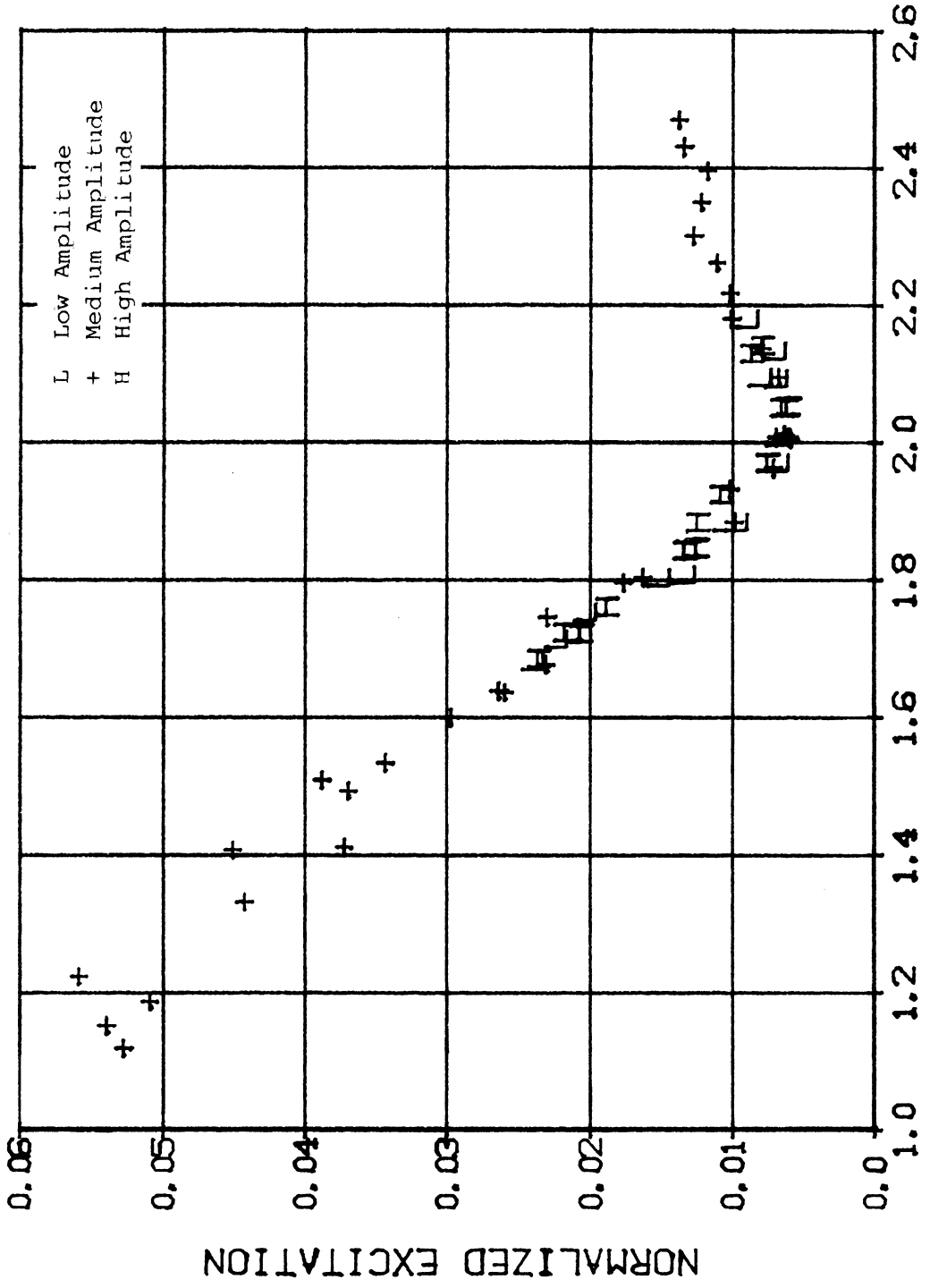

FIGURE 46: AMPLITUDE DEPENDENCE TEST, NORMALIZED LINEAR EXCITATION VS SHIP LENGTH/WAVELENGTH. $F_N = 0.132$. LOW, MEDIUM, AND HIGH AMPLITUDES. MODEL RESTRAINED.

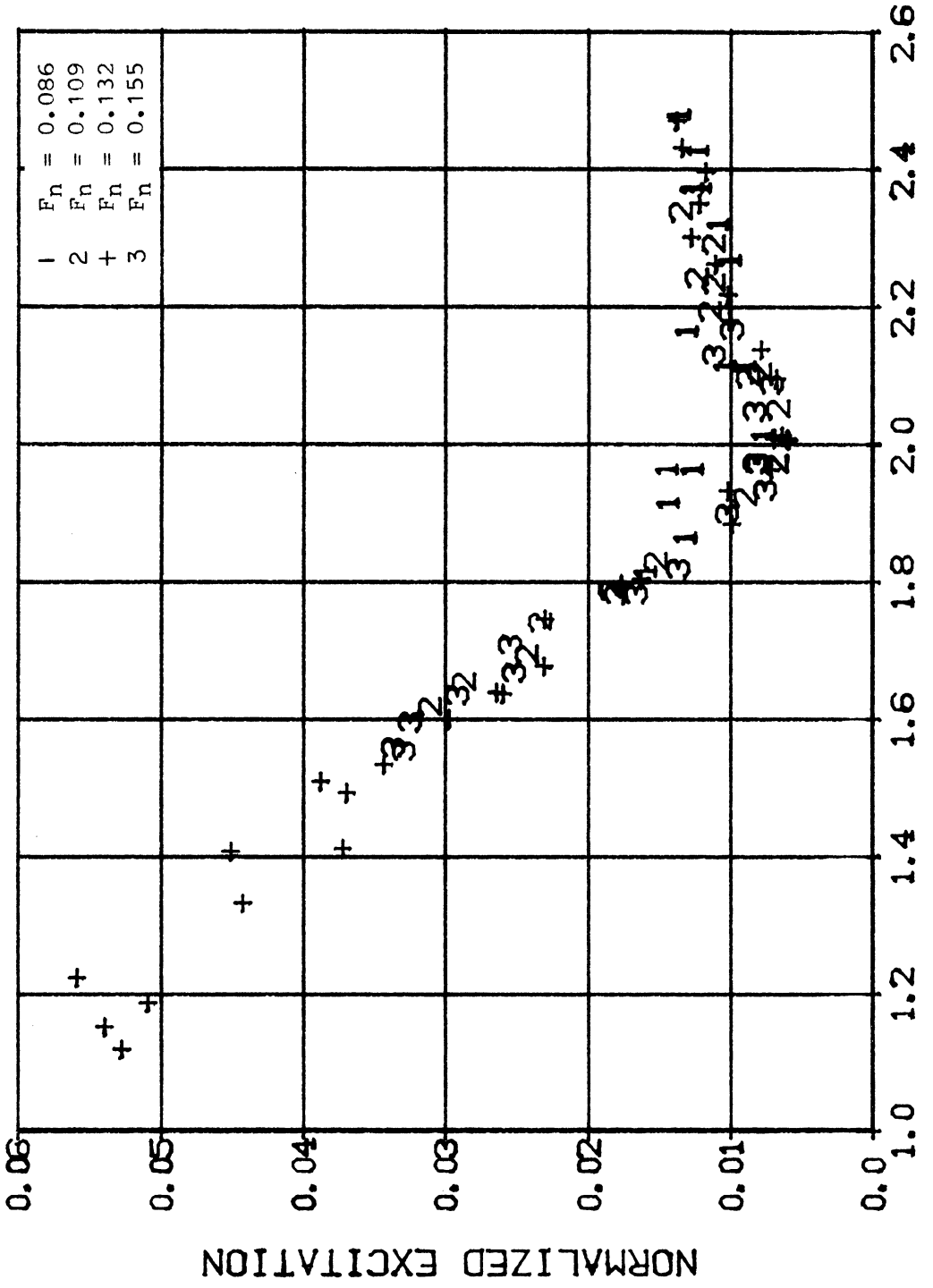

FIGURE 47: SPEED DEPENDENCE TESTS, NORMALIZED LINEAR EXCITATION VS SHIP LENGTH/WAVELENGTH. F_N = 0.086, 0.109, 0.132, 0.155. MODEL RESTRAINED.

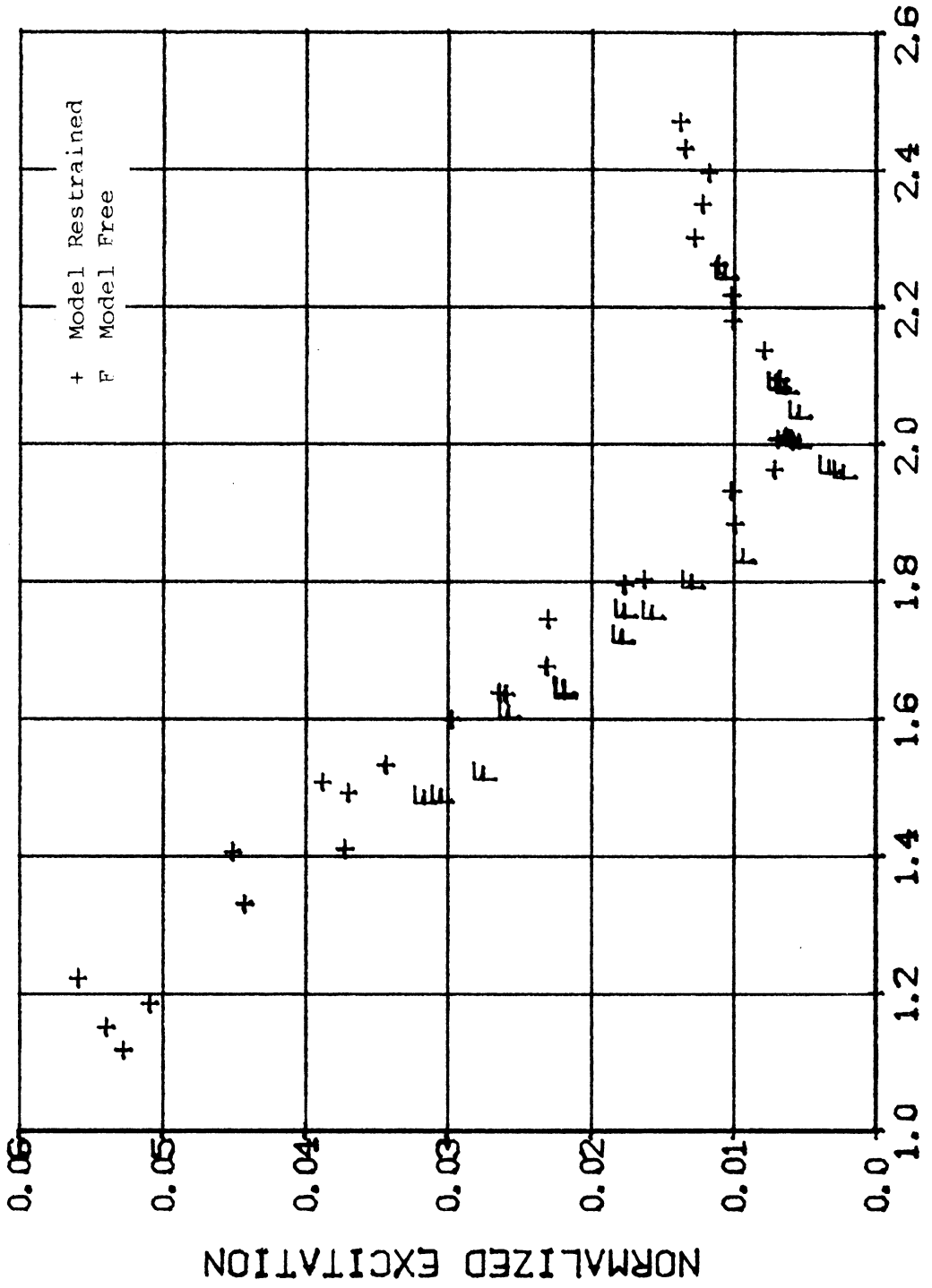

FIGURE 48: NORMALIZED LINEAR EXCITATION VS. SHIP LENGTH/ WAVELENGTH. $F_N = 0.132$. MODEL RESTRAINED AND MODEL FREE TO HEAVE AND PITCH.

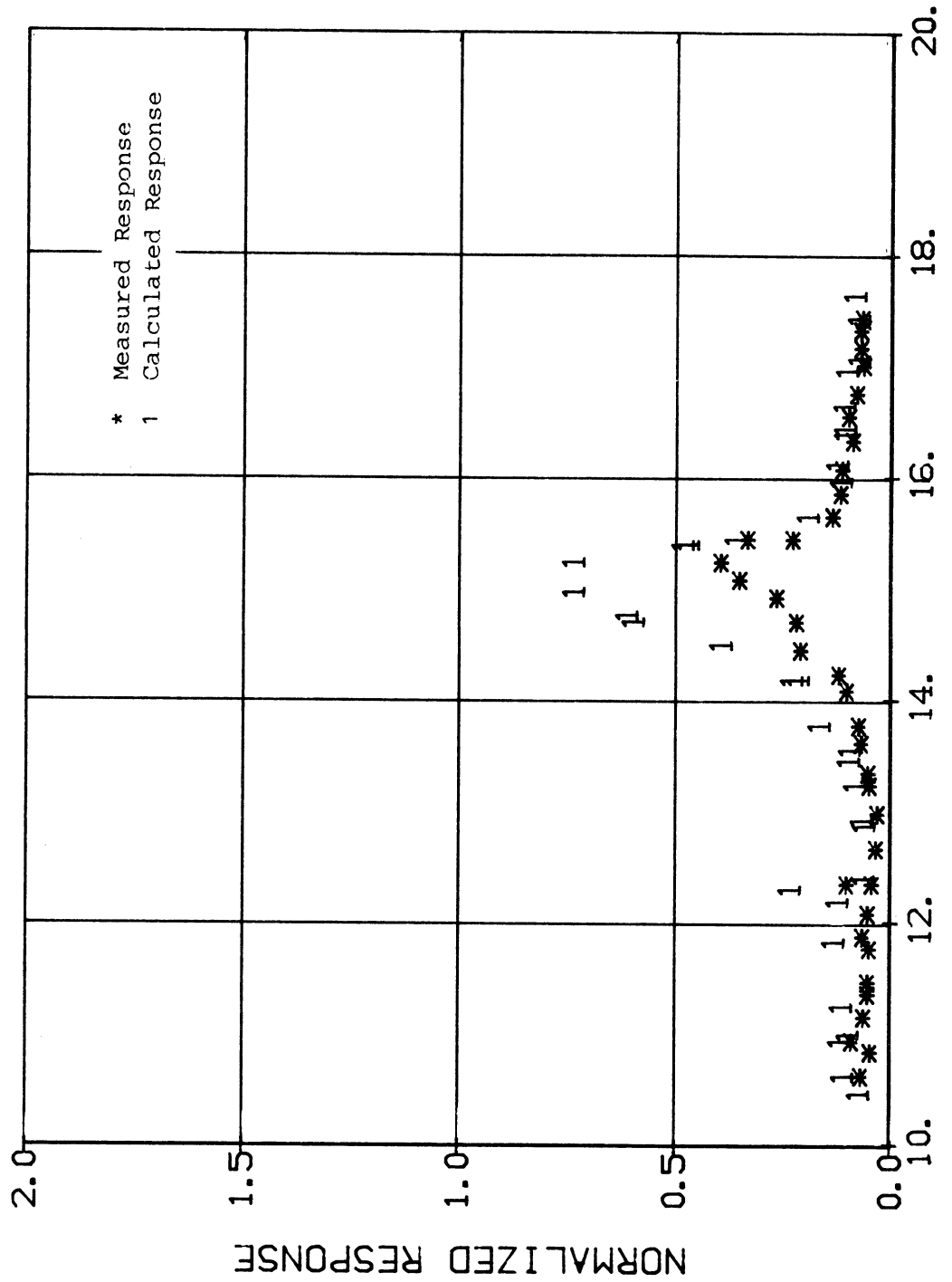

FIGURE 49: COMPARISON OF CALCULATED AND MEASURED NON-LINEAR RESPONSE. MODEL RESTRAINED.

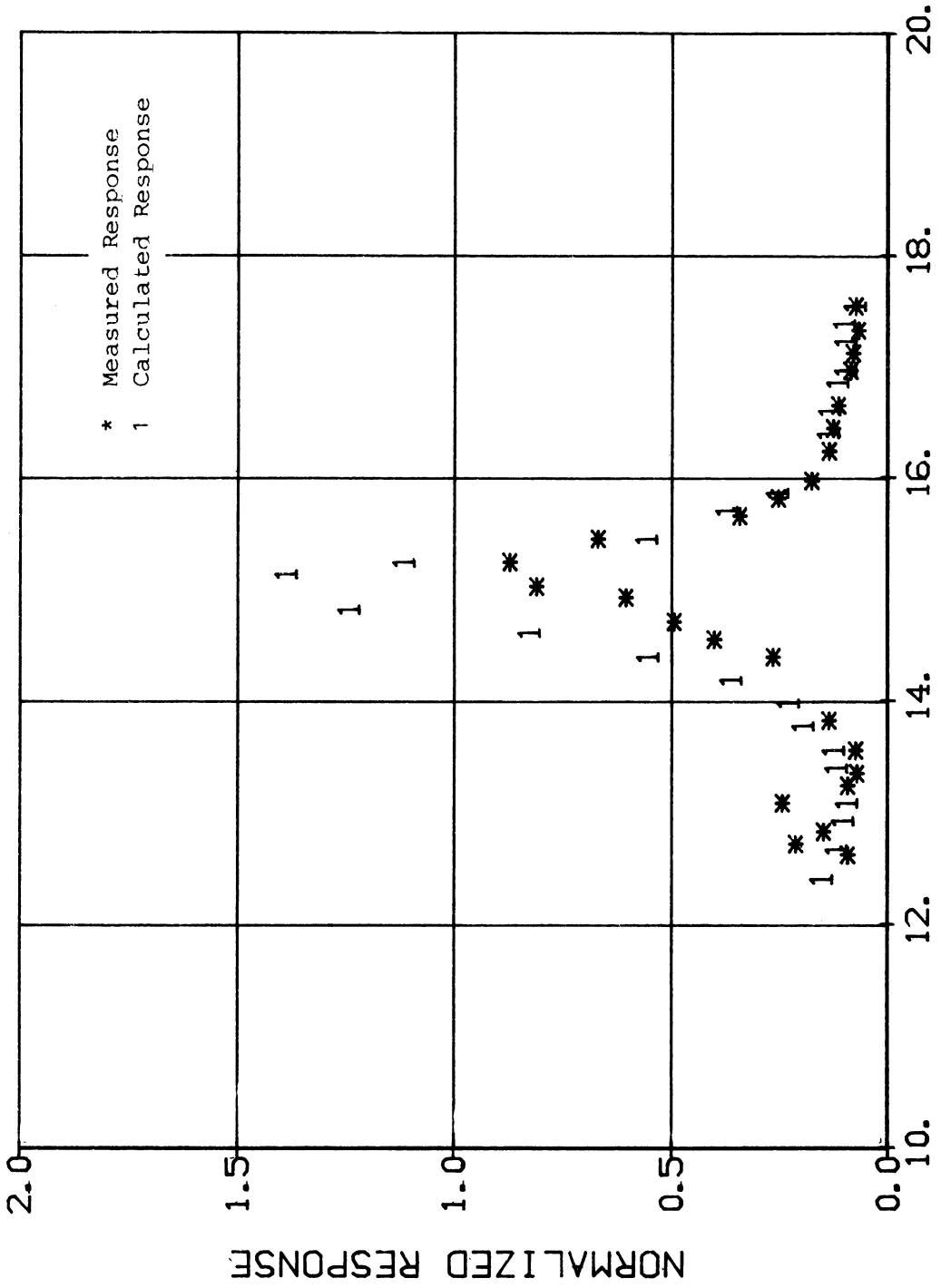

FIGURE 50: COMPARISON OF CALCULATED AND MEASURED NON-LINEAR RESPONSE. MODEL FREE TO HEAVE AND PITCH.

IV. CALCULATION OF THE NON-LINEAR SPRINGING EXCITATION SPECTRUM

Presented in this section is a method for calculating the second order springing excitation through use of the experimental results given in section III. This non-linear excitation, given as a one-sided spectral density $S_E^{(2)+}$ versus encounter frequency, ω, can be combined with the linear excitation spectrum $S_E^{(1)+}$ to give the total springing excitation spectrum, S_E^{+}, as a function of encounter frequency. The total excitation can in turn be used to calculate the total linear and nonlinear springing induced bending moment at midships. It is assumed that all the nonlinear behavior is in the excitation. As seen from Figures 44, 49 and 50 this is not an entirely valid assumption.

Development of a Computational Formula

As discussed in the introduction, assume that the major contribution to the non-linear springing behavior of a Great Lakes bulk carrier comes from the time dependent excitation term e_2. Here e_2 is the total normalized 2 noded springing excitation written as

$$e_2(t) = e_2^{(1)}(t) + e_2^{(2)}(t) \quad , \tag{12}$$

where $e_2^{(1)}$ and $e_2^{(2)}$ are the first and second order excitations respectively. If $e_2(t)$ has a sinusoidal time dependence of $\exp(i\omega t)$, where ω is the frequency of encounter, then $E_2^{(1)}$ is the amplitude of the excitation due to incident waves of frequency ω and $E_2^{(2)}$ is the amplitude of the excitation due to all pairs of waves whose sums are equal to ω.

The uncoupled differential equation describing the normalized springing response, q_2, for a hinged ship is given from equation (3) as

$$\ddot{q}_2(a_{22}+A_{22}) + \dot{q}_2(b_{22}+B_{22}) + q_2C_{22} = m_0(1+\ell_A/\ell_F) + e_2 \quad . \tag{13}$$

The left hand side of equation (13) follows a linear relationship. For an explanation of the various coefficients see the comments following (3). It is only important here to note that

$$m_0 = -K_s(1 + \ell_A/\ell_F)q_2 \tag{14}$$

where m_0 is the midship bending moment and K_s is the internal spring constant.

Now define an internal spring constant, c_{22}, in the following manner:

$$c_{22} = K_s(1 + \ell_A/\ell_F)^2 \ ,$$

and also the damping ratio, ζ_D, as

$$\zeta_D = \frac{(b_{22}+B_{22})\omega_0}{2(c_{22}+C_{22})} = \frac{b_{22} + B_{22}}{2\sqrt{(c_{22}+C_{22})(a_{22}+A_{22})}}$$

where ω_0 is the natural frequency in springing.

By using the above definitions and equation (14), the solution for the springing response to sinusoidal excitation is

$$q_2 = \left[\frac{e_2}{\omega_0^2(a_{22}+A_{22})}\right]\left[\frac{1}{(1-\omega^2/\omega_0^2)+i2\zeta_D\omega/\omega_0}\right] \ . \tag{15}$$

Here i is used as an imaginary notation and is equal to $\sqrt{-1}$. By manipulating the above expressions, the bending moment at midship can be shown to be

$$m_0 = \left[\frac{-e_2}{(1-\omega^2/\omega_0^2)+i2\zeta_D\omega/\omega_0}\right]\left[1 - \frac{C_{22}}{\omega_0^2(a_{22}+A_{22})}\right]\left[\frac{1}{1+\ell_A/\ell_F}\right] \tag{16}$$

Since $e_2(t)$ is shown by equation(12) to have a linear and non-linear component, $m_0(t)$ can also be expressed as

$$m_0(t) = m_0^{(1)}(t) + m_0^{(2)}(t) \tag{17}$$

where $m_0^{(1)}(t)$ is the bending moment due to $e_2^{(1)}(t)$ and $m_0^{(2)}(t)$ is the bending moment due to $e_2^{(2)}(t)$. If $e_2^{(1)}(t)$ represents the excitation due to an incident wave of unit amplitude and frequency ω, then $m_0^{(1)}(t)$ has an

amplitude that can be written as $M_0^{(1)}(\omega_e)$ and thus represents the first order transfer function. In a similar fashion, let $E_2^{(2)}(\omega_1,\omega_2)$ be the amplitude of the second order excitation due to incident waves of unit amplitudes and encounter frequencies of ω_1 and ω_2. Then $M_0^{(2)}$ becomes the second order transfer function. Strictly speaking, $M_0^{(2)}$ should be written as $M_0^{(2)}(\omega_1,\omega_2)$ where the frequencies ω_1 and ω_2 must satisfy the relation $\omega_1 + \omega_2 = \omega$.

If there exists a one sided sea spectrum of $S^+(\omega)$, then we can use equations (12) and (16) to calculate the total response spectrum composed of both first and second order parts. Let $S_M^+(\omega)$ be the total midship bending moment response spectrum at some encounter frequency ω. Then Neal (1974) or Yamanouchi (1974) have shown that

$$S_M^+(\omega) = S_M^{(1)+}(\omega) + S_M^{(2)+}(\omega) \tag{18}$$

where $S_M^{(1)+}(\omega)$ is the usual first order response spectrum given as

$$S_M^{(1)+}(\omega) = |M_0^{(1)}(\omega)|^2 \, S^+(\omega) \tag{19}$$

and $S_M^{(2)+}(\omega)$ is the second order response spectrum given as

$$S_M^{(2)+}(\omega) = \int_{-\infty}^{\infty} d\mu \; |M_0^{(2)}(\omega-\mu,\mu)|^2 \, S^+(|\omega-\mu|) \, S^+(|\mu|) \; . \tag{20}$$

If certain assumptions are made about the behavior of the integrand of equation (20), simplification is possible. First, equation (20) can be separated into two regions of integration, $-\infty<\mu\leq 0$ and $0\leq\mu<\infty$. When $\mu<0$, the integral represents the contribution of the non-linear bending moment at ω_0 due to two waves, one at a frequency $|\mu|$ and another at a frequency $\omega_0+|\mu|$. It is unlikely that this contribution is significant and so the integral over the negative range of μ will be considered small.

Following equation (16), we may write

$$M_0^{(2)}(\omega-\mu,\mu) = -H^{(2)}(\omega-\mu,\mu) \cdot q(\omega) \tag{21}$$

where

$$q(\omega) = \left[\frac{1}{(1-\omega^2/\omega_o^2) + i2\zeta_D\omega/\omega_o}\right]\left[1 - \frac{C_{22}}{\omega_o^2(a_{22}+A_{22})}\right]\left[\frac{1}{1+\ell_A/\ell_F}\right] \tag{22}$$

It follows that

$$S_M^+(\omega) = |q(\omega)|^2[S_E^{(1)}(\omega) + S_E^{(2)}(\omega)] \tag{23}$$

where $S_E^{(1)}(\omega) = |H^{(1)}(\omega)|^2 S^+(\omega)$

and $S_E^{(2)}(\omega) = \int_0^\infty d\mu \ |H^{(2)}(\omega-\mu,\mu)|^2 S^+(|\omega-\mu|)S^+(\mu)$.

It is clear that $S_E^{(1)}(\omega)$ and $S_E^{(2)}(\omega)$ are the first and second order spectral densities of the springing excitation. If we restrict our attention to frequencies whose sum equals ω and if we note that the integrand in the above equation is symmetric about $\mu = \omega/2$, then $S_E^{(2)}(\omega)$ can be expressed alternatively as

$$S_E^{(2)}(\omega) = 2 \int_0^{\omega_e/2} d\mu |H^{(2)}(\omega-\mu,\mu)|^2 S^+(|\omega-\mu|)S^+(\mu) \tag{24}$$

An experimental investigation of the linear component $S_E^{(1)}(\omega)$ was conducted by Troesch (1980) in an earlier study. Here the subject of interest is the non-linear component $S_E^{(2)}(\omega)$.

In order to calculate the non-linear excitation component over a range of encounter frequency values ω , the magnitude of the second order transfer function $H^{(2)}(\omega-\mu,\mu)$ must be known for wide ranges of its arguments μ and $\omega-\mu$. However, the experimental results suggest an approximation which limits to a considerable extent the amount of information required to calculate $S_E^{(2)}(\omega)$.

Consider Figures 10 and 12 in section III. The first is a normalized plot of $H^{(2)}(\omega-\mu,\mu)$ as a function of ω (model scale), with μ specified by $\mu=\frac{\omega}{2}$. The second is a normalized plot of $H^{(2)}(\omega-\mu,\mu)$ versus ω, with μ specified by $\mu = \frac{\omega}{2} - 0.712$. A comparison of the two curves shows that, for a given ω, there is little change in the magnitude of the transfer function as μ varies from $\frac{\omega}{2} - 0.712$ to $\frac{\omega}{2}$. This indicates that the magnitude of $H^{(2)}(\omega-\mu,\mu)$ is essentially constant for a range of μ near $\mu = \frac{\omega}{2}$, i.e. over the high end of the interval of integration in equation (24). For the typical single-peaked narrow band wave spectrum, the product $S^+(\mu)S^+(\omega-\mu)$ will be largest for values of μ near $\mu = \frac{\omega}{2}$. The significant contribution to the integral in equation (24) will therefore come from a region in which $H^{(2)}(\omega-\mu,\mu)$ varies only slightly. For this reason the following approximation can be made

$$S_E^{(2)}(\omega) \simeq |H^{(2)}(\omega/2,\omega/2)|^2 \cdot 2 \int_0^{\omega/2} d\mu S^+(\omega-\mu)S^+(\mu) \qquad (25)$$

in which $H^{(2)}(\omega-\mu,\mu)$ has been assumed to be constant over the entire interval of integration, taking its value at $\mu = \frac{\omega}{2}$.

Since the encounter frequency ω is a function of Froude number F_n and ship length to wavelength ratio L/λ we can write

$$H^{(2)}(\frac{\omega}{2},\frac{\omega}{2}) = H^{(2)}(L/\lambda,L/\lambda,F_n) \qquad (26)$$

Now consider Figure 23. This is a plot of the normalized excitation transfer function versus L/λ with Froude number as a parameter. It is clear that $H^{(2)}$ varies slowly over the broad range of Froude numbers tested. It is therefore reasonable to neglect the speed dependence over small changes of Froude number, or

$$H^{(2)}(L/\lambda,L/\lambda,F_n) \simeq H^{(2)}(L/\lambda,L/\lambda) \; . \qquad (27)$$

Equation (25) can then be written

$$S_E^{(2)}(\omega) \simeq |H^{(2)}(L/\lambda, L/\lambda)|^2 \cdot 2 \int_0^{\omega/2} d\mu S^+(|\omega-\mu) S^+(\mu) \quad . \tag{28}$$

For purposes of numerical computation equation (22) can be rewritten in the discrete frequency form of

$$S_E^{(2)}(n\Delta\omega) \simeq |H^{(2)}(L/\lambda, L/\lambda)|^2 \sum_{m=0}^{n-1} \Delta\omega \; S+(n\Delta\omega - m\Delta\omega) S^+(m\Delta\omega) \tag{29}$$

in which $\Delta\omega$ is some selected increment of encounter frequency, and λ is the wavelength corresponding to the frequency of encounter $\omega = \frac{1}{2} n\Delta\omega$. A trapezoidal integration formula is implied. Equation (29) is the basis for the method of calculation outlined below.

Algorithm for Calculation of the Non-linear Excitation Spectrum in Head Seas

The second order excitation component can be calculated by the following algorithm. The spectral density of the incident sea is assumed to be given as a function of absolute frequency σ . The result of the computations will be a set of values of the spectral density of non-linear springing excitation $S_E^{(2)}(\omega)$ for evenly spaced values of encounter frequency ω .

1. Select an increment of encounter frequency $\Delta\omega$. Values of $S_E^{(2)}(\omega)$ will be calculated for frequencies $\omega = n\Delta\omega$. Smaller values of $\Delta\omega$ will result in improved accuracy and an increased amount of computational work.

2. For each value of n calculate the absolute frequency σ_n .

$$\sigma_n = \frac{-1 + \sqrt{1 + (4Un\Delta\omega/q)}}{2U/q} \tag{30}$$

The ship's speed U , the gravitational constant q , and $\Delta\omega$ must be in consistant units.

3. Obtain values of the wave spectral density function, $S^+(n\Delta\omega)$, for each n where

$$S^+(n\Delta\omega) = S^+(\sigma_n)/(1+2\sigma_n U/g) \tag{31}$$

4. Calculate the excitation spectral density $S_E^{(2)}(n\Delta\omega)$ for each n by the following steps:

a. Calculate I_n where

$$I_n = \sum_{m=0}^{n-1} \Delta\omega \; S^+(n\Delta\omega - m\Delta\omega) S^+(m\Delta\omega) \tag{32}$$

b. Calculate L/λ_n where

$$L/\lambda_n = L[-\sqrt{g} + \sqrt{g + 2Un\Delta\omega}]^2/8\pi U^2 \tag{33}$$

c. Enter Figure 16 with L/λ_n and read the normalized transfer function $(H_n^{(2)})_{norm}$.

d. Calculate $H_n^{(2)}$

$$H_n^{(2)} = 2\pi\rho g B L \left(\frac{L}{\lambda_n}\right)(H_n^{(2)})_{norm} \tag{34}$$

e. Calculate the spectral density of non-linear excitation $S_E^{(2)}(n\Delta\omega)$ by

$$S_E^{(2)}(n\Delta\omega) = [H_n^{(2)}]^2 I_n \tag{35}$$

Example

As an example, a non-linear bending moment spectrum is determined here for the wave spectrum shown in Figure 51 (taken from Ploeg (1971)). The calculations are carried out for a ship speed of 21.56 ft/sec (14.7 mph). The increment of encounter frequency is taken to be $\Delta\omega = 0.1$ radians/sec , and the effects of heave and pitch are neglected.

Table II shows the results of steps 2 and 3 of the computations. Tables III, IV, and V show calculations of I_n from step 4.a for n = 18, 19, and 20, respectively. Calculations of I_n for other n values are not shown. Table VI shows calculations of $S_E^{(2)}(n\Delta\omega)$ for each n . The parameter L/λ_n is found using equation (33), and is then used to determine $H_{n\,norm}$ from Figure 16. The transfer function $H_n^{(2)}$ is then computed from equation (34). Finally, equation (35) is used to find $S_E^{(2)}(n\Delta\omega)$.

The linear excitation spectrum $S_E^{(1)+}(n\Delta\omega)$ is calculated using experimental data given by Troesch (1980). The details of the computations are not shown here.

Once the linear and non-linear excitation spectral components $S_E^{(1)+}(n\Delta\omega)$ and $S_E^{(2)+}(n\Delta\omega)$ are known, the corresponding components of the bending moment spectrum can be calculated using equations (21), (22), and (23), with

$$\omega_o = 1.904 \text{ radians/sec},$$

$$\zeta_D = 0.0154 ,$$

$$1 - \ell_A/\ell_F = 2.025 ,$$

$$1 - \frac{C_{22}}{\omega_o^2(a22 + A22)} = 0.857 .$$

Computed values of the non-linear bending moment spectrum $S_M^{(2)+}(n\Delta\omega)$ are given in Table VII.

Table VIII shows the values obtained for the linear component $S_M^{(1)+}(n\Delta\omega)$, the non-linear component $S_M^{(2)+}(n\Delta\omega)$, and the total bending moment spectrum $S_M^{+}(n\Delta\omega)$. Figure 52 shows the results of the computations: a spectral density

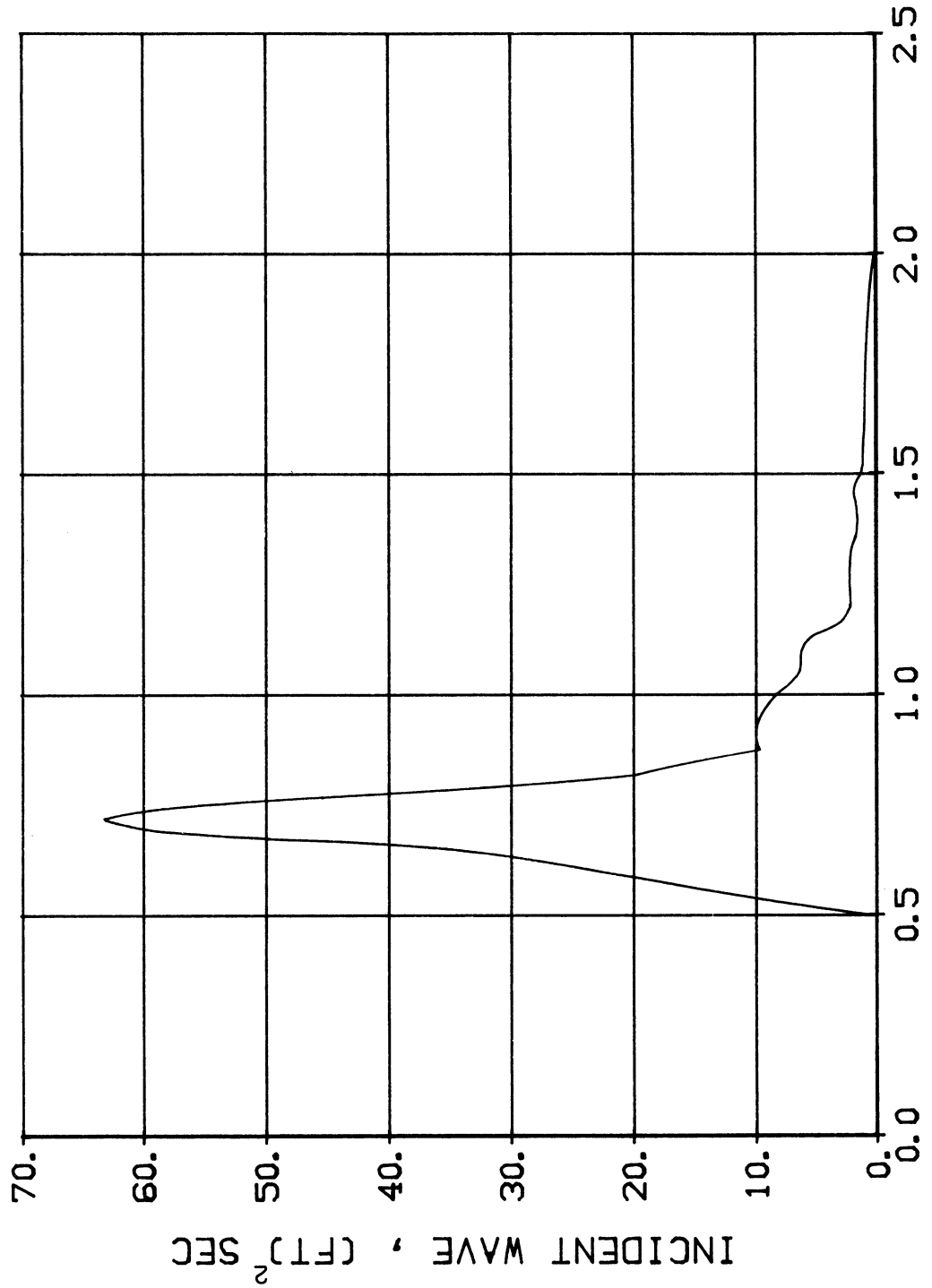

FIGURE 51: INCIDENT WAVE SPECTRUM USED IN THE EXAMPLE.
MEASURED AT EAGLE HARBOR, 28 NOV. 1966.
SIGNIFICANT WAVEHEIGHT = 18.29 FT. (TAKEN FROM PLOEG (1971)).

TABLE II: Transformation of the Incident Wave Spectrum onto the Encounter Frequency Axis.

n	$n\Delta\omega$	σ_n	$S^+(\sigma_n)$	$S^+(n\Delta\omega)$
0	0	0	0	0
1	0.1	0.9	0	0
2	0.2	0.18	0	0
3	0.3	0.26	0	0
4	0.4	0.33	0	0
5	0.5	0.40	0	0
6	0.6	0.46	0	0
7	0.7	0.52	3.5	2.06
8	0.8	0.58	17.5	9.85
9	0.9	0.63	28.0	15.18
10	1.0	0.69	56.5	29.35
11	1.1	0.74	57.5	28.87
12	1.2	0.79	33.0	16.03
13	1.3	0.83	18.5	8.76
14	1.4	0.88	9.8	4.50
15	1.5	0.93	9.9	4.41
16	1.6	0.97	9.3	4.04
17	1.7	1.01	8.0	3.40
18	1.8	1.05	6.3	2.62
19	1.9	1.10	6.2	2.51
20	2.0	1.14	4.5	1.78
21	2.1	1.17	3.0	1.17
22	2.2	1.21	2.0	0.76

(cont.)

n	$n\Delta\omega$	σ_n	$S^+(\sigma_n)$	$S^+(n\Delta\omega)$
23	2.3	1.25	2.0	0.75
24	2.4	1.29	2.1	0.77
25	2.5	1.32	2.1	0.76
26	2.6	1.36	1.7	0.60
27	2.7	1.40	1.3	0.45
28	2.8	1.43	1.6	0.55
29	2.9	1.46	1.7	0.57
30	3.0	1.50	1.1	0.37
31	3.1	1.53	1.0	0.33
32	3.2	1.56	1.0	0.32
33	3.3	1.60	0.8	0.25
34	3.4	1.63	0.8	0.25
35	3.5	1.66	0.7	0.22
36	3.6	1.69	0.6	0.18
37	3.7	1.72	0.6	0.18
38	3.8	1.75	0.6	0.18
39	3.9	1.78	0.6	0.18
40	4.0	1.81	0.6	0.18
41	4.1	1.84	0.6	0.17
42	4.2	1.87	0.5	0.14
43	4.3	1.89	0.5	0.14
44	4.4	1.92	0.4	0.11
45	4.5	1.95	0.3	0.08
46	4.6	1.98	0.2	0.05
47	4.7	2.01	0	0

TABLE III: Calculation of I_n for n = 18

m	n-m	$S^+(m\Delta\omega)$	$S^+(n\Delta\omega-m\Delta\omega)$	$S^+(m\Delta\omega)S^+(n\Delta\omega-m\Delta\omega)$
0	18	0	2.62	0
1	17	0	3.40	0
2	16	0	4.04	0
3	15	0	4.41	0
4	14	0	4.50	0
5	13	0	8.76	0
6	12	0	16.03	0
7	11	2.06	28.87	59.47
8	10	9.85	29.35	289.10
9	9	15.18	15.18	230.43
10	8	29.35	9.85	289.10
11	7	28.87	2.06	59.47
12	6	16.03	0	0
13	5	8.76	0	0
14	4	4.50	0	0
15	3	4.41	0	0
16	2	4.04	0	0
17	1	3.40	0	0

$$\sum = 927.57$$

$$I_{18} = \Delta\omega \times \sum = 92.8$$

TABLE IV: Calculation of I_n for n = 19

m	n-m	$S^+(m\Delta\omega)$	$S^+(n\Delta\omega-m\Delta\omega)$	$S^+(m\Delta\omega)S^+(n\Delta\omega-m\Delta\omega)$
0	19	0	2.51	0
1	18	0	2.62	0
2	17	0	3.40	0
3	16	0	4.04	0
4	15	0	4.41	0
5	14	0	4.50	0
6	13	0	8.76	0
7	12	2.06	16.03	33.02
8	11	9.85	28.87	284.37
9	10	15.18	29.35	445.53
10	9	29.35	15.18	445.53
11	8	28.87	9.85	284.37
12	7	16.03	2.06	33.02
13	6	8.76	0	0
14	5	4.50	0	0
15	4	4.41	0	0
16	3	4.04	0	0
17	2	3.40	0	0
18	1	2.62	0	0

$$\sum = 1525.84$$

$$I_{19} = \Delta\omega \times \sum = 152.6$$

TABLE V: Calculation of I_n for n = 20

m	n-m	$S^+(m\Delta\omega)$	$S^+(n\Delta\omega-m\Delta\omega)$	$S^+(m\Delta\omega)S^+(n\Delta\omega-m\Delta\omega)$
0	20	0	1.78	0
1	19	0	2.51	0
2	18	0	2.62	0
3	17	0	3.40	0
4	16	0	4.04	0
5	15	0	4.41	0
6	14	0	4.50	0
7	13	2.06	8.76	18.05
8	12	9.85	16.03	157.90
9	11	15.18	28.87	438.25
10	10	29.35	29.35	861.42
11	9	28.87	15.18	438.25
12	8	16.03	9.85	157.90
13	7	8.76	2.06	18.05
14	6	4.50	0	0
15	5	4.41	0	0
16	4	4.04	0	0
17	3	3.40	0	0
18	2	2.62	0	0
19	1	2.51	0	0

$$\sum = 2089.82$$

$$I_{20} = \Delta\omega \times \sum = 209.0$$

TABLE VI: Calculation of Non-linear Excitation from Eagle Harbor Spectrum (Model Restrained)

n	L/λ_n	$(H_n^{(2)})_{norm}$	$H_n^{(2)}$	I_n	$S_E^{(2)}+(n\Delta w)$
1	0.012			0	0
2	0.044			0	0
3	0.093			0	0
4	0.158			0	0
5	0.235			0	0
6	0.324			0	0
7	0.424			0	0
8	0.532			0	0
9	0.649			0	0
10	0.773			0	0
11	0.904			0	0
12	1.042			0	0
13	1.185			0	0
14	1.334	0.036	1.966×10^6	0.4	1.546×10^{12}
15	1.488	0.022	1.340×10^6	4.1	7.362×10^{12}
16	1.647	0.022	1.483×10^6	16.0	3.519×10^{12}
17	1.810	0.030	2.223×10^6	42.0	2.076×10^{14}
18	1.977	0.024	1.943×10^6	92.8	3.503×10^{14}
19	2.148	0.025	1.319×10^6	152.6	2.655×10^{14}
20	2.323	0.025	2.378×10^6	209.0	1.182×10^{15}
21	2.502	0.020	2.049×10^6	237.3	9.963×10^{14}

TABLE VII: Calculation of Non-linear Bending Moment Spectrum

n	$S_E^{(2)+}(n\Delta\omega)$	$q(n\Delta\omega)$	$S_M^{(2)+}(n\Delta\omega)$ $(ft\text{-}lbs)^2 sec$	$S_M^{(2)+}(n\Delta\omega)$ $(ft\text{-}L^T)^2 sec$
1	0		0	0
2	0		0	0
3	0		0	0
4	0		0	0
5	0		0	0
6	0		0	0
7	0		0	0
8	0		0	0
9	0		0	0
10	0		0	0
11	0		0	0
12	0		0	0
13	0		0	0
14	1.546×10^{12}	0.920	1.309×10^{12}	2.609×10^{5}
15	7.362×10^{12}	1.113	9.102×10^{12}	1.818×10^{6}
16	3.519×10^{13}	1.434	7.236×10^{13}	1.442×10^{7}
17	2.076×10^{14}	2.067	8.870×10^{14}	1.768×10^{8}
18	3.503×10^{14}	3.839	5.163×10^{15}	1.029×10^{9}
19	2.655×10^{14}	13.636	4.937×10^{16}	9.839×10^{9}
20	1.182×10^{15}	3.905	1.802×10^{16}	3.591×10^{9}
21	9.963×10^{14}	1.930	3.711×10^{15}	7.396×10^{8}

TABLE VIII: Calculation of Combined Linear and Non-linear Bending Moment Spectrum

n	$S_M^{(1)+}(n\Delta\omega)$ $(ft\text{-}LT)^2 sec$	$S_M^{(2)+}(n\Delta\omega)$ $(ft\text{-}LT)^2 sec$	$S_M^{+}(n\Delta\omega)$ $(ft\text{-}LT)^2 sec$
1	0	0	0
2	0	0	0
3	0	0	0
4	0	0	0
5	0	0	0
6	0	0	0
7			
8	1.639×10^{10}	0	1.639×10^{10}
9	1.659×10^{9}	0	1.659×10^{9}
10	1.393×10^{10}	0	1.393×10^{10}
11	8.147×10^{9}	0	8.147×10^{9}
12	3.528×10^{9}	0	3.528×10^{9}
13	8.367×10^{9}	0	8.367×10^{9}
14	1.041×10^{9}	2.609×10^{5}	1.042×10^{9}
15	3.378×10^{9}	1.818×10^{6}	3.380×10^{9}
16	5.083×10^{9}	1.442×10^{7}	5.098×10^{9}
17	5.162×10^{9}	1.768×10^{8}	5.339×10^{9}
18	2.491×10^{10}	1.029×10^{9}	2.594×10^{10}
19	8.004×10^{10}	9.839×10^{9}	8.988×10^{10}
20	6.281×10^{9}	3.591×10^{9}	9.872×10^{9}
21	1.135×10^{9}	7.396×10^{8}	1.875×10^{9}

curve of the combined linear and non-linear springing induced bending moment as a function of encounter frequency.

Calculations which take into account the effects of heave and pitch can be undertaken in a similar manner by using Figure 26 instead of Figure 16 in step 4.c. The resulting bending moment spectrum is shown in Figure 53.

In this example, when the effects of vertical rigid-body motion are neglected, the linear component of the combined bending moment spectrum accounts for 91% of the peak value, and the non-linear component contributes the remaining 9%. Of the area under the curve in the region near resonance (i.e., in the frequency range between 1.7 and 2.1 radians/sec), linear analysis accounts for 86%, and 14% is due to non-linear effects.

When heave and pitch effects are included, linear analysis accounts for only 70% of the peak spectral value, and the non-linear spectral component contributes 30%. The linear component accounts for only 76% of the area under the "combined" curve in the frequency range between 1.7 and 2.1 radians/sec, and the remaining 24% arises from non-linear effects.

It must be noted that the calculations leading from the springing excitation spectra to the bending moment spectra shown in Figures 50 and 51 are based upon the hypothesis that the second order excitation is the only source of non-linear effects. The use of equation (23) is correct only if this assumption holds. However, as discussed in section III, comparisons of experimentally measured excitation and response indicate that the assumption is questionable at frequencies near resonance, and will result in over-prediction of the bending moment magnitudes at frequencies near the natural springing frequency. See, for example, Figures 49 and 50.

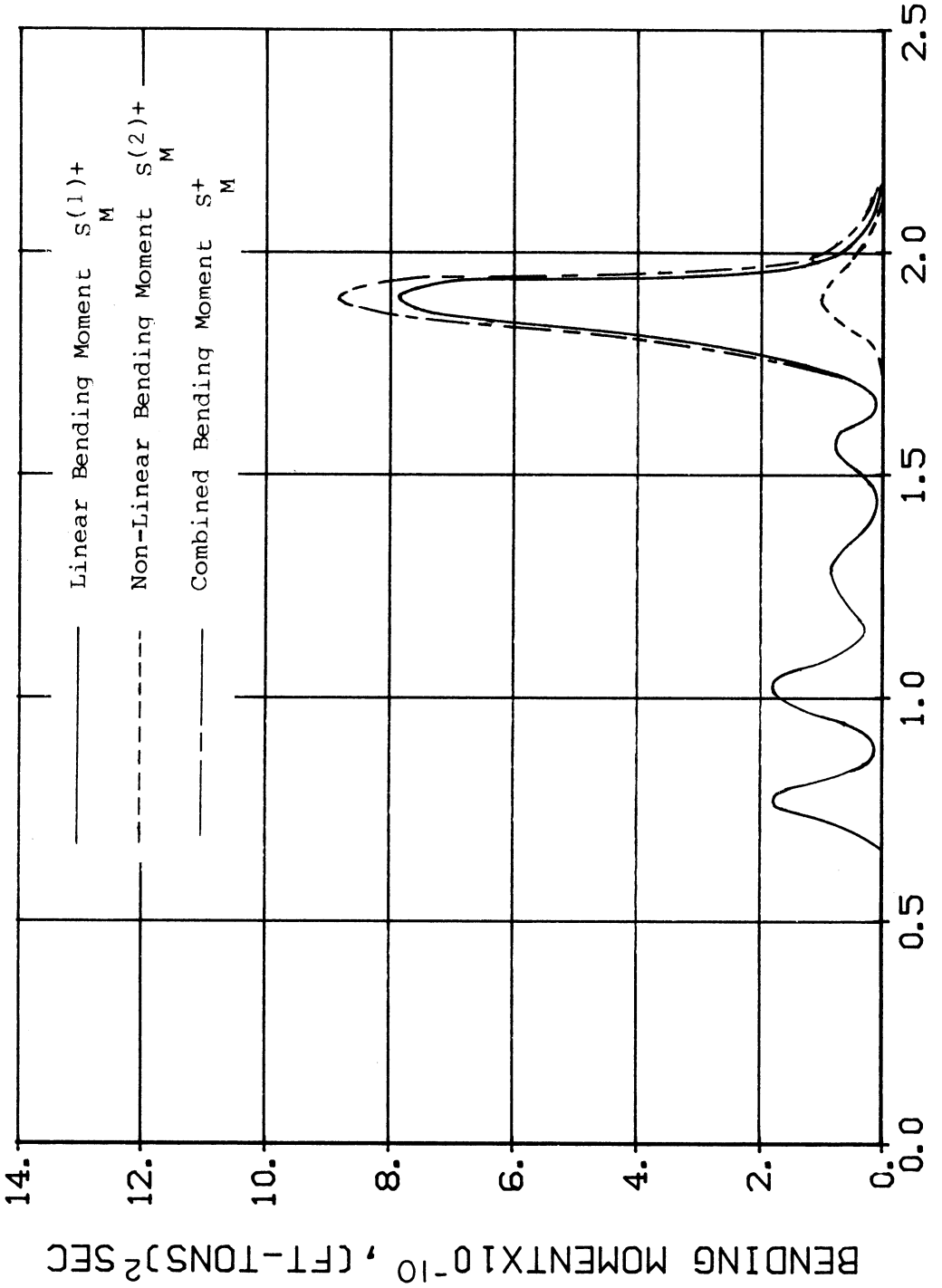

FIGURE 52: BENDING MOMENT SPECTRUM CALCULATED IN THE EXAMPLE. EFFECTS OF HEAVE AND PITCH NEGLECTED.

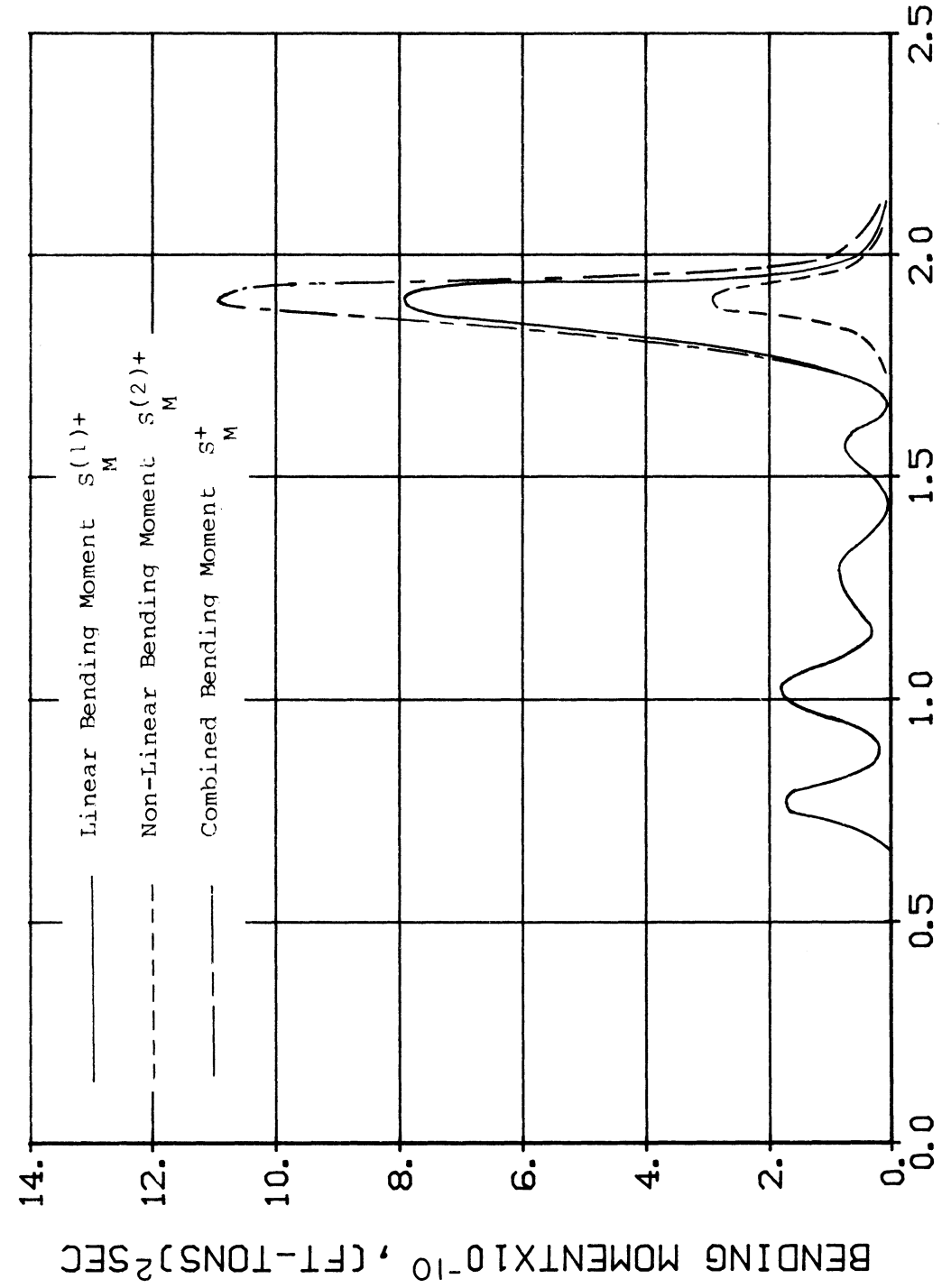

FIGURE 53: BENDING MOMENT SPECTRUM CALCULATED IN THE EXAMPLE. EFFECTS OF HEAVE AND PITCH INCLUDED.

V. *RECOMMENDATIONS FOR FUTURE RESEARCH*

The results presented in this work indicate the significance of nonlinear springing. However, various questions raised by the experiments have yet to be answered. As a consequence, the following areas are recommended for future research:

- Theoretical calculations should be performed to compare with experiment. The most straightforward approach would be to try and model the nonlinear excitation on a body fixed in waves. This would eliminate the effect of vessel motions and simplify considerably the proposed boundary value problem.

- Experiments and theory should be used to explain why the excitation for the restrained and free conditions were different. See, for example Figures 26 and 27. (The same type of behavior was also demonstrated in the response tests as shown in Figure 44.) It is clear, that even with small vessel motions, heave and pitch couple with nonlinear springing to increase the generalized springing excitation.

- The off diagonal behavior, characterized by changing ω_- and holding ω_+ fixed, should be explored. The results as shown in Figure 13 exhibit a large amount of scatter making it difficult to identify any significant trends. The study of the off diagonal term can be done using either theory or experiments.

- The assumption that the reactive hydrodynamic forces, A_{2j} the springing added mass and B_{2j} the springing damping, follow a linear relationship does not appear to be valid. Figures 49 and 50 clearly show this. The measured response is considerably reduced over the calculated response.

This suggests an important nonlinear damping force. The research investigating this nonlinear damping should be both experimental and theoretical.

REFERENCES

Bishop, R., et. al. (1977), "A Unified Dynamic Analysis of Ship Response to Waves," *Roy. Inst. Nav. Arch.* Spring Meeting.

Hoffman, D., and Van Hoof, R. (1976), "Experimental and Theoretical Evaluation of Springing on a Great Lakes Bulk Carrier," USCG Report CG-D-74.

Jensen, J.J., and Pedersen, T. (1978), "Wave-Induced Bending Moments in Ships - A Quadratic Theory," *Roy. Inst. Nav. Arch.*

Jensen, J.J., and Pedersen, T. (1981), "Bending Moments and Shear Forces in Ships Sailing in Irregular Waves," *JSR*, Vol. 25, No. 4, pp. 243-251.

Longuet-Higgins, M.S. (1963), "The Effects of Nonlinearities on Statistical Distributions in the Theory of Sea Waves," *JFM*, 17, pp. 459-480.

Maeda, H. (1980), "On the Theory of Coupled Ship Motions and Vibrations," Department of Naval Architecture and Marine Engineering, The University of Michigan.

Neal, E. (1974), "Second-Order Hydrodynamic Forces Due to Stochastic Excitation," Tenth Naval Hydrodynamics Symposium, Cambridge, Massachusetts.

Ploeg, J. (1971), "Wave Climate Study - Great Lakes and Gulf of St. Lawrence," SNAME T&R Bulletin 2107.

Troesch, A.W. (1980), "Ship Springing - An Experimental and Theoretical Study," Department of Naval Architecture and Marine Engineering, The University of Michigan, Ann Arbor, Michigan.

Yamanouchi, Y. (1974), "Ship's Behavior on Ocean Waves as a Stochastic Process," International Symposium of the Dynamics of Marine Vehicles and Structures in Waves, London, 178-192.

APPENDIX: DATA ANALYSIS TECHNIQUE

The method of analysis leading to the evaluation of the linear and non-linear transfer functions is presented in this Appendix. Given first is a development of the underlying theory. Following is a discussion of the application of this theory to the model test situation.

Preliminary Theory

Let $e_2(t)$ denote the springing excitation as a function of time. We wish to relate this excitation to the undisturbed incident wave elevation $\zeta(t)$, also measured as a function of time at some specified location which is fixed with respect to the moving ship.

We can express the excitation in terms of the wave elevation by making use of a second order formula given by Yamanouchi (1974).

$$e_2(t) = \int_{-\infty}^{\infty} h_1(\tau)\zeta(t-\tau)d\tau + \int_{-\infty}^{\infty}\int_{-\infty}^{\infty} h_2(\tau_1,\tau_2)\zeta(t-\tau_1)\zeta(t-\tau_2)d\tau_1 d\tau_2 \qquad \text{(A-1)}$$

Here $h_1(\tau)$ is the impulse response function and $h_2(\tau_1,\tau_2)$ is the quadratic impulse response function.

Let

$$e_2(t) = e_2^{(1)}(t) + e_2^{(2)}(t) \ , \qquad \text{(A-2)}$$

where $e_2^{(1)}$ is the linear (first order) excitation

$$e_2^{(1)} = \int_{-\infty}^{\infty} h_1(\tau)\zeta(t-\tau)d\tau \ , \qquad \text{(A-3)}$$

and $e_2^{(2)}$ is the non-linear (second order) excitation

$$e_2^{(2)}(t) = \int_{-\infty}^{\infty}\int_{-\infty}^{\infty} h_2(\tau_1,\tau_2)\zeta(t-\tau_1)\zeta(t-\tau_2)d\tau_1 d\tau_2 \quad . \tag{A-4}$$

Suppose that the wave elevation $\zeta(t)$ can be written as a Fourier series

$$\zeta(t) = \sum_{n=1}^{\infty} \eta(n\Delta\omega)e^{in\Delta\omega t} \quad , \tag{A-5}$$

where $\Delta\omega$ is some incremental frequency of encounter and the coefficients $\eta(n\Delta\omega)$ are complex. Substitution of the series (A-5) into the expression for the linear excitation (A-3) gives

$$e_2^{(1)}(t) = \int_{-\infty}^{\infty} h_1(\tau) \sum_{n=1}^{\infty} \eta(n\Delta\omega)e^{in\Delta\omega(t-\tau)}d\tau$$

$$= \sum_{n=1}^{\infty} \eta(n\Delta\omega)e^{in\Delta\omega t} \int_{-\infty}^{\infty} h_1(\tau)e^{-in\Delta\omega\tau}d\tau$$

$$= \sum_{n=1}^{\infty} \eta(n\Delta\omega)H^{(1)}(n\Delta\omega)e^{in\Delta\omega t} \tag{A-6}$$

where $H^{(1)}(n\Delta\omega)$ is the complex first order transfer function

$$H^{(1)}(n\Delta\omega) = \int_{-\infty}^{\infty} h_1(\tau)e^{-in\Delta\omega\tau}d\tau \quad . \tag{A-7}$$

Substitution of the Fourier series (A-5) into the expression for the non-linear excitation (A-4) gives

$$e_2^{(2)}(t) = \int_{-\infty}^{\infty}\int_{-\infty}^{\infty} h_2(\tau_1,\tau_2)\left|\sum_{n=1}^{\infty} \eta(n\Delta\omega)e^{in\Delta\omega(t-\tau_1)}\right|\left|\sum_{m=1}^{\infty} \eta(m\Delta\omega)e^{im\Delta\omega(t-\tau_1)}\right|$$

$$= \sum_{n=1}^{\infty}\sum_{m=1}^{\infty} \eta(n\Delta\omega)\,\eta(m\Delta\omega)e^{i(n+m)\Delta\omega t} \int_{-\infty}^{\infty}\int_{-\infty}^{\infty} h_2(\tau_1,\tau_2,)e^{-in\Delta\omega\tau_1}\,e^{-im\Delta\omega\tau_2}\,d\tau_1 d\tau_2$$

$$= \sum_{n=1}^{\infty} \sum_{m=1}^{\infty} \eta(n\Delta\omega)\eta(m\Delta\omega)H^{(1)}(n\Delta\omega,m\Delta\omega)e^{i(n+m)\Delta\omega t} , \qquad (A-8)$$

where $H^{(2)}(n\Delta\omega,m\Delta\omega)$ is the complex second order transfer function defined by

$$H^{(2)}(n\Delta\omega,m\Delta\omega) = \int_{-\infty}^{\infty} \int_{-\infty}^{\infty} h_2(\tau_1,\tau_2)e^{-in\Delta\omega\tau_1} e^{im\Delta\omega\tau_2} d\tau_1 d\tau_2 . \qquad (A-9)$$

The total springing excitation can now be written to second order as

$$e_2(t) = \sum_{k=1}^{\infty} \eta(k\Delta\omega)H^{(1)}(k\Delta\omega)e^{ik\Delta\omega t}$$

$$+ \sum_{n=1}^{\infty} \sum_{m=1}^{\infty} \eta(n\Delta\omega)\eta(m\Delta\omega)H^{(2)}(n\Delta\omega,m\Delta\omega)e^{i(n+m)\Delta\omega t} . \qquad (A-10)$$

We next express $e_2(t)$ as a Fourier series.

$$e_2(t) = \sum_{k=1}^{\infty} E_2(k\Delta\omega)e^{ik\Delta\omega t} \qquad (A-11)$$

Combining the expressions (A-10) and (A-11) we obtain

$$\sum_{k=1}^{\infty} E_2(k\Delta\omega)e^{ik\Delta\omega t} = \sum_{k=1}^{\infty} \eta(k\Delta\omega)H^{(1)}(k\Delta\omega)e^{ik\Delta\omega t}$$

$$+ \sum_{n=1}^{\infty} \sum_{m=1}^{\infty} \eta(n\Delta\omega)\eta(m\Delta\omega)H^{(2)}(n\Delta\omega,m\Delta\omega)e^{i(n+m)\Delta\omega t} . \qquad (A-12)$$

The double sum can be re-ordered

$$\sum_{n=1}^{\infty} \sum_{m=1}^{\infty} \eta(n\Delta\omega)\eta(m\Delta\omega)H^{(2)}(n\Delta\omega,m\Delta\omega)e^{i(n+m)\Delta\omega t}$$

$$= \sum_{k=2}^{\infty} \sum_{n=1}^{k-1} \eta(n\Delta\omega)\eta(k\Delta\omega-n\Delta\omega)H^{(2)}(n\Delta\omega,k\Delta\omega-n\Delta\omega)e^{ik\Delta\omega t} \qquad (A-13)$$

to give

$$\sum_{k=1}^{\infty} E_2(k\Delta\omega)e^{ik\Delta\omega t} = \sum_{k=1}^{\infty} \eta(k\Delta\omega)H^{(1)}(k\Delta\omega)e^{ik\Delta\omega t}$$

$$+ \sum_{k=2}^{\infty}\sum_{n=1}^{k-1} \eta(n\Delta\omega)\eta(k\Delta\omega-n\Delta\omega)H^{(2)}(n\Delta\omega,k\Delta\omega-n\Delta\omega)e^{ik\Delta\omega t} \qquad \text{(A-14)}$$

or

$$\sum_{k=1}^{\infty} E_2(k\Delta\omega)e^{ik\Delta\omega t} = \eta(\Delta\omega)H^{(1)}(\Delta\omega)e^{i\Delta\omega t}$$

$$+ \sum_{k=2}^{\infty}\left[\left[\eta(k\Delta\omega)H^{(1)}(k\Delta\omega) + \sum_{n=1}^{k-1} \eta(n\Delta\omega)\eta(k\Delta\omega-n\Delta\omega)H^{(2)}(n\Delta\omega,k\Delta\omega-n\Delta\omega)\right]\right]e^{ik\Delta\omega t}. \qquad \text{(A-15)}$$

From this it follows that

$$E_2(k\Delta\omega) = \eta(k\Delta\omega)H^{(1)}(k\Delta\omega) \qquad , k=1$$

$$= \eta(k\Delta\omega)H^{(1)}(k\Delta\omega) + \sum_{n=1}^{k-1} \eta(n\Delta\omega)\eta(k\Delta\omega-n\Delta\omega)H^{(2)}(n\Delta\omega,k\Delta\omega-n\Delta\omega), \quad k\geq 2 . \qquad \text{(A-16)}$$

Defining

$$E_2^{(1)}(k\Delta\omega) = \eta(k\Delta\omega)H^{(1)}(k\Delta\omega) \qquad \text{(A-17)}$$

and

$$E_2^{(2)}(k\Delta\omega) = 0 \qquad , \quad k=1$$

$$= \sum_{n=1}^{k-1} \eta(n\Delta\omega)\eta(k\Delta\omega-n\Delta\omega)H^{(2)}(n\Delta\omega,k\Delta\omega-n\Delta\omega), \quad k\geq 2 , \qquad \text{(A-18)}$$

we can decompose the Fourier coefficient $E_2(k\Delta\omega)$ into its linear and non-linear components.

$$E_2(k\Delta\omega) = E_2^{(1)}(k\Delta\omega) + E_2^{(2)}(k\Delta\omega) \qquad \text{(A-19)}$$

Experimental Determination of the Linear and Non-Linear Transfer Functions

The primary purpose of the experiments is the determination of the non-linear transfer function $H^{(2)}(n\Delta\omega, k\Delta\omega - n\Delta\omega)$ in equation (A-16). A secondary purpose is the evaluation of the linear transfer function $H^{(1)}(k\Delta\omega)$ for comparison with Troesch (1980). Discussed here is the method by which these transfer functions are determined from recorded time histories of the incident wave elevation and the springing excitation. The same method is used to treat measurements of springing response.

Consider a case in which the model encounters an incident wave system composed of two sinusoidal waves with encounter frequencies $\omega_1 = p\Delta\omega$ and $\omega_2 = q\Delta\omega$. The Fourier series (A-5) representing the wave elevation would then have only two non-zero terms.

$$\zeta(t) = \eta(p\Delta\omega)e^{ip\Delta\omega t} + \eta(q\Delta\omega)e^{iq\Delta\omega t} \qquad \text{(A-20)}$$

From equation (A-16) we find that the Fourier series (A-11) representing the springing excitation would, in general, have five non-zero terms. Two of these would represent the linear excitations caused by the two wave components.

$$E_2(p\Delta\omega) = E_2^{(1)}(p\Delta\omega) = \eta(p\Delta\omega)H^{(1)}(p\Delta\omega) \qquad \text{(A-21)}$$

$$E_2(q\Delta\omega) = E_2^{(1)}(q\Delta\omega) = \eta(q\Delta\omega)H^{(2)}(q\Delta\omega) \qquad \text{(A-22)}$$

Two more would arise through non-linear effects at "harmonics" of the wave frequencies, i.e. at $\omega = 2p\Delta\omega$ and $\omega = 2q\Delta\omega$.

$$E_2(2p\Delta\omega) = E_2^{(2)}(2p\Delta\omega) = \eta(p\Delta\omega)\eta(p\Delta\omega)H^{(2)}(p\Delta\omega, p\Delta\omega) \quad , \qquad \text{(A-23)}$$

$$E_2(2q\Delta\omega) = E_2^{(2)}(2q\Delta\omega) = \eta(q\Delta\omega)\eta(q\Delta\omega)H^{(2)}(q\Delta\omega, q\Delta\omega) \quad , \qquad \text{(A-24)}$$

the last would arise as a non-linear excitation at the sum of the wave frequencies, i.e. at $\omega = p\Delta\omega + q\Delta\omega$.

$$E_2(p\Delta\omega+q\Delta\omega) = E_2^{(2)}(p\Delta\omega+q\Delta\omega) = 2\eta(p\Delta\omega)\eta(q\Delta\omega)H^{(2)}(p\Delta\omega,q\Delta\omega) \quad . \tag{A-25}$$

If the wave elevation and springing excitation were recorded as functions of time, and the Fourier coefficients were calculated for each time history, we could use equations (A-21) through (A-25) to obtain the following values of the linear and non-linear transfer functions:

$$H^{(1)}(p\Delta\omega) = \frac{E_2(p\Delta\omega)}{\eta(p\Delta\omega)} \quad , \tag{A-26}$$

$$H^{(1)}(q\Delta\omega) = \frac{E_2(p\Delta\omega)}{\eta(q\Delta\omega)} \quad , \tag{A-27}$$

$$H^{(2)}(p\Delta\omega,q\Delta\omega) = \frac{E_2(2p\Delta\omega)}{\eta(p\Delta\omega)\eta(p\Delta\omega)} \quad , \tag{A-28}$$

$$H^{(2)}(q\Delta\omega,q\Delta\omega) = \frac{E_2(2q\Delta\omega)}{\eta(q\Delta\omega)\eta(q\Delta\omega)} \quad , \tag{A-29}$$

$$H^{(2)}(p\Delta\omega,q\Delta\omega) = \frac{E_2(p\Delta\omega+q\Delta\omega)}{2\eta(p\Delta\omega)\eta(q\Delta\omega)} \quad . \tag{A-30}$$

Further data could be obtained through this method by testing at several different combinations of wave encounter frequencies $p\Delta\omega$ and $q\Delta\omega$.

Unfortunately, this method is overly idealistic. It is not possible in practice to produce perfectly sinusoidal waves in the towing tank. If an attempt is made to generate an incident wave pattern composed of sinusoidal

waves at two discrete frequencies $p\Delta\omega$ and $q\Delta\omega$, creating the situation analyzed above, the Fourier analysis of the surface elevation will show that non-zero Fourier components will be present at frequencies adjacent to $\omega = p\Delta\omega$ and $\omega = q\Delta\omega$ in addition to the components at the intended frequencies. As will be shown, this energy "leakage" is of no consequence in the evaluation of the linear transfer function, but must be taken into account in the determination of the non-linear transfer function.

In order to simplify the discussion as much as possible we consider a case in which energy leakage is minimal. We will assume that an attempt has been made to generate a wave system with components at encounter frequencies $\omega = p\Delta\omega$ and $\omega = q\Delta\omega$, but that Fourier analysis has shown that non-zero Fourier components were present at frequencies $\omega = (p-1)\Delta\omega, p\Delta\omega, (p+1)\Delta\omega$ and $\omega = (q-1)\Delta\omega, q\Delta\omega, (q+1)\Delta\omega$.

From equation (A-16) we find that the linear excitation component at $\omega = p\Delta\omega$ is given by

$$E_2(p\Delta\omega) = E_2^{(2)}(p\Delta\omega) = \eta\,(p\Delta\omega)H^{(1)}(p\Delta\omega) \quad . \tag{A-31}$$

This is the same as equation (A-21), and equation (A-26) is again a valid expression for the linear transfer function at $\omega = q\Delta\omega$. Likewise, equations (A-22) and (A-27) again apply at $\omega = q\Delta\omega$. In general, we find that

$$E_2(p'\Delta\omega) = E_2^{(1)}(p'\Delta\omega) = \eta(p'\Delta\omega)H^{(1)}(p'\Delta\omega) \tag{A-32}$$

and

$$H^{(1)}(p'\Delta\omega) = \frac{E_2(p'\Delta\omega)}{\eta(p'\Delta\omega)} \tag{A-33}$$

are valid in treating the linear behavior for $p' = p$ and $p' = q$.

However, in this more realistic case, equation (A-23) is no longer a valid expression for the "harmonic" excitation at $\omega = 2\Delta p$. We have instead

$$E_2(2p\Delta\omega) = E_2^{(2)}(2p\Delta\omega) = 2\eta[(p-1)\Delta\omega]\eta[(p+1)\Delta\omega]H^{(2)}[(p-1)\Delta\omega,(p+1)\Delta\omega]$$

$$+ \eta[p\Delta\omega]\eta[p\Delta\omega]H^{(2)}[p\Delta\omega,p\Delta\omega] \ , \qquad \text{(A-34)}$$

and it is obvious that equation (A-28) cannot be used. In order to extract data from equation (A-34) we must employ the following approximation. We assume that for small changes in its arguments the transfer function $H^{(2)}$ is nearly constant. Then, if $\Delta\omega$ is sufficiently small,

$$E_2(2p\Delta\omega) = E_2^{(2)}(2p\Delta\omega) \simeq [2\eta[(p-1)\Delta\omega]\eta[p+1)\Delta\omega] + \eta[p\Delta\omega]\eta[p\Delta\omega]] \cdot H^{(2)}[p\Delta\omega,p\Delta\omega]$$

$$\simeq H^{(2)}[p\Delta\omega,p\Delta\omega] \sum_{n=1}^{2p-1} \eta(n\Delta\omega)\eta(2p\Delta\omega-n\Delta\omega) \ , \qquad \text{(A-35)}$$

and we obtain an approximate value for $H^{(2)}$ from

$$H^{(2)}[p\Delta\omega,p\Delta\omega] \simeq \frac{E_2(2p\Delta\omega)}{\sum_{n=1}^{2p-1} \eta(n\Delta\omega)\eta(2p\Delta\omega-n\Delta\omega)} \ . \qquad \text{(A-36)}$$

Similar treatment of the non-linear excitation components at frequencies $\omega = 2q\Delta\omega$ and $\omega = p\Delta\omega + q\Delta\omega$ results in expressions analogous to equation (A-36). We give the general formula

$$H^{(2)}[p'\Delta\omega,q'\Delta\omega] \simeq \frac{E_2(p'\Delta\omega + q'\Delta\omega)}{\sum_{n=1}^{p'+q'} \eta(n\Delta\omega)\eta(p'\Delta\omega+q'\Delta\omega-n\Delta\omega)} \ . \qquad \text{(A-37)}$$

"Harmonic" excitation is analyzed by using equations (A-35) and (A-36) with

$p' = q' = p$. "Sum frequency" excitation is treated with $p' = p$, $q' = q$. As implied in the development, the approximations are valid only when the significant wave energy is concentrated at encounter frequencies near the intended frequencies $\omega = p\Delta\omega$ and $\omega = q\Delta\omega$ as shown in Figures 5 and 7.

Equations (A-33) and (A-37) are the basis for the data analysis procedure used to produce the experimental results given in section III. During each test run the surface elevation ζ and springing excitation e_2 were measured as functions of time, and both time histories were stored in digitized form in the memory of a Tektronix 4052 computer. Fourier coefficients were calculated for each record by a Fast Fourier Transform FFT technique. Evaluation of the linear transfer function at frequencies $\omega = p\Delta\omega$ and $\omega = q\Delta\omega$ was then possible using equation (A-33). A convolution subroutine was used to compute the sum

$$S = \sum_{n=1}^{p'+q'} \eta(n\Delta\omega)\eta(p'\Delta\omega+q'\Delta\omega-n\Delta\omega) \qquad \text{(A-38)}$$

for $p' = q' = p$; $p' = q' = q$; and $p' = p$, $q' = q$. The values of the non-linear transfer function for the three non-linear excitation components were then calculated by equation (A-37).